UNIVERSITÀ
POLITECNICA
DELLE MARCHE

FACOLTA' DI INGEGNERIA

Corso di Laurea Magistrale in Biomedical Engineering-

Engineering of Medical Devices

Finite element analysis of different configurations of pediatric oncologic implants for proximal femoral resection

Relatore:

Prof. Marco Mandolini

Tesi di laurea di:

Federica Canu

Correlatore:

Prof. Bernardo Innocenti, PhD

Mattia Sisella, PhD *Candidate*

Anno Accademico 2025-2026

Dedica

I. Table of Contents

II. Table of Figures

III. List of tabels

Abstract

Introduction

Pediatric malignant bone tumors, particularly osteosarcoma, frequently require extensive bone resections and complex reconstructive procedures. In skeletally immature patients, proximal femoral reconstruction represents a major biomechanical challenge due to reduced bone dimensions, ongoing skeletal growth and the need to preserve the remaining bone stock. In this context, the interaction between the prosthetic stem and the residual femur plays a crucial role in determining implant stability and physiological load transfer.

The aim of this thesis is to investigate the biomechanical behavior of the residual femoral bone following proximal femoral resection through finite element analysis (FEA), focusing on the combined effect of different resection levels and prosthetic stem lengths.

Materials and methods

A patient-specific numerical model was developed starting from computed tomography (CT) images of a 14-year-old pediatric patient treated at Meyer Children's Hospital in Florence, Italy. Cortical bone, trabecular bone and growth plate regions were segmented and reconstructed using 3D Slicer, while numerical simulations were performed in Abaqus. The oncological reconstruction was performed using the modular LINK Megasystem-C prosthetic system. Different oncological reconstruction configurations were developed by varying both the proximal femoral resection level and the intramedullary stem length of the prosthesis. An axial load of 250 N was applied along the mechanical axis to simulate physiological loading conditions representative of static standing with bilateral support. Stress distribution within the bone was evaluated by dividing the femur into 5 regions of interest.

Results

Numerical analysis focused primarily on the evaluation of Von Mises stress distribution within the residual cortical bone. The results show that both stem length and resection level influence the mechanical response of the femur.

In all investigated configurations, the average stress within the cortical bone remained below 5 MPa. The highest stress levels were consistently observed at the bone–implant interface, and around the stem tip.

Increasing stem length promoted a more distal transfer of loads and generally reduced stress levels within the residual bone. Similarly, increasing the proximal femoral resection length resulted in a progressive decrease in cortical stress values.

Discussion

The findings suggest that both stem length and resection level affect load transfer within the pediatric femur. The reduction in stress observed with longer stems and more extensive resections indicates a progressive shift of load transmission from the residual bone to the stem, potentially increasing the risk of stress shielding. Conversely, shorter stems promoted greater proximal load transfer, resulting in a more physiological mechanical environment but also higher local stress concentrations. These results highlight the importance of balancing implant stability and preservation of physiological bone loading when planning pediatric proximal femoral reconstructions.

Conclusion

The present study highlights the importance of considering both resection level and stem length during pediatric proximal femoral reconstruction. The developed patient-specific finite element model provides a useful framework for investigating bone–implant biomechanics and may support future optimization of surgical planning and prosthetic design in skeletally immature patients.

Abstract in Italiano

Introduzione
I tumori ossei maligni pediatrici, in particolare l'osteosarcoma, richiedono frequentemente ampie resezioni ossee e complesse procedure ricostruttive. Nei pazienti scheletricamente immaturi, la ricostruzione del femore prossimale rappresenta una rilevante sfida biomeccanica a causa delle ridotte dimensioni ossee, della crescita scheletrica ancora in corso e della necessità di preservare l’osso residuo. In questo contesto, l'interazione tra lo stelo protesico e il femore residuo svolge un ruolo fondamentale nel determinare la stabilità dell'impianto e il trasferimento fisiologico dei carichi.
L'obiettivo di questa tesi è studiare il comportamento biomeccanico dell'osso femorale residuo in seguito a resezione del femore prossimale tramite analisi agli elementi finiti (Finite Element Analysis, FEA), focalizzandosi sull'effetto combinato di differenti livelli di resezione e diverse lunghezze dello stelo protesico.

Materiali e Metodi
È stato sviluppato un modello numerico patient-specific a partire da immagini di tomografia computerizzata (CT) di un paziente pediatrico di 14 anni trattato presso l'Ospedale Pediatrico Meyer di Firenze. Le regioni corrispondenti all'osso corticale, all'osso trabecolare e alla placca di accrescimento distale sono state segmentate e ricostruite mediante il software 3D Slicer, mentre le simulazioni numeriche sono state eseguite in Abaqus. La ricostruzione oncologica è stata realizzata utilizzando il sistema protesico modulare LINK Megasystem-C. Sono state sviluppate diverse configurazioni ricostruttive variando sia il livello di resezione del femore prossimale sia la lunghezza dello stelo intramidollare della protesi. Un carico assiale di 250 N è stato applicato lungo l'asse meccanico per simulare condizioni fisiologiche di carico rappresentative della posizione eretta statica con appoggio bilaterale. La distribuzione degli stress all'interno dell'osso è stata valutata suddividendo il femore in cinque regioni di interesse.

Risultati
L'analisi numerica si è concentrata principalmente sulla valutazione della distribuzione degli stress di Von Mises all'interno dell'osso corticale residuo. I risultati mostrano che sia la lunghezza dello stelo sia il livello di resezione influenzano la risposta meccanica del femore. In tutte le configurazioni analizzate, lo stress medio all'interno dell'osso corticale è rimasto inferiore a 5 MPa. I valori più elevati di stress sono stati osservati in corrispondenza dell'interfaccia osso-impianto e nella regione circostante la punta dello stelo.
L'aumento della lunghezza dello stelo ha favorito un trasferimento più distale dei carichi e ha generalmente ridotto i livelli di stress nell'osso residuo. Analogamente, l'aumento della

lunghezza di resezione del femore prossimale ha determinato una progressiva diminuzione dei valori di stress nell'osso corticale.

Discussione

I risultati suggeriscono che sia la lunghezza dello stelo sia il livello di resezione influenzano i meccanismi di trasferimento del carico all'interno del femore pediatrico. La riduzione degli stress osservata per steli più lunghi e resezioni più estese indica un progressivo trasferimento del carico dall'osso residuo allo stelo protesico, con un potenziale aumento del rischio di stress shielding. Al contrario, gli steli più corti favoriscono un maggiore trasferimento prossimale del carico, determinando un ambiente meccanico più fisiologico ma associato a maggiori concentrazioni locali di stress. Questi risultati evidenziano l'importanza di bilanciare la stabilità dell'impianto e la preservazione di un carico fisiologico dell'osso durante la pianificazione delle ricostruzioni oncologiche del femore prossimale in età pediatrica.

Conclusioni

Lo studio evidenzia l'importanza di considerare sia il livello di resezione sia la lunghezza dello stelo durante la ricostruzione del femore prossimale in pazienti pediatrici. Il modello agli elementi finiti patient-specific sviluppato fornisce uno strumento utile per l'analisi della biomeccanica osso-impianto e potrebbe contribuire alla futura ottimizzazione della pianificazione chirurgica e della progettazione protesica nei pazienti pediatrici.

1 Introduction

Pediatric malignant bone tumors are rare but highly aggressive musculoskeletal diseases that affect children and adolescents during the critical years of skeletal growth. Among these, osteosarcoma represents the most common primary malignant bone tumor, followed by Edwing's sarcoma. They frequently involve long bones such as the femur, particularly in regions characterized by elevated growth activity.

Over the last decades, major advances in chemotherapy protocols, imaging techniques and surgical procedures have progressively shifted the standard treatment from limb amputation to limb-salvage surgery. This evolution has significantly improved both survival rates and postoperative quality of life by allowing preservation of the affected limb and partial recovery of physiological functionality.

Despite these clinical advances, reconstruction following proximal femoral tumor resection remains particularly challenging in skeletally immature patients.

Unlike adult subjects, pediatric patients present ongoing skeletal growth, active growth plates and reduced bone dimensions, all of which complicate both surgical management and prosthetic reconstruction. Furthermore, the proximal femur plays a fundamental biomechanical role in load transmission between the hip joint and the lower limb. Consequently, the removal of large proximal femoral segments substantially alters the physiological stress distribution within the residual bone and modifies the overall mechanical behavior of the femur–implant system.

In this context, modular oncological prostheses have become one of the most widely adopted reconstructive solutions after tumor resection. Their modularity allows adaptation of the implant geometry to different patient anatomies and resection lengths while ensuring adequate structural stability. However, the interaction between the prosthetic stem and the residual bone remains a critical aspect influencing long-term clinical outcomes.

In particular, the amount of residual bone preserved after surgery and the length of the intramedullary stem directly affect the transfer of mechanical loads from the implant to the surrounding cortical bone. Non-physiological stress distributions may consequently develop, potentially leading to stress shielding phenomena, bone resorption, cortical weakening and increased risk of mechanical failure at the bone–implant interface.

Biomechanical investigation of these phenomena is particularly important in pediatric orthopedic oncology, where long-term implant survival and preservation of the residual bone stock are essential considerations. Nevertheless, the biomechanical behavior of pediatric oncological femoral reconstructions is still insufficiently investigated in literature, especially regarding the combined influence of different resection levels and prosthetic stem lengths on the mechanical response of the remaining bone.

Finite Element Analysis (FEA) has become an increasingly important tool in orthopedic biomechanics for the study of bone–implant interactions and stress transfer mechanisms. Numerical simulations allow the evaluation of different surgical and prosthetic configurations under controlled loading conditions without the ethical and practical limitations associated with experimental studies in pediatric patients. In addition, patient-specific finite element models derived from computed tomography (CT) imaging provide the possibility to reproduce realistic anatomical geometries and investigate the mechanical response of reconstructed skeletal structures with high reliability.

To perform the biomechanical analyses, a patient-specific numerical workflow was developed starting from CT images of a pediatric patient affected by proximal femoral tumour. The anatomical structures of the femur, including cortical bone, trabecular bone and growth plate regions, were reconstructed through medical image segmentation using 3D Slicer. The resulting three-dimensional geometries were subsequently imported into Abaqus CAE 2019 for finite element modelling, prosthetic reconstruction and numerical simulations under physiological loading conditions representative of static standing.

The aim of this thesis is to investigate the biomechanical behavior of the residual femoral bone following proximal femoral resection through FEA. Attention is dedicated to evaluating the combined effect of different resection levels and prosthetic stem lengths on stress transfer within the reconstructed femur. Different oncological reconstruction configurations were generated and systematically compared to analyze how variations in residual bone length and stem length influence load transfer mechanisms and local stress concentrations within the residual femur.

The study focuses primarily on the evaluation of Von Mises stress and other relevant mechanical indicators associated with potential bone weakening and implant overloading. Through the comparison of the different configurations, this work aims to provide biomechanical insights into the mechanical behavior of pediatric proximal femoral reconstructions and to contribute to a better understanding of the factors affecting residual bone preservation and implant stability. Ultimately, the results of this study may support future optimization of prosthetic design and patient-specific surgical planning strategies in pediatric orthopedic oncology.

2 State of the art

2.1 Femur bone

2.1.1 Adult femur anatomy

The femur is the longest, strongest, and heaviest bone in the human body and represents the primary load-bearing structure of the lower limb. Anatomically, it is classified as a long bone and can be divided into three principal regions: the proximal epiphysis, the diaphysis, and the distal epiphysis. It's the only bone of the thigh and accounts for approximately one-quarter of an individual's total body height [1,2].

The proximal epiphysis consists of the femoral head, femoral neck, and the greater and lesser trochanters.

The spherical femoral head articulates with the acetabulum of the pelvis, forming the hip joint, a synovial ball-and-socket joint that allows a wide range of motion while maintaining joint stability. On its medial aspect, the femoral head presents a small depression known as the fovea capitis, which serves as the attachment site for the ligament of the head of the femur. The femoral neck connects the head to the shaft and is oriented at an angle of approximately 125–130° relative to the diaphysis, commonly referred to as the neck–shaft angle. This anatomical configuration contributes to the efficient transmission of loads from the pelvis to the lower limb.

The greater trochanter is a large prominence located lateral to the femoral neck and serves as the attachment site for several muscles acting across the hip joint. The lesser trochanter provides insertion for powerful hip flexor muscles. The two trochanters are connected anteriorly by the intertrochanteric line and posteriorly by the intertrochanteric crest, important anatomical landmarks of the proximal femur [2].

The diaphysis constitutes the central shaft of the femur and exhibits a slight anterior curvature. It is primarily responsible for transmitting mechanical loads generated during standing, walking, and other daily activities. Internally, the shaft contains the medullary cavity, which houses bone marrow and is surrounded by a thick cortical shell that provides structural stiffness and resistance to bending and compression. On the posterior aspect of the shaft, the linea aspera forms a prominent longitudinal ridge that serves as the attachment site for numerous muscles of the thigh.

The distal epiphysis expands into the medial and lateral femoral condyles, which articulate with the tibia and patella to form the knee joint. The condyles are separated posteriorly by the intercondylar fossa, while anteriorly they merge to form the patellar surface, which articulates with the patella during knee motion. The medial and lateral epicondyles provide attachment sites for ligaments and muscles contributing to knee stability [2].

Structurally, the femur is composed of two main types of bone tissue: cortical bone and trabecular bone. Cortical bone, also known as compact bone, forms the external shell of the femur and provides most of its mechanical strength. Trabecular bone, also referred to as cancellous bone, is mainly located within the proximal and distal epiphyses and consists of a porous network of interconnected trabeculae that efficiently distribute stresses and absorb mechanical energy.

The primary functions of the femur are weight bearing, load transmission, and gait stabilization. While standing, the weight of the upper body is transferred through the femoral heads to the lower limbs, while during locomotion the femur acts as the main structural element responsible for transmitting forces between the hip and knee joints.

The interaction between cortical and trabecular bone, together with the anatomical configuration of the femur, ensures both mechanical strength and efficient load transfer throughout the skeletal system [1,2].

The main anatomical landmarks of the femur are illustrated in Figure 2.1. The figure shows the anterior and posterior views of the bone, highlighting the proximal, diaphyseal, and distal regions together with the principal anatomical structures.

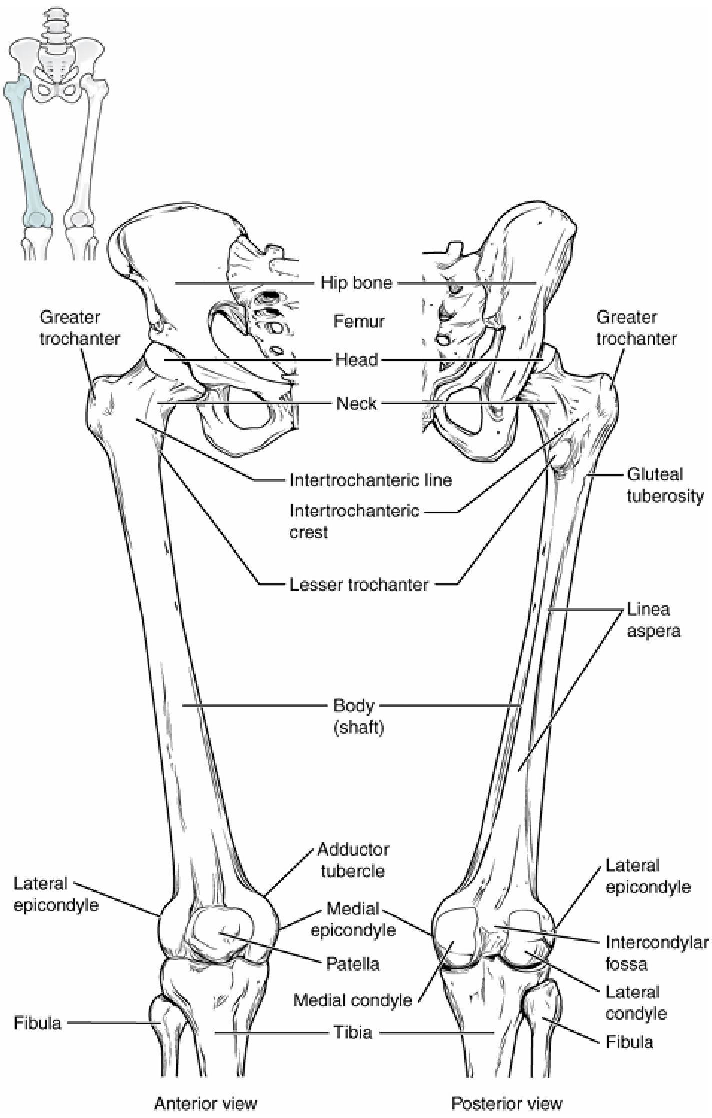

Figure 2.1: Main anatomical landmarks of the human femur. Adapted from OpenStax Anatomy and Physiology 2e [2].

The femoral shaft is not perfectly aligned with the vertical direction but exhibits a physiological inclination toward the body's midline. Consequently, the anatomical axis of the femur, defined as the line passing through the center of the diaphysis, differs from the mechanical axis of the lower limb. The mechanical axis is generally defined as the line connecting the center of the femoral head to the center of the knee joint and represents the principal direction of load transmission during standing and gait. The angle between these axes plays an important role in lower-limb biomechanics [2].

As shown in Figure 2.2, the medial inclination of the femur contributes to the formation of the quadriceps angle (Q-angle), a parameter commonly used to describe lower-limb alignment. The Q-angle reflects the oblique orientation of the femoral shaft relative to the overall alignment of the lower extremity.

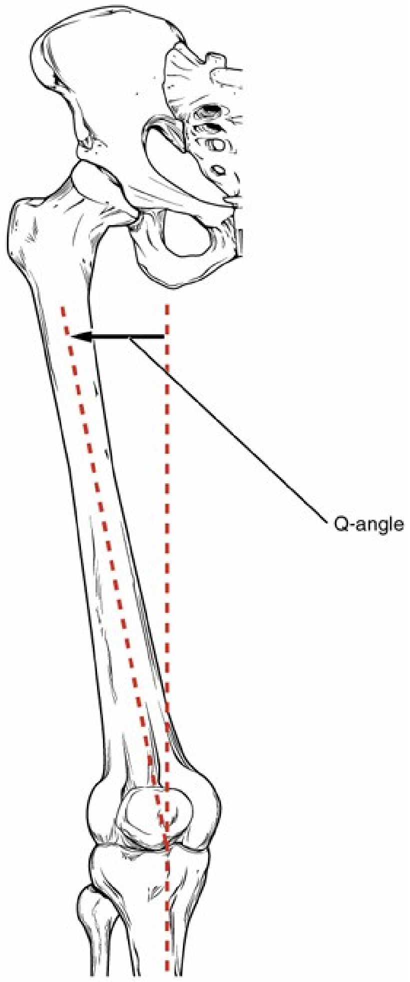

Figure 2.2: Schematic representation of the femoral anatomical axis and its inclination relative to the vertical direction. Adapted from OpenStax Anatomy and Physiology 2e [2].

2.1.2 Biomechanics of the proximal femur

The hip is a ball-and-socket synovial joint that provides six degrees of freedom, allowing flexion-extension, abduction-adduction, internal-external rotation, as well as limited translational motions. Its stability is primarily ensured by the congruent geometry between the femoral head and the acetabulum, together with the surrounding ligaments and muscles.

The proximal femur is subjected to complex loading conditions generated by body weight and muscle forces.

According to Wolff's law, the trabecular architecture of the proximal femur develops along principal compression and tension trajectories, reflecting the physiological loads transmitted through the hip joint. The geometry of the femoral neck, particularly the neck-shaft angle and femoral anteversion, plays a fundamental role in determining load transmission and muscle lever arms.

During double-leg stance, body weight is distributed approximately equally between the two lower limbs. In contrast, during single-leg stance, the body weight acts medial to the supporting hip, generating a moment that tends to tilt the pelvis toward the unsupported side. To maintain pelvic stability, the hip abductor muscles generate an opposing moment. The combined action of body weight and abductor muscles produces a resultant hip joint reaction force that is transmitted through the femoral head and neck. Experimental and analytical studies have shown that this reaction force may reach approximately three to six times body weight during normal gait, making the proximal femur one of the most highly loaded regions of the musculoskeletal system. These loading conditions are particularly relevant in biomechanical analyses of proximal femoral reconstructions and orthopedic implants. [3,4]

Figure 2.3 illustrates the biomechanical equilibrium of the hip during single-leg stance. The body weight (K) generates a moment around the supporting hip that tends to tilt the pelvis toward the contralateral side. This moment is counteracted by the force generated by the hip abductor muscles (M), mainly the gluteus medius and minimus. The combination of body weight and muscle forces produces the resultant hip joint reaction force (R), which is transmitted through the femoral head and proximal femur. Since the abductor lever arm is shorter than the body weight lever arm, muscle forces must be considerably larger than body weight, resulting in hip joint reaction forces that can reach several times body weight during gait. [3,4]

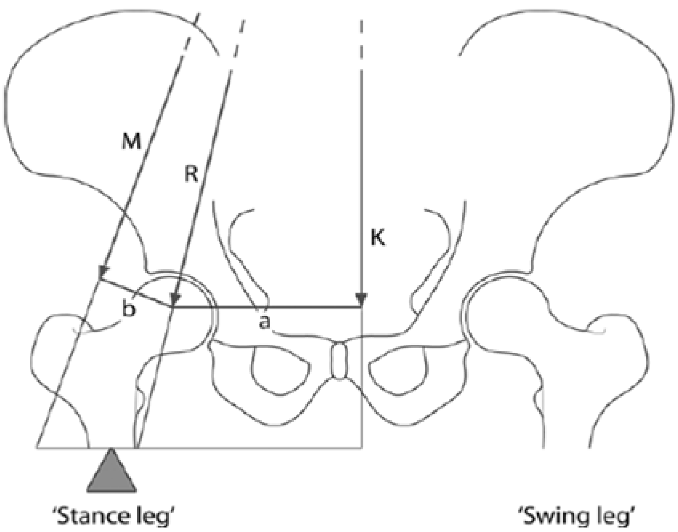

Figure 2.3: Biomechanical model of the hip during single-leg stance showing body weight (K), abductor muscle force (M), and hip joint reaction force (R). Adapted from [3].

2.2 Pediatric femur

Compared with the adult femur, the pediatric femur has several anatomical characteristics associated with ongoing skeletal growth and incomplete ossification. During childhood and adolescence, the femur consists of both ossified and cartilaginous regions that progressively mature through endochondral ossification.

The epiphyseal regions contain a greater proportion of trabecular bone than in the mature skeleton and are surrounded by relatively thin cortical shells. Furthermore, several anatomical structures, particularly within the proximal and distal epiphyses, are not completely ossified and therefore may be difficult to identify using conventional CT imaging [5,6].

Ossification of the femur begins during fetal development with the formation of a primary ossification center within the diaphysis, while multiple secondary ossification centers appear progressively after birth. These secondary centers develop in the distal femoral epiphysis, femoral head, and trochanteric regions, and gradually fuse with diaphysis throughout childhood and adolescence. Consequently, skeletal maturity is reached only during late adolescence, when the epiphyseal plates close and the secondary ossification centers become fully integrated with the femoral shaft [2].

One of the most distinctive anatomical features of the pediatric femur is the presence of the growth plates (physes). These cartilaginous structures are located between the epiphysis and metaphysis and remain active until skeletal maturity, providing the mechanism responsible for longitudinal bone growth [5,6].

The growth plate is composed of highly specialized cartilage tissue organized into different cellular zones, including the reserve zone, proliferative zone, and hypertrophic zone.

The reserve zone is located adjacent to the epiphysis and contains relatively few rounded chondrocytes embedded within an abundant extracellular matrix. These cells exhibit limited proliferative activity and are considered a reservoir of progenitor cells that contribute to the maintenance and organization of the growth plate.

The proliferative zone is characterized by flattened chondrocytes arranged in longitudinal columns parallel to the long axis of the bone. In this region, active cell division and extracellular matrix production occur, contributing directly to longitudinal bone growth. The columnar organization of chondrocytes defines the primary direction of femoral elongation during skeletal development.

The hypertrophic zone is located closest to the metaphysis and contains enlarged chondrocytes that cease proliferation and undergo terminal differentiation. These cells promote matrix mineralization and stimulate vascular invasion, ultimately leading to the replacement of cartilage by bone tissue through endochondral ossification. Because of its highly specialized structure, the hypertrophic zone represents the mechanically weakest region of the growth plate and is the area most susceptible to injury. [7]

During endochondral ossification, chondrocytes proliferate, enlarge, and are progressively replaced by mineralized bone tissue, allowing continuous elongation of the femur throughout childhood and adolescence.

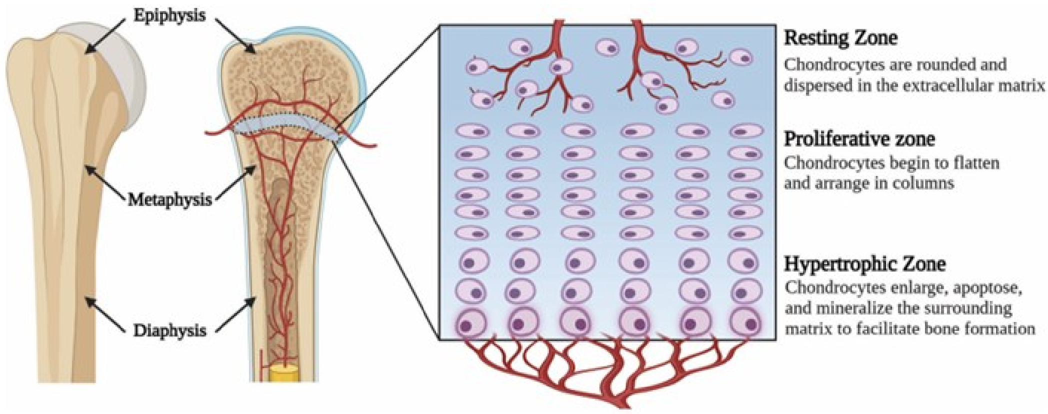

Figure 2.4: Histological and zonal structure of the growth plate [7].

From a biomechanical perspective, the growth plate represents a mechanically weaker and more deformable region than the surrounding bone due to its high-water content, cartilaginous composition, and lower degree of mineralization. Several studies have demonstrated that mechanical loading influences growth plate activity and may affect both growth rate and growth direction. Compressive hydrostatic stresses tend to inhibit growth, whereas shear stresses may stimulate endochondral ossification processes.

Experimental studies have shown that the growth plate exhibits anisotropic mechanical properties, being considerably more compliant along the longitudinal direction of bone growth than in the transverse directions.

Furthermore, mechanical properties vary among the different zones of the physis. The reserve zone has been reported to be the stiffest region, whereas the proliferative and hypertrophic zones exhibit lower elastic moduli and greater deformability. These characteristics contribute to the heterogeneous stress distribution within the growth plate and partly explain its susceptibility to growth disturbances and physeal injuries under abnormal loading conditions [7].

Because of their fundamental role in skeletal development, preservation of the growth plates is a major consideration during pediatric orthopedic surgery. Damage to these structures may alter normal growth patterns, potentially leading to deformities or limb-length discrepancies. Consequently, accurate geometric and mechanical representation of the growth plate is particularly important in biomechanical studies involving pediatric femoral reconstructions. [5,6]

Figure 2.5 shows the anatomical differences between an adult bone and a child's one, in the last one it's highlighted the presence of proximal and distal physis with a dot blue line.

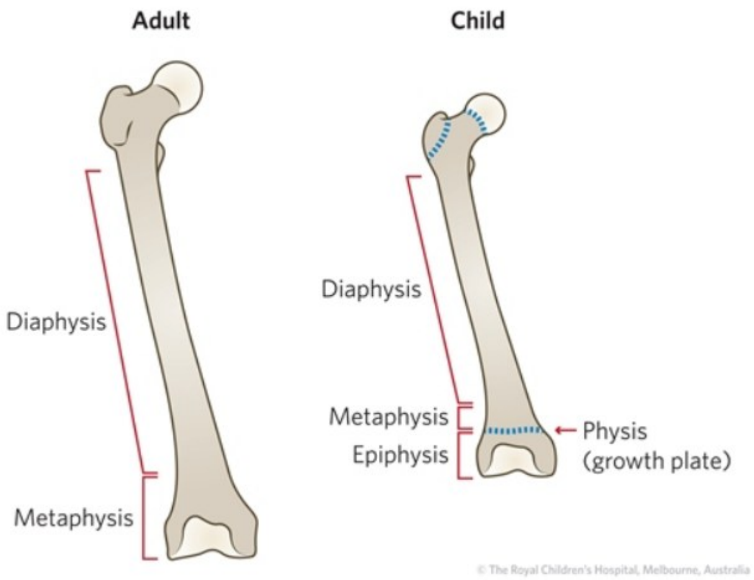

Figure 2.5: Anatomical differences between adult and child bones [8].

2.3 Pediatric Bone material's properties

2.3.1 Bone development during skeletal growth

Pediatric bone is a dynamic tissue undergoing continuous structural, compositional, and mechanical changes throughout growth. During skeletal development, cortical bone progressively evolves from a highly porous and immature structure into a denser and mechanically competent tissue able to withstand the increasing physiological loads.

Histological analyses of femoral immature bone sample [6] have shown that fetal and infantile cortical bone is characterized by a scaffold-like architecture with large porous channels and a substantial amount of osteoid, corresponding to a not yet mineralized bone matrix. As growth goes on, this immature structure is gradually replaced by a denser cortical organization composed mainly of mineralized tissue.

In subjects between 2 and 14 years of age, the bone volume fraction, that is the ration between the volume occupied by the bone tissue and the total volume of the sample analyzed, has been reported to increase by approximately 22% compared with fetal and infantile bone, while the osteoid volume decreases by nearly 90%, reflecting the progressive maturation of the skeletal tissue.

Significant modifications also occur in the organization of collagen fibers. Early pediatric bone is mainly composed of woven bone, characterized by a disorganized arrangement of collagen fibers.

With increasing age, bone remodeling progressively replaces woven bone with lamellar bone organized into secondary osteons. This transition results in a more ordered microstructure, with collagen fibers becoming preferentially aligned along the principal loading directions, thereby improving the mechanical efficiency of the tissue.

Bone mineralization also increases during growth. Quantitative analyses have shown that the average mineral content of cortical bone is approximately 10% higher in children aged 2–14 years compared with fetal and infantile specimens. At the same time, the distribution of mineral becomes more homogeneous, indicating a progressive reduction in tissue heterogeneity and a more uniform mechanical response. [6]

These structural and compositional changes are directly reflected in the mechanical properties of the tissue.

Experimental studies have demonstrated that the elastic modulus of cortical bone increases by approximately 160% between fetal/infantile stages and childhood, while ultimate tensile strength increases by approximately 83%.

Consequently, growing bone progressively acquires greater stiffness and strength, allowing it to withstand the increasing mechanical demands associated with body growth and daily activities.

Figure 2.6 summarizes the evolution of the mechanical response of cortical bone during skeletal growth. Samples from children aged 2–14 years have shown substantially higher elastic modulus and ultimate strength than fetal and infantile bone, reflecting the progressive maturation of the skeletal tissue. Conversely, failure strain tended to decrease with age, indicating a reduction in tissue deformability. [6]

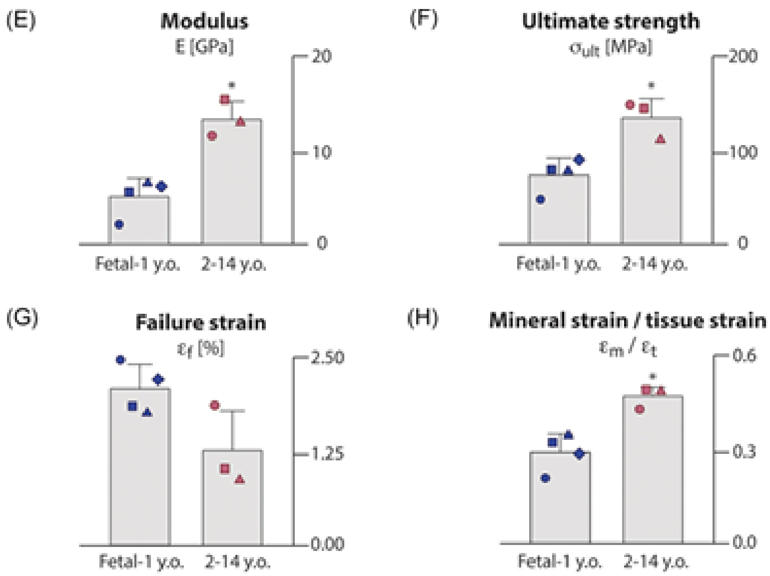

Figure 2.6: Comparison of selected mechanical properties of cortical bone between fetal/infantile specimens and children aged 2–14 years. (E) elastic modulus; (F) Ultimate strength; (G) Failure strain; (H) Mineral strain/tissue strain. Adapted from [6].

2.3.2 *Differences between pediatric and adult bone*

Bone tissue undergoes significant changes during growth and maturation, resulting in mechanical and structural differences between pediatric and adult bone. Compared with adult cortical bone, pediatric cortical bone shows lower mineralization and density, which directly affects its mechanical behavior.

Experimental studies performed on human cortical bone samples collected from children aged 4–15 years and adults aged 22–61 years demonstrated that pediatric bone presents a lower compressive Young's modulus (−34%), lower yield stress (−38%), lower ultimate compressive stress (−33%), and lower ash density (−17%) than adult bone. Conversely, pediatric bones showed a higher ultimate strain (+24%), indicating a greater capacity for deformation before failure as shown in Figure 2.10 [9].

These findings suggest that children's bones are generally less stiff and less strong than adult bones but exhibit greater ductility. This behavior is primarily related to the lower degree of mineralization observed during skeletal growth. Indeed, ash density, which reflects the mineral content of bone tissue, was found to be strongly correlated with both bone stiffness and strength, regardless of the age of the subject.

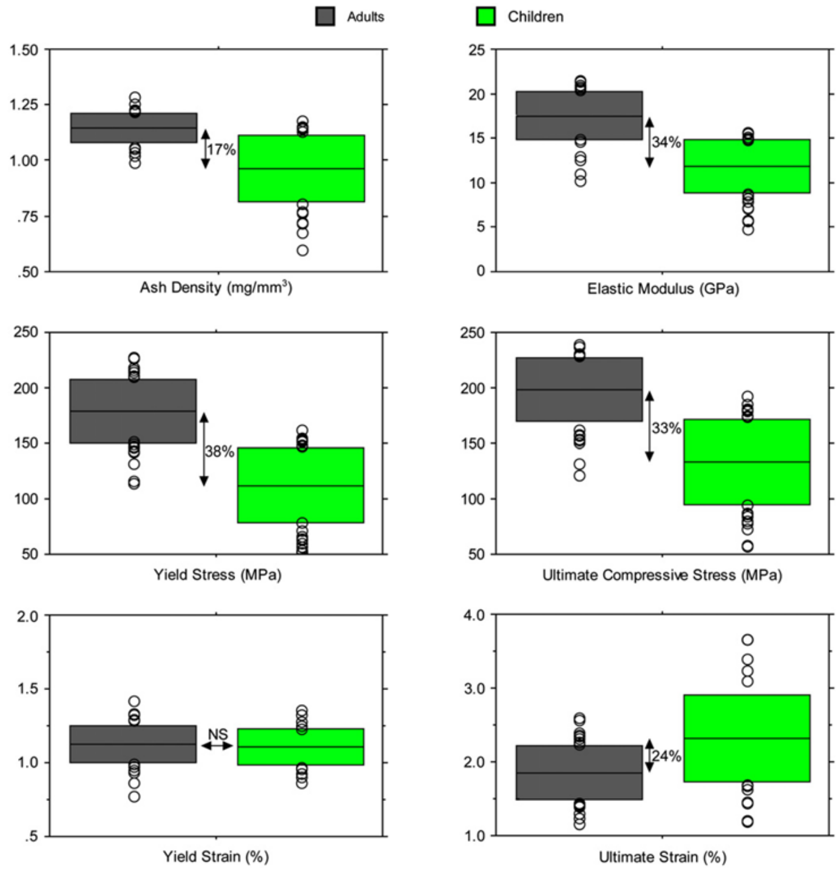

Figure 2.7: Comparison of the mechanical properties and ash density of pediatric and adult cortical bone, from [9].

From a clinical perspective, these characteristics explain why pediatric bone tends to deform more before fracture. Such differences must be considered when developing patient-specific finite element models, designing orthopedic implants, or planning reconstructive procedures in pediatric patients [9].

Although the studies presented above consistently highlight the differences between pediatric and adult bone, the mechanical properties reported for pediatric cortical and trabecular bone vary considerably throughout the literature. This variability is mainly related to differences in patient age, anatomical site, experimental protocol, and measurement technique.

To provide a comprehensive overview of the available data, the mechanical properties reported in the literature for pediatric cortical and trabecular bone were collected and summarized in Table 2. As will be discussed in the Materials and Methods section, the material properties adopted in the study were selected from the articles whose patient population most closely matched the age of the investigated subject, to ensure a physiologically representative description of the pediatric femur.

Table 1 Elastic modulus and Poisson's ratio values reported in the literature for pediatric cortical bone, trabecular bone, and growth plate cartilage and adopted in previous finite element studies.

Material	Elastic Modulus [MPa]	Poisson Coefficient	Reference
Cortical Bone	11800	0.29	[10]
	11200	0.3	[11]
	20000	0.3	[18]
Growth Plate	6	0.49	[18]
Trabecular Bone	2942	0.3	[18]
	15-325	0.2	[10]
	5.33	0.2	[11]

As shown in Table 2, a big variability exists among the material properties reported for pediatric tissues in the literature. This variability is particularly evident for trabecular bone, whose elastic modulus ranges from a few MPa to several GPa.

2.4 Pediatric Bone Tumor

Cancer represents the second leading cause of death among children aged 0–14 years in the United States. In 2023, nearly 10,000 children between 0 and 14 years of age and more than 5,000 adolescents aged 15–19 years were expected to be diagnosed with cancer [12].

Among pediatric malignancies, solid tumors account for approximately 40% of all cases and include several entities such as brain tumors, neuroblastoma, Wilms tumors, rhabdomyosarcoma, Ewing sarcoma and osteosarcoma [12]. Although these represent some of the most frequently diagnosed pediatric solid tumors, they are still classified as rare pediatric cancers [12].

The current treatment strategy for most pediatric solid tumors remains limited to surgical resection, radiation therapy, and chemotherapy. Even with recent advancements in therapeutic options, there has been limited improvement in survival for most pediatric cancers, including solid malignancies such as metastatic sarcomas.

Osteosarcoma and Edwing's sarcoma are the most common primary malignant bone tumors in children and adolescents and young adults. [12, 13,14]

2.4.1 Osteosarcoma

According to the literature, osteosarcoma (OS) is the most common primary malignant bone tumor [7,12,14].

It exhibits a bimodal age distribution, with the first and most prominent incidence peak occurring during adolescence and a second peak observed in adults over 60 years of age.

In children and adolescents, the incidence is approximately 3–4.5 cases per million individuals per year [12].

Epidemiological studies have shown that patients younger than 25 years account for approximately 56.8% of all osteosarcoma cases, highlighting the strong association between this disease and the growing skeleton.

The overall incidence in this age group is approximately 4.5 cases per million population, with a peak incidence observed during adolescence, reaching 7.6 cases per million between 10 and 14 years of age and 8.2 cases per million between 15 and 19 years of age. A slightly higher incidence has been reported in males compared with females.

The disease most frequently occurs during the second decade of life, coinciding with periods of rapid skeletal growth. [14]

The disease most commonly affects the metaphyseal regions of long bones, particularly the femur, tibia, fibula and humerus, which are characterized by rapid skeletal growth.

Radiologically, osteosarcoma typically appears as a lytic intramedullary lesion capable of destroying the surrounding cortical bone while extending into adjacent soft tissues.[12]

Clinically, patients often present persistent localized pain that may be last for several months before diagnosis. As the disease progresses, pain intensity typically increases and may be associated with swelling, tenderness, warmth, and alterations in gait caused by reduced weight-bearing on the affected limb.

Diagnosis is generally based on a combination of clinical examination, radiographic imaging and histological confirmation through biopsy. Radiographic findings may include characteristic bone destruction patterns, sclerosis, pathological fractures and periosteal reactions. [13]

Current treatment relies on a multimodal approach combining chemotherapy and surgical resection. The primary objective of surgery is to achieve complete tumor removal with adequate oncological margins while preserving as much healthy bone as possible. Advances in chemotherapy and limb-salvage techniques have significantly improved survival outcomes, with five-year survival rates approaching 70% for patients with localized diseases.

However, prognosis remains substantially poorer in the presence of metastases, with survival rates decreasing to below 40%. [12,14]

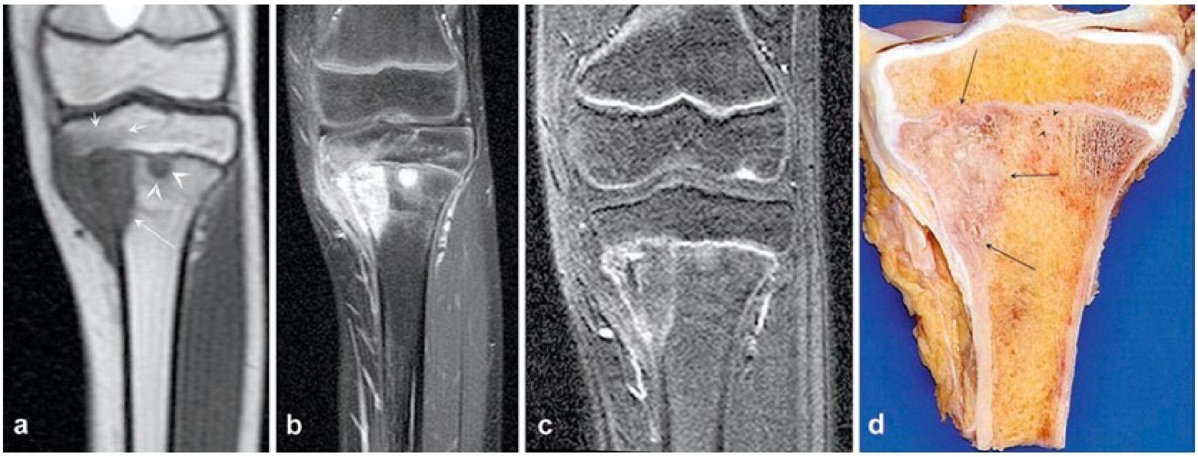

Figure 2.8: A 12-year-old boy with a tibial osteosarcoma in the left leg. a) Coronal T1-W MRI and b) coronal fat-saturated late contrast enhanced T1-W MRI display the metaphyseal tumour (long arrow) and a medial, small skip lesion (arrowheads). Epiphyseal signal abnormalities (small arrows) and late enhancement are also observed, but dynamic enhanced subtracted coronal view at 30 s (c) does not display any early enhancement within the epiphysis. d) Pathological analysis confirms involvement of metaphysis and growth plate, and normality of the epiphysis. [15]

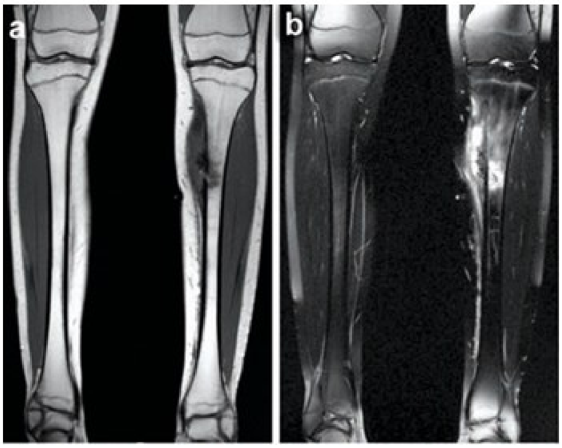

Figure 2.9: A 14-year-old girl with a tibial osteosarcoma in the left leg. MR views: a) coronal T1-W, b) coronal fat saturated T2-W. [15]

Figure 2.10: Preoperative radiographs showing osteosarcoma of the proximal femur. [17]

2.4.2 *Ewing's Sarcoma*

Ewing sarcoma (EwS) is a rare but highly aggressive malignant bone tumor primarily affecting children, adolescents, and young adults. The annual incidence in the United States is approximately one case per 1.5 million individuals. The tumor most commonly arises in the pelvis and in the proximal regions of long bones, including the femur and tibia.

Histologically, Ewing sarcoma is characterized by small round blue cells with prominent nuclei and limited stromal tissue.

Radiographically, Ewing sarcoma typically presents as an osteolytic lesion with a characteristic "moth-eaten" appearance, frequently associated with periosteal reactions such as the classical onion-skin pattern or Codman’s triangle.

Clinically, patients often present with localized pain, swelling, and functional impairment of the affected limb.

The introduction of multimodal treatment strategies combining chemotherapy and surgery has significantly improved outcomes for patients with localized disease, with overall survival rates currently reaching approximately 70–75%.

However, prognosis remains considerably poorer for patients presenting with metastatic disease at diagnosis, whose survival rate decreases to approximately 20–25%.

Consequently, complete surgical resection with adequate oncological margins remains a fundamental component of treatment, often requiring extensive bone removal and subsequent reconstructive procedures. [12]

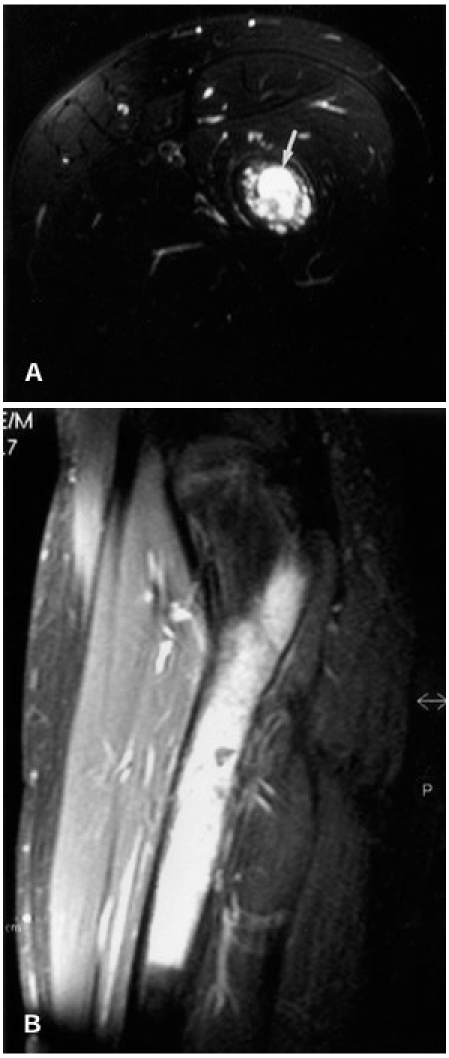

Figure 2.11: A 14-year-old boy with intraosseous Ewing's sarcoma of the proximal femur. (A) Axial T2-weighted MR image. (B) Sagittal contrast-enhanced T1-weighted MR image showing the extent of the tumor. Adapted from [16]

Figure 2.12: 8-year-old patient with an Ewing's sarcoma of the left proximal femur. Antero posterior and lateral x-rays. [19]

2.5 Proximal Femoral Replacement

Proximal Femoral Replacement (PFR) is an orthopedic reconstructive procedure involving the replacement of the proximal portion of the femur with a prosthetic implant. This surgical technique is commonly performed following extensive bone loss caused by primary bone tumors, metastatic lesions, severe trauma, or failed revision arthroplasties. In pediatric orthopedic oncology, PFR represents an important limb-salvage strategy following resection of malignant bone tumors affecting the proximal femur. This innovative approach has successfully decreased the need for amputation to less than 10% of cases.[20]

Although tumors in this anatomical region are less common than those occurring around the knee joint, reconstruction of the proximal femur presents unique clinical and biomechanical challenges. In particular, the amount of residual bone available after tumor resection strongly influences implant fixation, load transfer mechanisms, and the long-term durability of the reconstruction.[19]

Today, limb salvage surgery is considered the standard treatment for malignant tumors. After bone tumor resection, the use of a megaprosthesis is considered the most common method of reconstruction. This is true for adults and for fully grown patients; for growing patients, expandable prostheses can be a solution if the size of the bone segment permits the insertion of such a big device.

In very small patients, in whom a prosthesis cannot be used, other strategies must be applied. Indeed, children have different anatomies, so both resection and reconstruction are more difficult than in adults; moreover, modular prostheses are not commercially available in the required small sizes.

In fact, the main problems are related to bone growth, which could cause a precocious implant to mobilize due to the increasing bone diameter and, obviously, the leg length discrepancy [21].

Reconstructive strategies following proximal femoral resection can be generally divided into biological reconstructions and endoprosthetic reconstructions.

2.5.1 Biological Reconstruction

Biological reconstruction techniques, including autografts, allografts, and allograft–prosthetic composites, aim to restore skeletal defects using biological tissues.

Autografts consist of bone tissue taken from the patient, whereas allografts are obtained from human donors.

Among biological reconstruction techniques, APCs have emerged as a hybrid solution combining the biological advantages of allografts with the immediate mechanical stability provided by prosthetic components [21].

These reconstructions are particularly attractive in pediatric patients, where preservation of bone stock is essential for future revision procedures and long-term skeletal development [21,22].

In addition to restoring skeletal continuity, APCs may promote biological integration due to the higher biological activity of the pediatric bone tissue with respect to the adult's one, the APCs also facilitate soft-tissue reattachment, and allow a more physiological load transfer between the implant and the host bone once graft union has been achieved.

In very young patients, conventional modular or expandable prostheses may not be suitable because of the limited dimensions of the residual bone and the ongoing growth of the skeleton.

Furthermore, long intramedullary stems may increase the risk of stress shielding by transferring a greater proportion of the mechanical load directly to the femoral shaft, potentially reducing physiological loading of the surrounding immature bone.

For these reasons, APC reconstructions have been proposed as an alternative strategy in selected pediatric cases [21,22].

A notable example was reported by Zoccali et al. [21], who described a proximal femoral reconstruction in an infant patient affected by Ewing's sarcoma, as shown in Figure 2.7.

The reconstruction consisted of a femoral stem cemented into a humeral allograft and stabilized using a carbon-fiber plate.

An adult humerus is of the right size to replace a child's lower limb segments, and the distal humerus can be shaped, maintaining a cortex stiff enough to support a prosthesis. At one-year follow-up, the patient was disease-free and able to walk with only a slight limp [21].

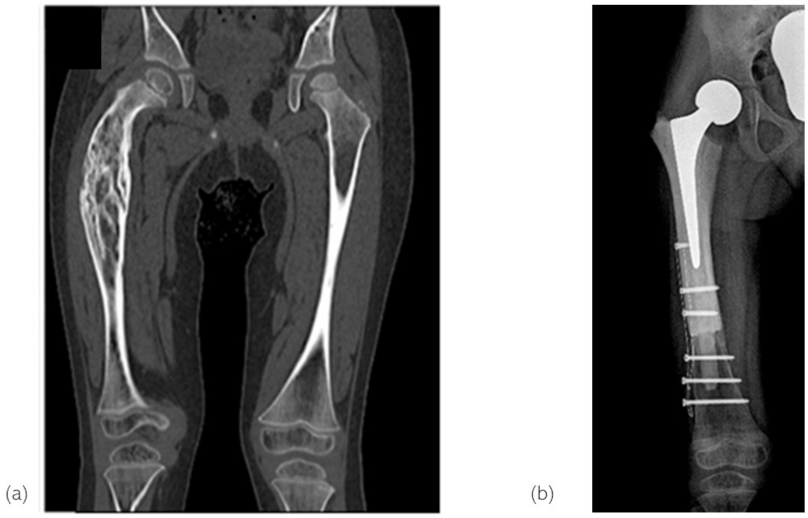

Figure 2.13: Biological reconstruction using an allograft–prosthetic composite following PFR in a pediatric patient. (a) Pre-operative CT scan. (b) Post-operative radiograph showing the reconstructed femur. Adapted from [21].

Further evidence supporting the use of APCs in pediatric patients was provided by Campanacci et al. [22], who reported the results of 10 skeletally immature patients treated with PFR and reconstruction using a short-stem allograft–prosthesis composite. The authors highlighted the potential advantages of APCs in preserving proximal femoral bone stock, facilitating biological tendon reattachment, and avoiding the use of long intramedullary stems in immature bone.

However, the study also demonstrated the limitations of this approach, reporting complications such as non-union, graft fracture, graft resorption, and limb-length discrepancy. Three patients ultimately required removal of the APC, with some reconstructions being substituted by modular endoprosthetic replacements.

These findings suggest that, although APCs represent a valuable biological reconstructive option in selected pediatric patients, they remain associated with several limitations, especially in the long-term.[22]

Osteointegration is generally restricted to the graft–host junction, making the reconstruction susceptible to graft resorption and non-union.

Furthermore, graft fracture represents one of the most common complications and frequently requires revision surgery.

The prolonged immobilization often required to protect the reconstruction may also complicate postoperative rehabilitation, particularly in very young patients.

Consequently, although APCs may provide a valuable reconstructive option when conventional prosthetic solutions cannot be implanted, their long-term durability and clinical outcomes remain less predictable than those of endoprosthetic reconstructions. For this reason, their use is generally limited to selected clinical scenarios in which preservation of bone stock and future reconstructive options are considered major priorities [21].

2.5.2 *Endoprosthetic reconstruction*

Endoprosthetic reconstruction can be achieved using either expandable or modular megaprosthetic systems.

2.5.2.1 Expandable prostheses

Expandable prostheses were developed to address one of the major challenges of limb-salvage surgery in skeletally immature patients: the limb-length discrepancy that is a consequence of the resection of active growth plates.

Following tumor resection, the contralateral limb continues its growth and this, may lead to significant differences in limb length at skeletal maturity. To overcome the problem, the expandable prosthetic systems were introduced, allowing progressive lengthening of the reconstruction during childhood and adolescence [24].

Over time, expandable prostheses evolved from first-generation devices requiring open surgical procedures for each lengthening, to second-generation minimally invasive systems, and finally to modern non-invasive designs that can be lengthened through external electromagnetic or magnetic mechanisms [23,24].

An example of this type of technology is the MUTARS® Xpand prosthesis, designed by the German company Implantcast GmbH.

All the components of the prosthesis are customized for each individual patient.

The elongation of the MUTARS® Xpand Prosthesis is performed via wireless energy transmission.

An electric motor (and receiver), called TAM, is built into the prosthesis which is controlled by an extracor poreal control unit (and electromagnetic energy transmitter) [25].

Figure 2.14 shows the components of the MUTARS® Xpand Prosthesis for proximal femur replacement.

Figure 2.14: MUTARS® Xpand Prosthesis for proximal femur replacement. [25]

Lengthening itself is done non-surgically in 0.035mm steps without the risk of vascular injury or nerve injury.

However, since the prosthesis is intended for use in children, it's so much slim as hence the mechanical load carrying capacity is, quite naturally, limited, for hip prosthesis so full weight bearing is possible for patients of up to 40 kg. For patients heavier than 40 kg partial weight bearing (via the use of crutches for example) is recommended for as long as the motor is in-situ. Also, high levels of physical activity can negatively influence the longevity of the prostheses. [25]

Although these implants can effectively reduce limb-length discrepancy and preserve limb function, they have high complication rates for what regard infection, aseptic loosening, mechanical failure, soft-tissue contractures, and the need for multiple revision procedures. Consequently, despite continuous technological improvements, expandable prostheses are generally reserved for selected pediatric patients with substantial remaining growth potential [23].

2.5.2.2 Modular megaprosthesis

Among the available reconstruction strategies, modular megaprostheses have become one of the most widely adopted solutions for extensive oncological resections.

Their popularity is mainly related to the possibility of achieving immediate mechanical stability, early postoperative mobilization, and intraoperative adaptability to different anatomical and surgical requirements.

The modular design allows reconstruction length and implant geometry to be adjusted according to the extent of bone resection while maintaining satisfactory functional outcomes.

Unlike biological reconstruction techniques, which rely on graft incorporation and healing processes, megaprosthetic reconstruction allows early mobilization and weight bearing, facilitating postoperative rehabilitation and improving patient quality of life.

For this reason, modular megaprostheses have become a standard option for the management of large skeletal defects resulting from primary bone tumors, metastatic disease, aggressive benign lesions, and complex revision procedures [26].

Several modular systems have been developed over the past decades. One of the early examples was the Howmedica Modular Resection System (HMRS), which allowed reconstruction of the proximal femur following tumor resection using modular components assembled according to the length of the resected segment. Clinical studies demonstrate satisfactory functional outcomes and long-term limb preservation, although complications such as hip instability, infection, and aseptic loosening remained important challenges [17].

Despite their clinical success, modular megaprostheses are not free from complications. Mechanical failures, aseptic loosening, prosthetic instability, infection, and soft-tissue deficiencies remain the most frequently reported causes of revision surgery.

In proximal femoral reconstructions, hip dislocation represents a particularly relevant complication because tumor resection often requires removal of the abductor musculature and surrounding soft tissues that contribute to joint stability [17].

The LINK Megasystem-C represents one of the most versatile modular megaprosthetic platforms. The system includes a wide range of interchangeable components that can be combined to reconstruct different anatomical regions of the lower limb, it will be further discussed in the next section.

Examples of proximal femoral reconstructions performed using modular megaprosthetic systems are shown in Figures 2.15 and 2.16.

Figure 2.15 shows a reconstruction performed with the LINK Megasystem-C system, while Figure 2.16 shows its clinical application in a pediatric patient affected by Ewing's sarcoma of the proximal femur.

Figure 2.15: Post-operative radiograph of a proximal femoral replacement performed using the LINK Megasystem-C modular megaprosthesis. Adapted from Salvini et al. [20].

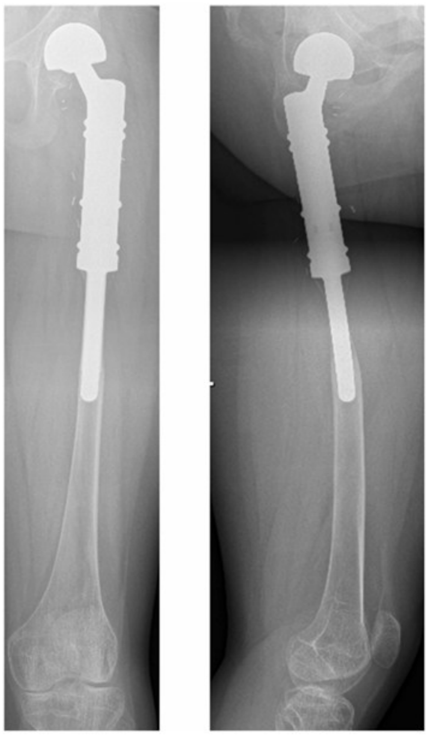

Figure 2.16: 11-years year-old patient affected by Edwing's sarcoma of the left proximal femur with a modular mega prosthesis inserted [19].

2.5.3 LINK Megasystem-C

The megaprosthesis used in the present study is the Megasystem-C Tumor and Revision System designed by LINK Orthopaedics, one of the leader manufacturers of orthopedic devices in the word with its base in Hamburg, Germany.

The modular oncological prosthetic system was designed for complex limb reconstruction procedures following tumor resections or severe bone loss conditions requiring large skeletal replacements.

Figure 2.17 shows the different configurations of Megasystem-C, from left to right there are:

distal femoral replacement with tibial components, proximal tibial replacement with femoral components, total femoral replacement with tibial components, the interport system that is an intercalary modular prosthesis designed for the reconstruction of diaphyseal bone defects while preserving both the adjacent joints, and lastly the proximal femoral replacement.

Figure 2.17: different configurations of the Megasystem-C [27].

A key feature of the LINK Megasystem-C is its modularity.

Many components are not specific to a single reconstruction type but can be used across different configurations.

For example, femoral heads, modular stems, coupling elements, and segmental bodies may be combined in various ways to create proximal femoral, distal femoral, total femoral, or intercalary reconstructions.

This interchangeable design allows a high degree of customization while reducing the number of implant-specific components required.

In the present thesis a proximal femoral replacement has been used for the study.

The assembly of the PFR is shown in Figure 2.18 and it consists of:

- an intramedullary stem that could be cemented or cementless and with different lengths;
- a neck segment that could have different lengths;
- a coupling component;
- a prosthetic head of different sizes;
- a support ring or stem segment.

Figure 2.18: assembly of the Megasystem-C used for proximal femoral replacement [27].

The surgical procedure for proximal femoral reconstruction begins with the resection of the proximal femur at the preoperatively planned level.

After removal of the diseased bone segment, the medullary canal of the remaining femur is prepared to accommodate the prosthetic stem. The preparation of the medullary cavity is performed using progressively sized awls. Depending on the selected implant configuration, stems with lengths of 100 mm, 130 mm, or 160 mm may be used.

In the case of cementless modular stems, the canal is reamed progressively until cortical contact is achieved over approximately 50 mm, ensuring adequate primary stability through press-fit fixation [27].

The final implant diameter must correspond to the last awl used during preparation.

For cemented stems, the medullary canal is prepared slightly larger, generally at least 2 mm wider than the stem diameter, to leave the space for the cement layer around the implant. Subsequently, a dedicated reamer is used to flatten the resection surface, creating a stable and uniform interface between the bone and the extramedullary component of the prosthesis.

After bone preparation, trial prosthetic components are assembled and inserted into the prepared femur. These trial implants allow the surgeon to evaluate leg length, rotational alignment, joint stability, and range of motion through flexion, extension, and rotational movements of the limb.

When necessary, the metaphyseal region is further prepared using a special hollow reamer to create the implant bed for the neck segment.

The selected neck component is then attached to the stem, and the desired anteversion angle is adjusted before temporary fixation with a trial screw.

Proper anteversion is essential to restore physiological hip biomechanics and reduce the risk of postoperative instability or dislocation.

Once the optimal configuration has been identified with the trial components, the definitive implant is assembled.

The coupling component for proximal femoral replacement is connected to the stem, followed by attachment of the prosthetic neck and femoral head.

The implant is then definitively fixed either through cemented fixation or through press-fit fixation.

From a biomechanical standpoint, proximal femoral replacement represents a demanding reconstruction because the implant must withstand significant compressive, bending, and torsional loads generated during daily activities such as standing and walking.

The modular design of the Megasystem-C system allows restoration of limb length and joint alignment while ensuring adequate mechanical stability and adaptability to patient-specific anatomical conditions [27].

2.6 Influence of prosthetic design parameters

Complications associated with proximal femoral megaprostheses include implant loosening, mechanical failure, bone resorption and hip instability. Many of these complications are closely related to the biomechanical interaction between the implant and the residual bone. Consequently, understanding how factors such as resection level and stem length influence stress distribution within the remaining femur is essential for optimizing implant design.

2.6.1 *Effect of resection level*

The level of bone resection represents one of the most critical parameters in proximal femoral oncological reconstruction, particularly in pediatric patients. Following tumor excision, the amount of residual bone directly influences implant fixation, load transfer mechanisms, mechanical stability and long-term preservation of the remaining femur.

In limb-salvage surgery, surgeons must achieve adequate oncological margins while simultaneously preserving as much healthy bone as possible to maintain favorable biomechanical conditions after reconstruction.

The residual bone must withstand the mechanical demands of the reconstruction and the ongoing physiological processes associated with growth and remodeling.

Excessive bone removal may compromise future revision possibilities, reduce cortical support available for fixation and increase the risk of long-term mechanical complications.

A crucial aspect associated with the resection level is the precision of the osteotomy plane. Resections performed close to the joint are technically demanding because they require accurate identification of tumor margins while simultaneously preserving the maximum amount of healthy bone tissue [22].

For this reason, image-based planning and computer-assisted surgical techniques have progressively gained importance in orthopedic oncology [22].

Depending on tumor extension and anatomical involvement, proximal femoral resections may be classified as metaphyseal, meta-diaphyseal or extended diaphyseal resections [28].

Figure 2.19 shows the classification proposed by Streitbürger et al. [28] relating the anatomical location of the osteotomy to the corresponding resection length.

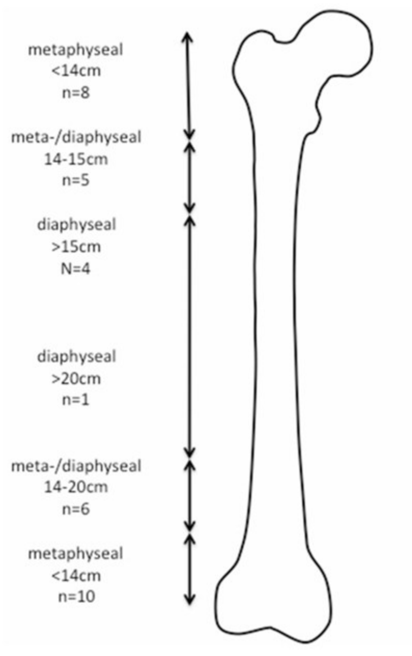

Figure 2.19: Classification of femoral resection levels according to the anatomical region involved and the corresponding resection length ranges [28].

Reported femoral resection lengths in oncological reconstruction vary considerably according to patient age, tumor location and surgical strategy, ranging between approximately 12 and 19 cm.

Table 1 summarizes the average resection lengths reported in the literature for both pediatric and adult patients, demonstrating how large bone resections are frequently required in oncological reconstruction procedures.

From a biomechanical point of view, resection level directly influences the mechanical behavior of the reconstructed femur.

Experimental and numerical studies have demonstrated that different osteotomy levels can significantly modify strain and stress distributions within the residual bone after implantation. More extensive resections were associated with greater deviations from physiological loading conditions and increased stress concentrations near the bone–implant interface [8,30].

Conversely, preservation of a larger amount of residual bone promoted a more physiological transfer of loads and reduced stress shielding effects [29,30].

These findings suggest that even relatively small variations in resection length may substantially affect the biomechanical environment of the reconstructed femur.

For these reasons, the present thesis investigates multiple proximal femoral resection configurations to evaluate how progressive bone loss affects stress distribution within the remaining pediatric femur with the modular LINK Megasystem-C system.

Table 2 Resection level range found in the literature: PP stands for pediatric patients, AP stands for adult patients, PFR stands for proximal femoral resection and DFR stands for distal femoral resection.

Mean Resection length	Patient Group	Location	References
15 cm (range: 6 – 29 cm)	PP	PFR	[22]
18.6 cm (range: 10 - 30 cm)	AP	PFR	[31]
17.6 cm (range: 8 – 32 cm)	PP	PFR	[19]
12.3 cm (± 1.6 cm)	AP	PFR	[20]
18.5 cm (range: 10 – 29 cm)	AP	DFR and PFR	[28]

2.6.2 *Role of stem length*

Stem length plays a fundamental role in determining the biomechanical behavior of femoral prosthetic reconstructions. In oncological surgery, especially after proximal femoral resection, the intramedullary stem is responsible for transferring loads from the prosthesis to the remaining bone. Consequently, variations in stem length can significantly influence stress distribution, implant stability and preservation of residual bone stock.

Several biomechanical studies have investigated the influence of stem length on load transfer within the femur. Li et al. [32] combined finite element analysis and biomechanical experiments to evaluate different cemented stem lengths.

Their results demonstrated that reducing stem length increased Von Mises stress within the proximal femur and promoted a more physiological load transfer, whereas longer stems transferred a greater proportion of the load distally along the femoral shaft. The authors concluded that stem shortening may reduce stress shielding while maintaining adequate mechanical stability [32].

However, reducing stem length may also decrease the initial mechanical stability of the implant, particularly in cases characterized by limited residual bone support. This aspect becomes especially critical in oncological reconstructions involving short proximal femoral segments, where the remaining bone often presents reduced cortical support and higher portion of trabecular bone [33].

Recent finite element studies investigating different stem configurations highlighted the importance of optimizing load transfer within the residual femur. Improved fixation strategies and optimized stem geometries were shown to reduce stress concentration at the bone–implant interface and promote a more homogeneous stress distribution within the cortical bone [33].

Arno et al. compared stemless, ultra-short and short cementless femoral implants and demonstrated that increasing stem length progressively reduced proximal femoral strain while increasing distal strain transmission.

The stemless and ultra-short designs showed strain distributions closer to those of the intact femur, suggesting a more physiological load transfer and a reduced stress shielding effect [38].

In pediatric oncological reconstructions, selecting an appropriate stem length becomes essential to achieve a balance between implant stability and reduction of stress shielding effects.

Based on these considerations, the present work investigates the biomechanical influence of different stem lengths combined with different proximal femoral resection levels, with the aim of evaluating how these parameters affect stress distribution within the residual femur and the overall mechanical behavior of the reconstructed bone–implant system.

2.7 Finite Element Analysis in orthopedic biomechanics

2.7.1 Principles of FEM

Finite Element Analysis (FEA), also called the finite element method (FEM), is a method for numerical solutions of field problems. A field problem requires the determination of spatial distribution of one or more dependent variables; this is described by differential equations or by an integral equation.

Finite element formulations, in ready-to-use form, are implemented in FEA programs, such as Abaqus or Ansys.

In finite element analysis, a complex structure is discretized into many small, interconnected regions known as finite elements.

Unlike infinitesimal elements used in analytical calculations, each finite element represents a limited portion of the geometry within which the variation of the field variable is approximated using simple mathematical functions, typically polynomial expressions. Although the actual physical behavior within the structure may be more complex, this approximation enables the numerical solution of engineering problems with acceptable accuracy.

The individual elements are connected through points called nodes, which constitute the fundamental locations where the unknown variables are calculated.

The collection of all elements and nodes forms the finite element mesh, which provides a numerical representation of the physical domain under investigation.

By solving the governing equations at the nodal locations, the values of the field variables can be determined throughout the entire structure.

Associated with each node is a set of degrees of freedom (DOFs), which represent the independent variables that can vary at that node.

In structural analyses, these DOFs typically correspond to translational displacements and, depending on the element formulation, rotational displacements.

The finite element solver calculates the values of the nodal DOFs, and the resulting displacement field is used to derive strains and stresses of the structure.

The accuracy of the solution depends on the quality and density of the mesh.

In general, higher is the number of elements better, the representation of the geometry and so the accuracy of the results, but also the computational effort increases.

The finite element workflow consists of three fundamental stages: problem classification, modeling, and discretization.

During the classification stage, the physical problem is identified and characterized according to the governing phenomena and analysis objectives.

In this stage the nature of the problem is identified, so for example whether it is time-dependent or not, in stress analysis the problem will be classified in static or dynamic.

Subsequently, in the modelling stage, the physical problem is transformed into a mathematical model suitable for numerical analysis.

Starting from the geometric representation of the structure, the analyst defines material properties, loading conditions, and boundary conditions while introducing appropriate simplifications.

Since finite element analysis solves the mathematical model rather than the real physical system, the accuracy of the results strongly depends on the assumptions adopted during this stage.

Consequently, decisions regarding which geometric features, material characteristics, and loading conditions are considered relevant may significantly influence the outcome of the simulation.

Finally, the model is discretized into a mesh of finite number of elements and nodes, used for the numerical solution.

Obviously, discretization introduces another approximation.

So, it's possible to talk about "modelling error" and "discretization error", the first one can be reduced by improving the model, the second one improving the number of elements.

In addition, as a computer does arithmetic, it introduces numerical errors.

The final stage is known as post-processing, during which the numerical results are visualized and interpreted.

Typical outputs in structural analyses include displacement fields, stress distributions and reaction forces.

These results are commonly displayed using graphical contour plots that facilitate the identification of critical regions within the structure.

Before drawing conclusions from the simulation, the results must be critically evaluated. The analyst should verify that the obtained values are physically meaningful and consistent with the expected behavior of the system.

This validation step is essential to identify modelling errors, inappropriate boundary conditions, or numerical inaccuracies that can compromise the reliability of the analysis. [34]

The overall finite element procedure, including model development, discretization, numerical solution, post-processing, and result validation, is summarized in Figure 2.20.

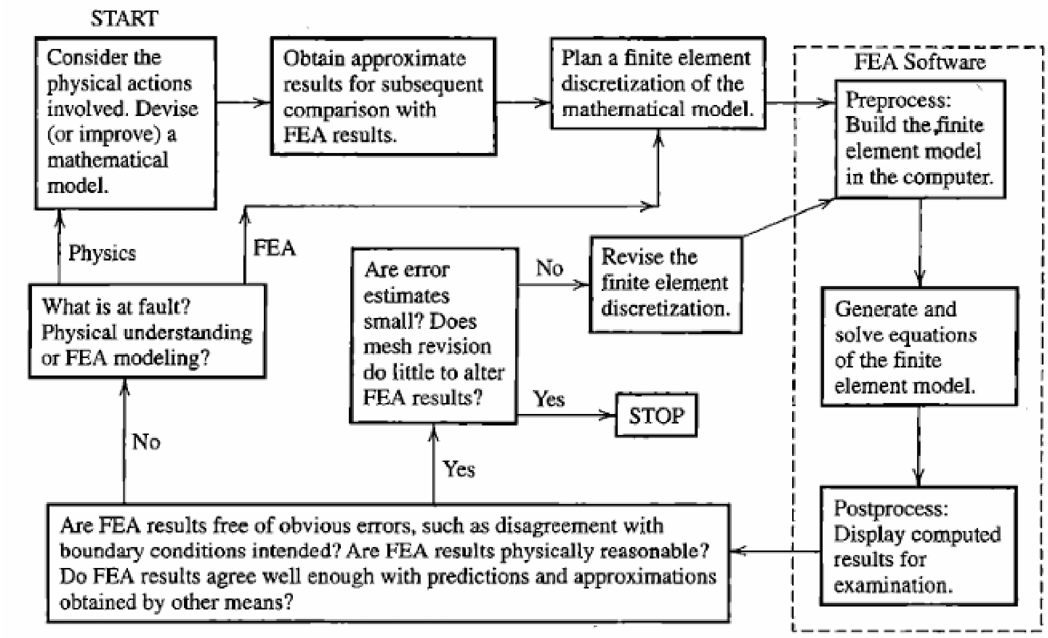

Figure 2.20: General workflow of the finite element analysis procedure, from Cook et al. [34].

2.7.2 *Application to bone structures*

FEA has become one of the most widely used computational tools in orthopedic biomechanics for investigating the mechanical behavior of bones, implants and prosthetic devices before clinical application, reducing both experimental costs and ethical concerns associated with in vivo investigations [35,36].

The first applications of the finite element method in orthopedics date back to the early 1970s, right after the introduction of modern hip and knee replacements.

During the 1970s and 1980s, finite element models were relatively simple and often limited to two-dimensional representations due to computational constraints. Nevertheless, they provided valuable insights into stress distribution and load transfer around orthopedic implants, helping researchers understand the causes of implant failure and loosening.

Then, the advances in medical imaging, computer hardware and numerical methods enabled the development of highly detailed three-dimensional patient-specific models. The number of elements that could be included in a simulation increased from a few hundred in early studies to hundreds of thousands or even millions in modern analyses. These improvements allowed researchers to design realistic anatomical geometries, anisotropic bone properties derived from CT scans and complex loading conditions that represent daily activities [35].

The development of a finite element model in biomechanics usually follows a structured workflow.

The process begins with the acquisition of patient-specific anatomical data through computed tomography (CT) or magnetic resonance imaging (MRI).

These images are subsequently segmented to reconstruct a three-dimensional representation of the bone. The implant geometry, usually obtained from CAD models provided by the manufacturer, is then virtually aligned with the reconstructed anatomy. After the assignment of the material properties, the boundary conditions and the physiological loading scenarios are defined. Finally, the problem can be discretized, and the numerical simulations are performed to evaluate stresses, strains, displacements, and other biomechanical parameters of interest. [36]

Today, FEA is employed throughout the design and evaluation process of orthopedic devices. Beyond the assessment of the initial mechanical behavior of implants, modern finite element models can simulate long-term phenomena such as bone remodeling, osseointegration, wear, damage accumulation and implant loosening.

Despite these advances, finite element modelling remains dependent on the accuracy of the model.

Nevertheless, it is now considered an essential tool for pre-clinical assessment, optimization and validation of orthopedic implants, reducing development costs and facilitating the evaluation of multiple design configurations before experimental testing of physical prototypes [35,36].

Despite the widespread use of FEA in orthopedic biomechanics, its application to pediatric musculoskeletal structures remains relatively limited. The limited research available in this area can be attributed to the technical and methodological challenges associated with creating accurate and reliable FEA models of pediatric hip joints. The complex anatomy and dynamic growth patterns of pediatric hips pose unique challenges in accurately representing geometry and material properties in finite element models. Additionally, acquiring subject-specific data for children, including CT or MRI scans, is often more difficult than in adults. These technical limits may have discouraged researchers from investigating this specific population. Nonetheless, the lack of research highlights the importance of conducting further studies to improve the understanding of pediatric biomechanics and support the development of optimized treatment strategies [21,23].

In orthopedic oncology, patient-specific data may become available during tumor resection procedures. To reduce the risk of local recurrence, the resected bone segment is typically larger than the actual tumor extension, providing the opportunity to obtain cortical bone samples from regions not affected by the disease. These specimens may contribute to a better characterization of the mechanical properties of pediatric bone and support the development of more accurate finite element models [23].

3 Method

3.1 Geometry acquisition

3.1.1 Segmentation

The study subject was a 14-year-old pediatric patient of the Meyer Hospital of Florence, Italy, affected by bone tumor. The CT scan images were obtained from the surgeon for subsequent analysis and can be observed in Figure 3.1.

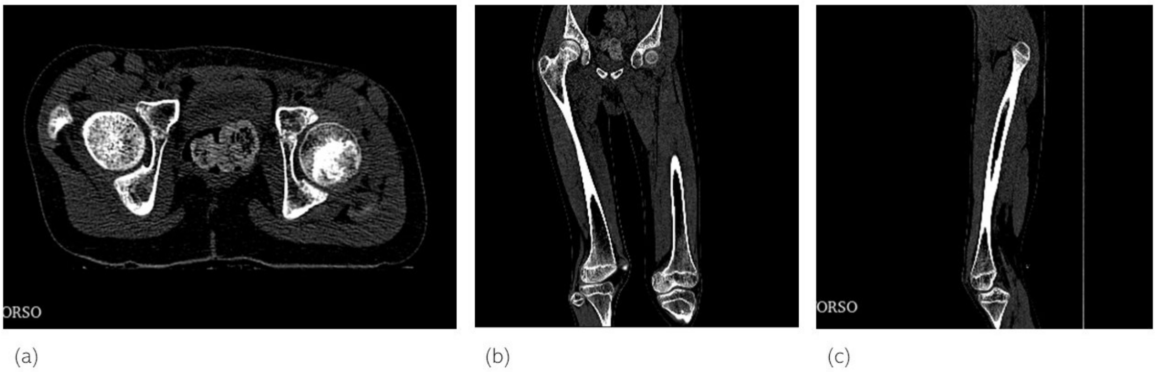

Figure 3.1: CT scan of the patient respectively in the :(a) axial view, (b) coronal view, (c) sagittal view.

The reconstruction of the femoral anatomical structures was carried out using 3D Slicer, an open-source software commonly employed for medical image processing and three-dimensional anatomical modelling. The segmentation task was divided into three main anatomical structures: I. Diaphysis II. Growth plates III. Epiphyses.

The proximal epiphysis was not segmented as an independent anatomical structure, and no detailed reconstruction of the proximal growth plate was performed, since this region was subsequently removed during the surgical resection required for prosthetic implantation. Consequently, the segmentation process in the proximal femoral region was limited to tracing the external boundaries of the femoral head, which was therefore incorporated directly into the diaphyseal geometry. The distal epiphysis and the distal growth plate were segmented as a separate anatomical structure to preserve the geometrical and biomechanical characteristics of the pediatric femur.

The cortical bone was identified through a threshold-based segmentation approach using Hounsfield Unit (HU) values. Specifically, a lower threshold of 100 HU and an upper threshold of 2428 HU were selected to isolate the denser cortical tissue while excluding surrounding soft tissues and most of the trabecular bone. After the automatic segmentation process, manual corrections were performed on individual CT slices to refine the geometry and improve the continuity of the reconstructed structure (Figure 3.2). Lower HU's values were set for the identification of the trabecular bone. In pediatric femurs, the distal epiphysis is predominantly composed of trabecular bone surrounded by a very thin cortical shell. Due to the limited thickness of the cortical layer, the distal epiphysis was modelled as a homogeneous trabecular region in the present study (Figure 3.3).

Due to its cartilaginous composition, the growth plate could not be accurately detected using automatic thresholding techniques. Consequently, its segmentation was performed entirely manually by tracing the structure slice-by-slice according to the anatomical information visible within the CT images (Figure 3.4). This approach was necessary because non-mineralized cartilage presents very limited contrast in standard CT acquisitions. Compared to adult femoral anatomy, pediatric femur segmentation introduces several additional difficulties. The presence of unossified cartilaginous regions requires extensive manual intervention, while the smaller dimensions of the pediatric structures demand careful adjustment of segmentation and post-processing parameters. Moreover, the lower contrast between cortical and trabecular bone regions makes the identification of the different tissues more challenging, requiring particular attention to maintain anatomical fidelity throughout the reconstruction process. The total segmentation can be observed in Figure 3.5.

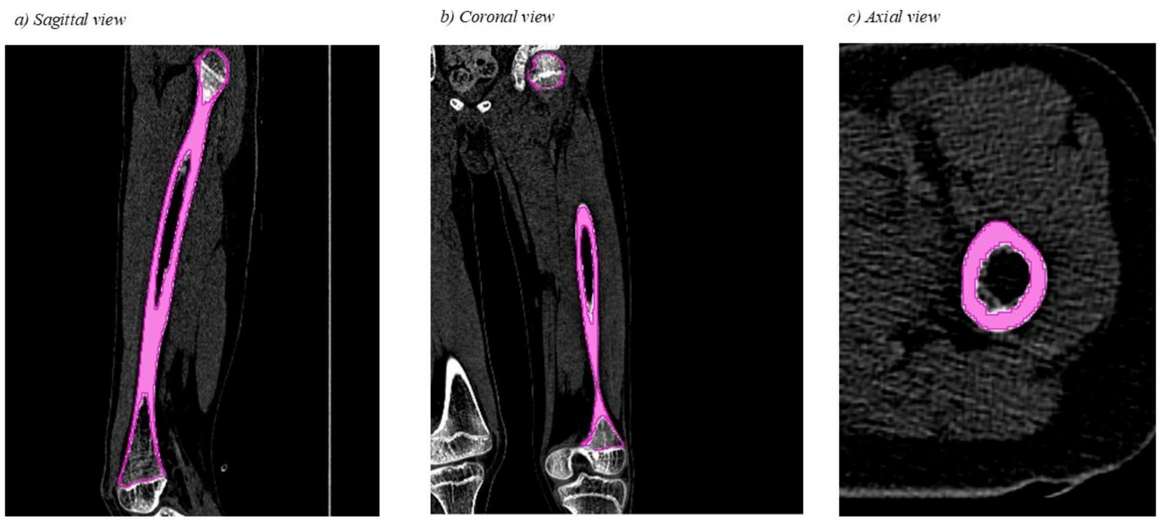

Figure 3.2: Cortical bone (violet) segmentation of the diaphysis and femoral head in the: (a) sagittal view, (b) coronal view, (c) axial view.

Figure 3.3: Segmentation of the distal epiphysis (blue) in the: (a) sagittal view, (b) coronal view, (c) axial view.

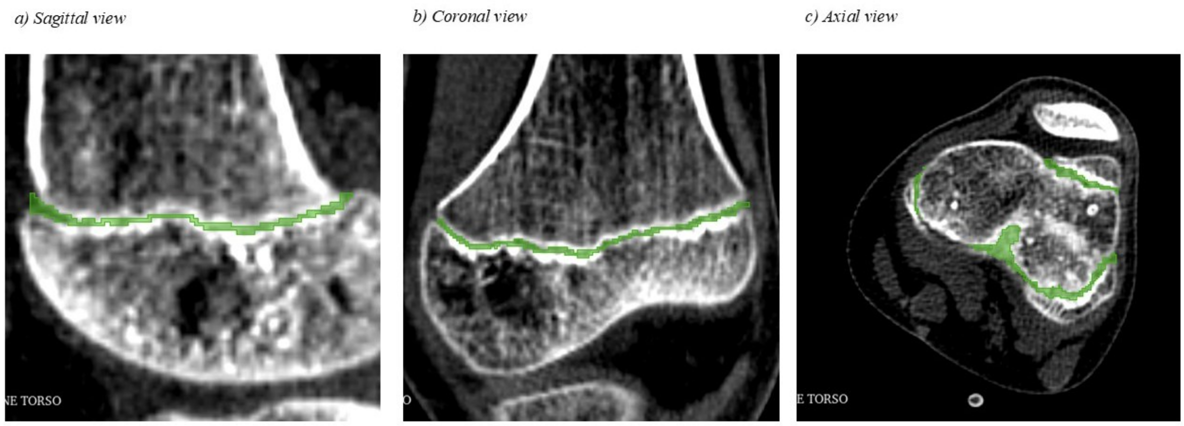

Figure 3.4: Distal growth plate (green) segmentation in the: (a) sagittal view, (b) coronal view, (c) axial view.

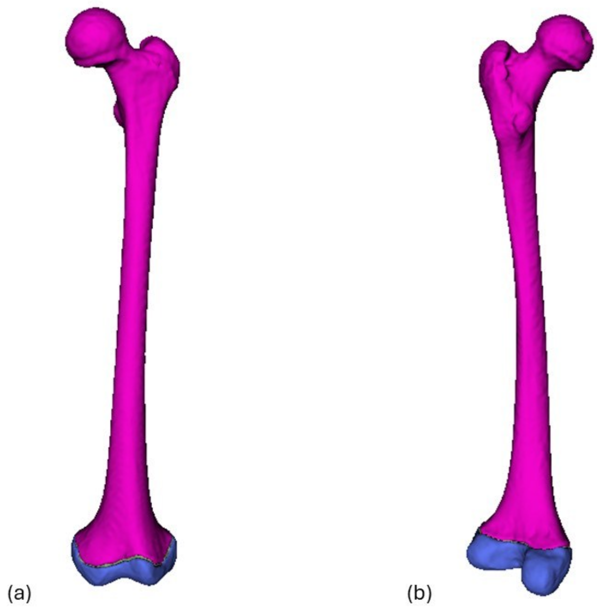

Figure 3.5: 3D of the segmented femur (cortical bone in violet, trabecular bone in blue and growth plate in green).

3.1.2 *Prosthesis geometry*

The prosthesis used in this study belongs to the Megasystem-C Tumor and Revision System developed by LINK Orthopedic.

The CAD models provided by the manufacturer included the main prosthetic components required for the reconstruction system:

- the neck segment massive,
- the coupling component,
- the stem segment,
- cementless stems

Figure 3.6 shows the three cementless stem configurations investigated in the present study. The stems differ in terms of intramedullary length (100 mm, 130 mm and 160 mm) and distal diameter, while maintaining the same proximal diameter of Ø 12 mm.

The longer stems exhibit a more pronounced tapering geometry, with progressively smaller distal diameters.

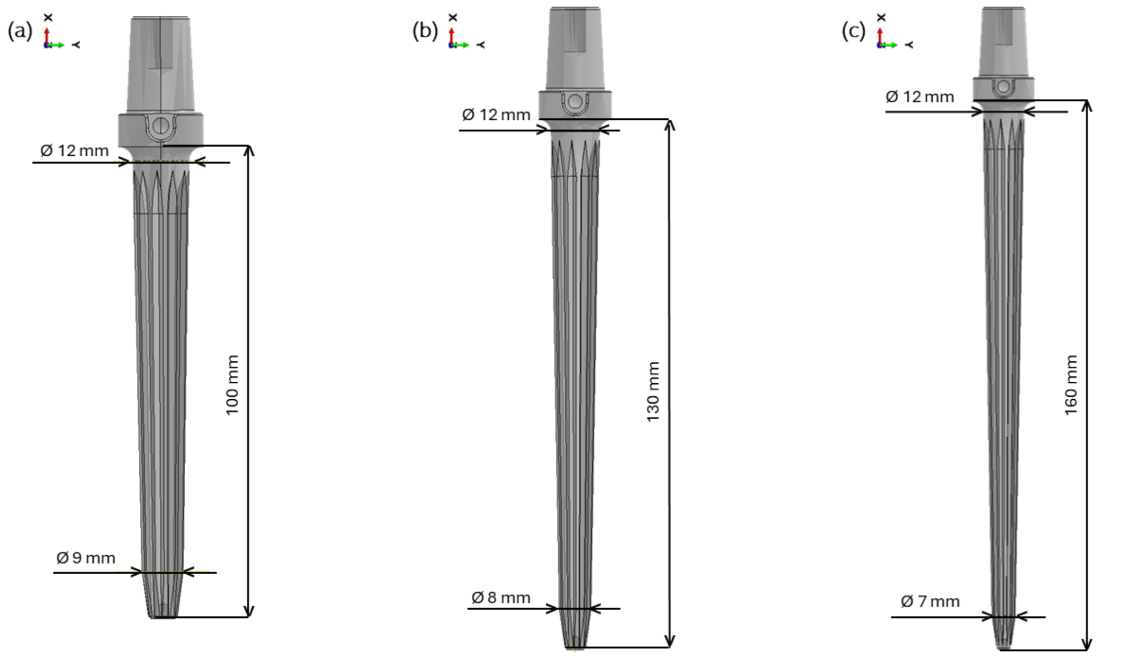

Figure 3.6: Link modular stems used in the current study: a) 100 mm stem; b) 130 mm stem; c) 160 mm stem.

To ensure numerical stability and facilitate mesh generation, the geometries were processed and simplified prior to finite element analysis. This included the removal of small features and geometrical details not relevant for the mechanical evaluation.

Figure 3.7 shows the modification of the neck segment geometry: (a) the original CAD model provided by LINK, including the internal mechanical components and cavities; (b) the simplified geometry adopted for the finite element model after removal of the internal mechanisms and reconstruction of the internal volume preserving the external geometry responsible for load transfer.

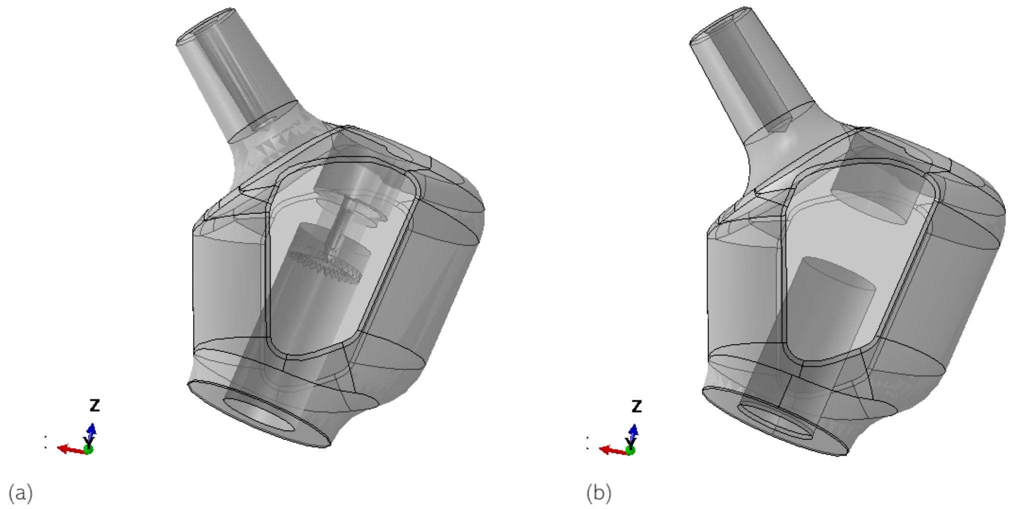

Figure 3.7: Modification of the neck segment geometry. (a) Original CAD model provided by LINK, including the internal mechanical components and cavities. (b) Simplified geometry adopted for the finite element model.

A similar simplification procedure was applied to the coupling component as shown in Figure 3.8.

The original geometry included serrated fixation features and connection details associated with the prosthetic assembly mechanism. These structures were replaced by a continuous cylindrical volume while maintaining the original external interfaces and dimensions. The adopted modifications reduced geometric complexity, improved mesh quality, and decreased computational cost without altering the global load transfer characteristics of the reconstruction.

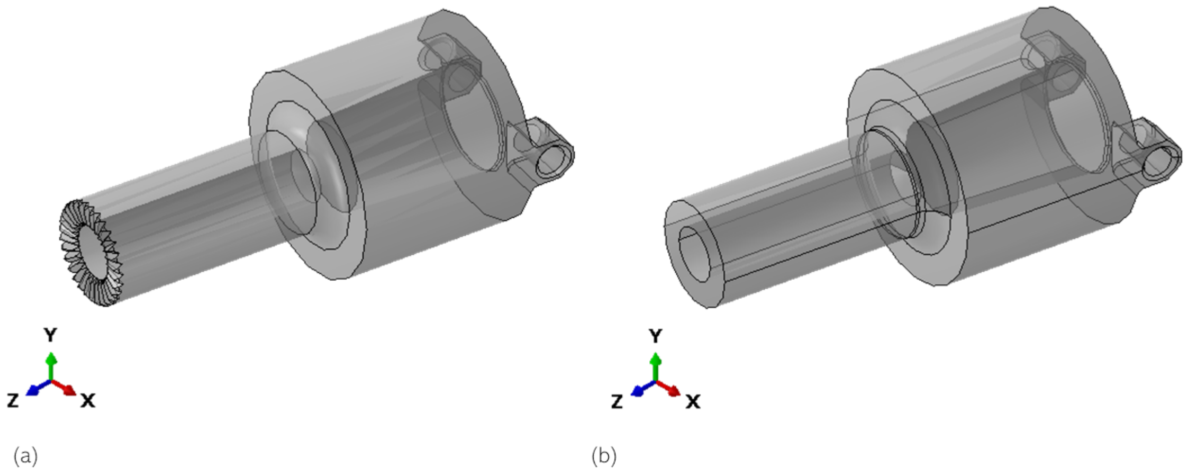

Figure 3.8: Modification of the coupling component geometry. (a) Original CAD model supplied by LINK, including the serrated fixation feature used for the prosthetic assembly. (b) Simplified geometry used in the finite element model.

Unlike the neck segment and the coupling component, the stem segment did not require any geometric simplification prior to finite element analysis. The original CAD geometry provided by LINK did not contain complex internal mechanisms or small features that could compromise mesh generation. Consequently, the stem segment was imported directly into the finite element model while preserving its original geometry and dimensions. The final prosthesis geometries are shown in Figure 3.9.

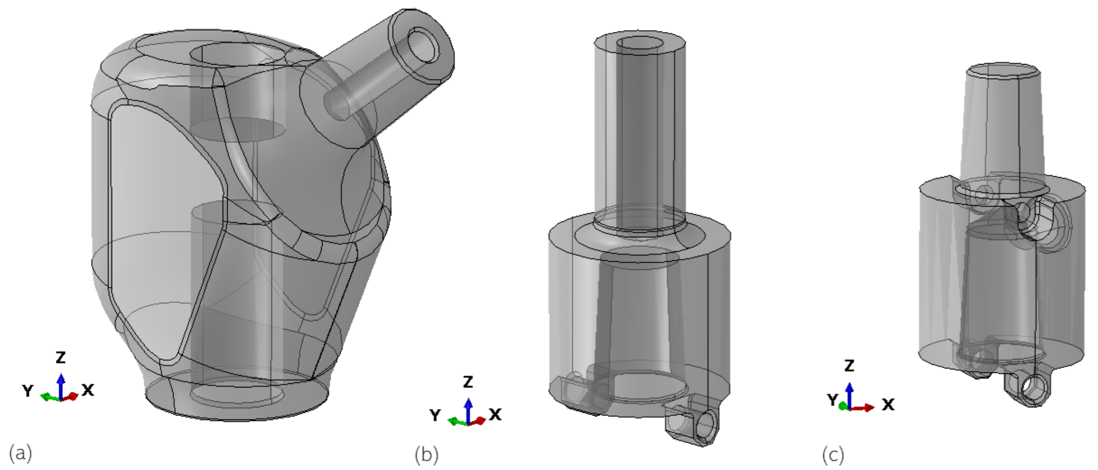

Figure 3.9: Overview of the prosthesis components used in the study: a) neck segment, b) coupling component; c) stem segment.

3.2 3D model reconstruction

The segmented structures were subsequently converted into three-dimensional solid geometries using wrapping algorithms to generate continuous surfaces, followed by smoothing procedures to improve geometric consistency. The quality of the segmentation was assessed through visual inspection of each CT slice to ensure anatomical accuracy.

Pediatric femur segmentation is inherently more challenging than adult bone segmentation due to the presence of active growth plates, reduced anatomical dimensions, and variable mineralization levels. These characteristics require careful manual intervention and optimized threshold selection to accurately identify cortical and trabecular bone regions while maintaining the fidelity of the original anatomy.

3.3 Numerical Model

The bone geometries were processed through a multi-stage workflow to ensure compatibility with finite element analysis:

1. Initial export from 3D Slicer: The segmented bone geometries were exported as STL files from 3D Slicer software
2. Format conversion in Geomagic: The STL files were imported into Geomagic Design X and converted to X_T format to ensure parametric geometry compatibility
3. Import into Abaqus: The X_T files were subsequently imported into Abaqus/CAE 2019 for finite element preprocessing.

3.3.1 *Material Assignment*

Material properties were assigned to each component according to values commonly adopted in the literature for pediatric orthopedic and biomechanical finite element analyses. The femoral bone was modelled by distinguishing cortical and trabecular regions, each assigned different mechanical properties to reproduce the heterogeneous behavior of bone tissue [10,11].

In addition, the growth plate was included in the model to better represent the anatomical and biomechanical characteristics of the pediatric femur.

The material properties were assigned to the prosthetic components according to the technical specifications reported in the LINK Megasystem-C catalogue [27]. In particular, the neck segment, stem segment and modular stem were modelled using Tilastan®, the commercial name adopted by LINK for the Ti6Al4V titanium alloy. This material is widely employed in orthopedic applications because of its favorable combination of mechanical strength, reduced density and excellent biocompatibility. Furthermore, its lower elastic modulus compared to cobalt–chromium alloys contribute to reducing stress shielding effects at the bone–implant interface.

The coupling component was instead assigned cobalt–chromium–molybdenum alloy (CoCrMo) properties, according to the manufacturer specifications [27].

CoCrMo is commonly used in oncological orthopedic prostheses due to its high stiffness, excellent wear resistance and corrosion resistance, making it particularly suitable for components subjected to elevated mechanical loads and contact stress.

All materials were considered homogeneous, isotropic and linearly elastic during the simulations. Regarding bone tissue, this assumption represents a simplification of the real mechanical behavior, since adult cortical bone is generally recognized as anisotropic due to its microstructural organization. However, for pediatric bone, the literature does not provide clear evidence demonstrating a pronounced anisotropic behavior comparable to that observed in adult bone tissue.

Preliminary simulations were also performed by introducing anisotropic properties for the cortical bone, but no significant differences were observed in the overall stress distribution results. Furthermore, several studies involving pediatric femoral models commonly adopt linear isotropic approximation for bone tissue. For these reasons, cortical and trabecular bone were ultimately modelled as isotropic linear elastic materials in the present study [10,11].

Table 3 Material properties used in FEM analysis

Material	Elastic Modulus [MPa]	Poisson Coefficient	Reference
Cortical Bone	11800	0.31	[10]
Trabecular Bone	2924	0.3	[18]
Growth Plate	6	0.48	[18]
Ti6Al4V	110000	0.35	[37]
CoCrMo	210000	0.29	[37]

3.3.2 *Assembly operations*

The prosthetic assembly procedure was developed following the surgical workflow adopted during the implantation of the LINK Megasystem-C reconstruction system. Initially, the different prosthetic components provided by the manufacturer, including the modular stem, stem segment, neck segment and coupling component, were assembled to obtain the complete prosthetic reconstruction model. Subsequently, a Boolean Union operation was performed to merge all the prosthetic components into a single geometrical part, simplifying the assembly management and ensuring continuity between the different modular elements during the finite element analysis.

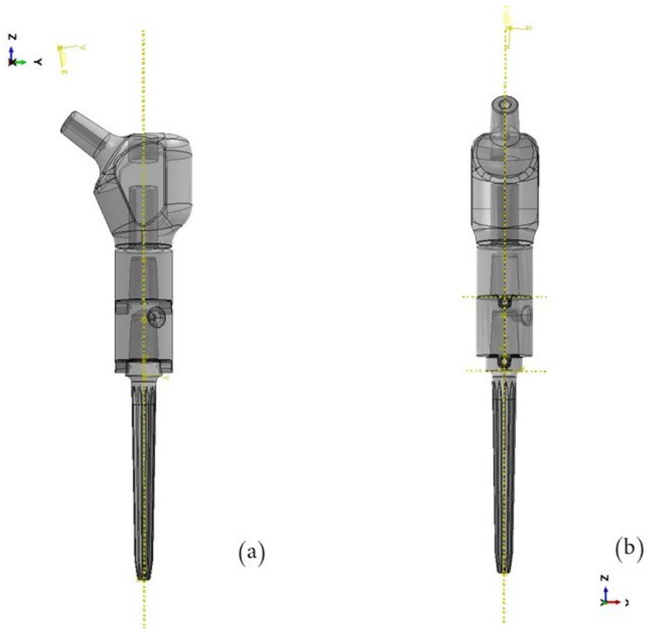

Figure 3.10: Alignment of the modular prosthesis components: (a) frontal view; (b) lateral view.

Separately, the femoral model was prepared for the implantation procedure. The femur consisted of four different anatomical regions: cortical bone, trabecular bone, distal epiphysis and growth plate. As a preliminary step, both the anatomical axis and the mechanical axis of the femur were identified in the Abaqus assembly environment. Two dedicated reference coordinate systems were then created accordingly, as shown in Figure 3.11.

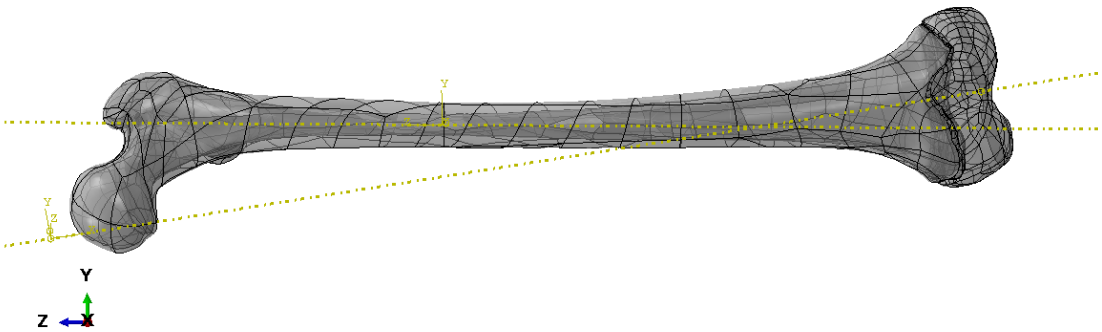

Figure 3.11: Overview of the femur assembly, made of cortical shell, trabecular core, growth plate and distal epiphysis. In yellow the anatomical and mechanical axes with the corresponding coordinate systems.

The anatomical coordinate system was defined to coincide with the global reference system of the model to simplify the alignment, while the mechanical loading axis was created from the center of the femoral head to the middle point of the distal diaphysis. In Figure 3-8 also the femoral neck axis is highlighted, the axis was needed to correctly align the prosthesis to the femur.

The prosthetic reconstruction was aligned with the femur using the previously identified anatomical and mechanical axes. Once the correct alignment had been achieved, the resection height was determined according to the desired surgical configuration. The bone resection was then performed using a cutting plane combined with a cell partition operation, allowing accurate separation of the proximal femoral region to be removed. The proximal portion of the femur, corresponding to the resected tumor area, was subsequently deleted and replaced by the prosthesis.

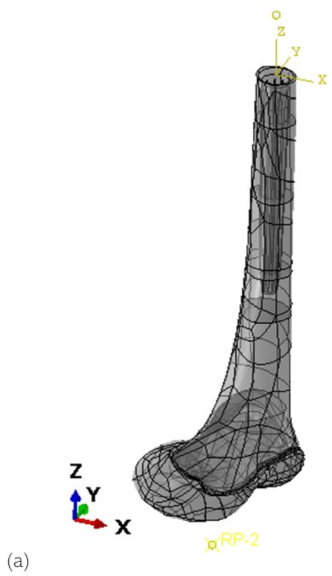

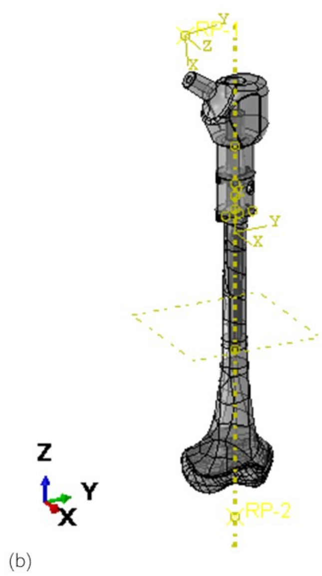

Figure 3.12: a) Resected femur with the intramedullary cavity for the prosthetic stem; b) overall view of the assembly.

Following the same sequence adopted during the surgical procedure, the intramedullary cavity required for prosthetic stem insertion was generated using a Boolean difference operation between the stem geometry and the femoral bone.

During this phase, a numerical modelling issue was encountered due to the very similar dimensions of the prosthetic stem and the trabecular bone region along the femoral shaft. In particular, the Boolean operation generated extremely small residual geometries within the trabecular region, leading to mesh generation failures caused by poor element quality.

To overcome this issue, the trabecular bone was removed from the femoral diaphysis and preserved only in the distal portion of the femur, extending approximately 25 mm proximally from the distal femoral base. This modelling choice was also considered anatomically realistic, since trabecular bone is not significantly present throughout the entire femoral shaft under physiological conditions. To identify the most appropriate transition region between cortical and trabecular bone, a qualitative evaluation of the CT images was performed to determine the anatomical location where the trabecular structure becomes macroscopically visible within the femur.

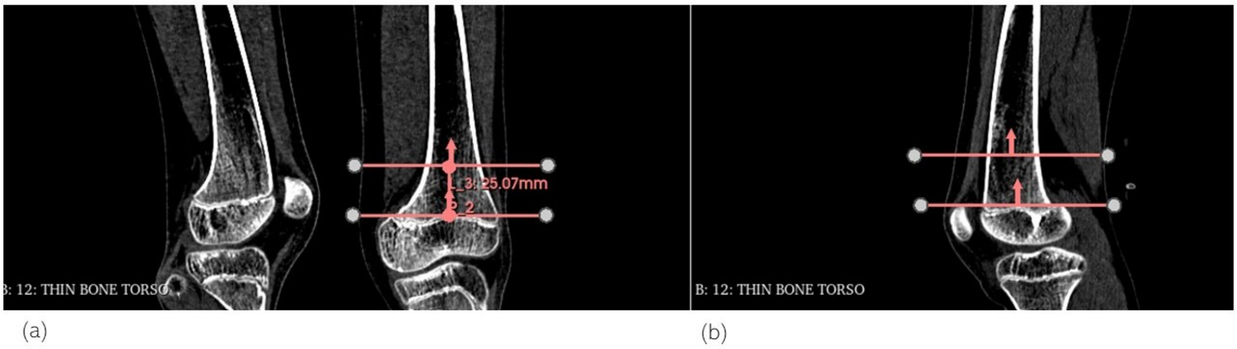

Figure 3.13: Identification of the distal trabecular bone region from patient-specific CT images using 3D Slicer: a) coronal view; b) sagittal view. The red reference lines were employed to evaluate the distal extent of the trabecular region.

Finally, a small clearance was intentionally maintained near the distal stem tip after the Boolean operation to avoid artificial stress singularities associated with the stem tip effect during finite element analysis.

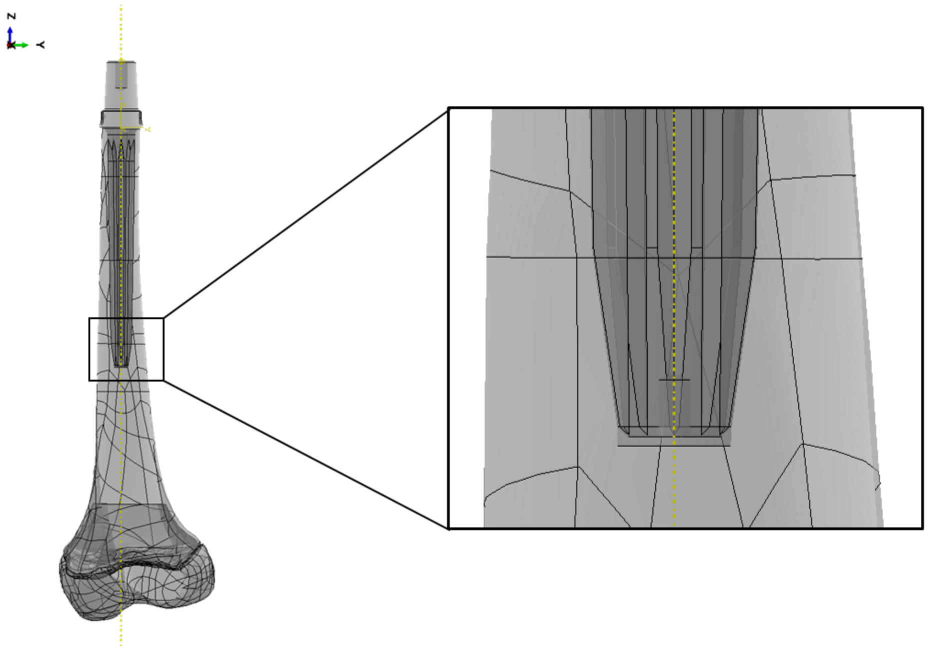

Figure 3.14: View of the resected femur with the implanted prosthetic stem. On the right part, a closed-up view of the distal stem tip region, where a small clearance was intentionally maintained to avoid the stem-tip effect during fem.

3.3.3 *Step definition*

For all simulations and for each analyzed configuration, the same two analysis steps were maintained to ensure consistency throughout the finite element study.

The initial step represented the reference configuration of the model and was used to initialize the simulation framework. During this phase, all prosthetic and bone components were assembled in a stress-free condition, allowing the proper definition of contacts and interactions between the femur and the prosthetic reconstruction system. This step ensured a stable initial state before the application of external loads.

The second step was defined as a *Static General* analysis step, it corresponded to the loading phase, in which the external forces were applied to evaluate the mechanical response of the femur.

Maintaining identical analysis steps, loading scenarios and boundary conditions across all simulations allowed a reliable evaluation of the influence of the different resection levels and stem lengths on stress distribution and overall structural behavior.

Table 4 Specific setting of the static general loading step.

Maximum number of increments	Initial increment size	Minimum Increment size	Maximum Increment size
100	0.01	1E-05	1

3.3.4 *Contact Interaction Definition*

Following assembly of the prosthetic and anatomical components, contact interactions were defined within the finite element model.

All interfaces were modelled using Tie constraints. This formulation assumes a perfect bonding condition between the contacting surfaces, preventing any relative displacement or rotation at the interface and ensuring complete load transfer between the connected parts.

For each tie interaction, the surface belonging to the component with the higher elastic modulus was generally assigned as the master surface, while the surface associated with the less rigid component was defined as the slave surface. The default Abaqus positioning tolerance was adopted, and rotational degrees of freedom were tied whenever applicable.

The only exception was the interface between the cementless stem and the residual femur, which was modelled using a frictional contact formulation to reproduce the mechanical behavior of a press-fit fixation.

A surface-to-surface contact interaction was defined between the external surface of the stem and the internal surface of the resected femur. Finite sliding was enabled to allow relative motion between the contacting surfaces during loading. The residual femur was assigned as the master surface, whereas the stem surface was defined as the slave surface.

Tangential behavior was modelled using the penalty friction formulation available in Abaqus. An isotropic friction coefficient of $\mu = 0.45$ was assigned to the bone–implant interface, according to values commonly reported in the literature for titanium–bone contact.[37]

This frictional interaction allows load transfer through both normal contact pressure and tangential friction forces, reproducing the primary stability mechanism of cementless stems.

To ensure a proper initial contact condition, the option "Adjust only to remove overclosure" was adopted. This setting eliminates local penetrations between the contacting surfaces at the beginning of the analysis while preserving the original geometry of the assembly.

3.3.5 *Load and Boundary Condition*

A fixed support boundary condition was applied at the distal epiphysis to simulate the physiological constraint provided by the knee joint, according to previous biomechanical studies [11,18].

This constraint prevented translational and rotational movement at the distal end of the femur. The mechanical load was applied to the upper surface of the prosthesis.

The load direction was defined along the axis extending from the center of the femoral head to the center of the distal epiphysis, representing the mechanical axis of the femur.

A load magnitude of 250 N was applied, corresponding to the physiological load experienced by the femur. This value was determined based on the patient's body weight of approximately 50 kg for a 14-year-old male subject.

According to previous biomechanical studies, simplified static finite element analyses frequently assume that the body weight is equally shared by both lower limbs during quiet standing. Consequently, a load corresponding to approximately half of the subject's body weight was applied. [11].

Therefore, the applied load was estimated as 50 kg ÷ 2 = 25 kg, corresponding to approximately 250 N.

Figure 3.15 shows the loading and boundary conditions adopted in the finite element model. The concentrated force applied along the mechanical axis of the femur is highlighted in red and originates from RP-1. The fixed boundary condition applied at RP-2 is highlighted in blue. The dashed yellow line represents the mechanical axis used to define the loading direction and the anatomical axis.

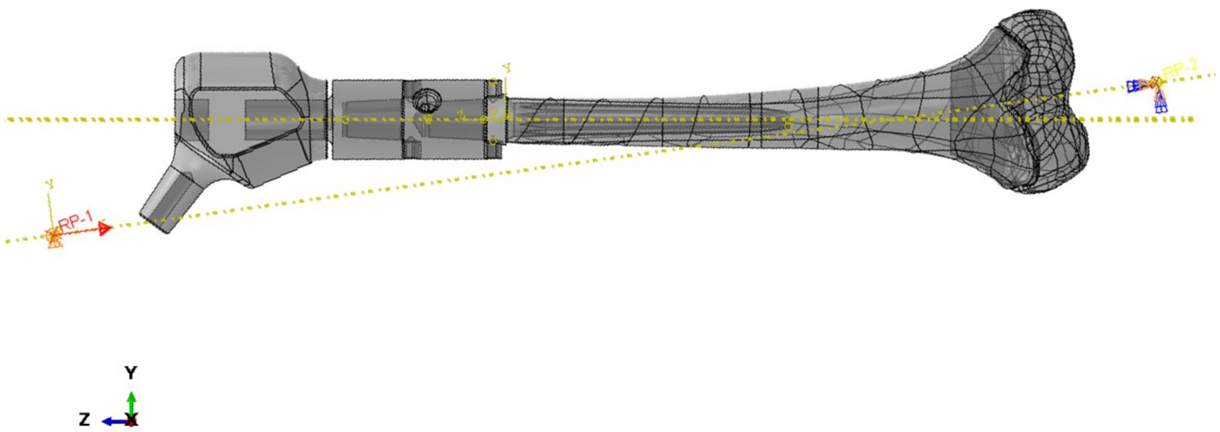

Figure 3.15: Loading and boundary conditions adopted in the finite element model.

The concentrated force was applied progressively using the tabular amplitude function shown in Table 5. The amplitude increased gradually from 0 to 1 throughout the analysis step, allowing the full load magnitude to be reached at the end of the simulation.

Table 5 Tabular amplitude used for the application of the external load during the finite element analysis.

	Time/Frequency	Amplitude
1	0	0
2	0.1	0.02
3	0.2	0.06
4	0.35	0.15
5	0.5	0.3
6	0.65	0.55
7	0.8	0.8
8	0.9	0.92
9	0.97	0.98
10	1	1

To uniformly distribute the load and boundary condition to the entire specific surfaces rather than concentrate at a single point, two references point were created along the mechanical axis of the femur:

1. A proximal reference point at 20 mm of distance from the loading surface of the prosthesis.
2. A distal reference point at 20 mm of distance from the center of the distal epiphysis to facilitate the boundary condition application.

A kinematic coupling constraint was established between the reference points and the specific surfaces. A boundary condition was applied to Reference Point 1 using the mechanical coordinate system.

The translational degrees of freedom perpendicular to the mechanical axis (U2 and U3) were constrained, while displacement along the longitudinal direction (U1) was left free. All rotational degrees of freedom were also left unconstrained.

This boundary condition was introduced to prevent rigid body motion in the transverse directions while allowing axial deformation of the reconstruction under the applied loading conditions, thereby reproducing a more physiologically realistic mechanical response.

What has been described is shown in Figure 3.16 and Figure 3.17.

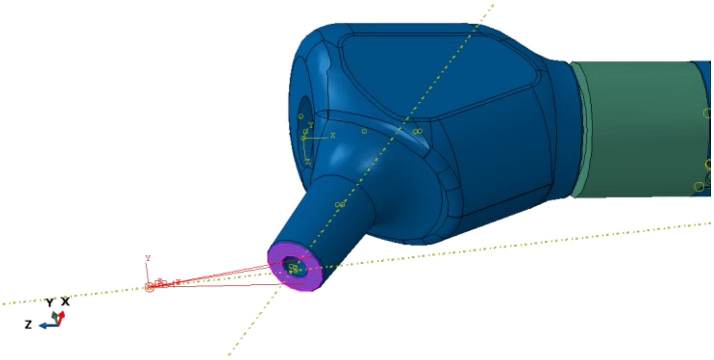

Figure 3.16: Proximal reference point: in violet the surface kinematically connected.

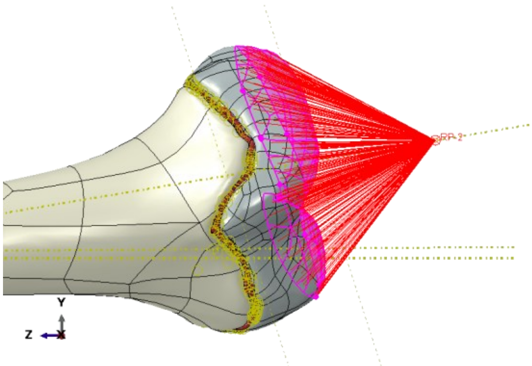

Figure 3.17: Distal reference point kinematically connected to the distal surface of the distal ephysis.

3.3.6 *Mesh definition*

A tetrahedral mesh was generated for the entire femoral reconstruction to discretize the geometry for finite element analysis. Tetrahedral elements were selected due to their ability to accurately conform to complex anatomical structures and irregular geometries while ensuring reliable stress predictions.

Specifically, second-order tetrahedral elements (C3D10) were used to mesh the prosthetic components, the intramedullary stem, and the growth plate. The prosthetic components and the stem exhibited relatively regular geometries that could be discretized without significant meshing difficulties using quadratic elements. Conversely, first-order tetrahedral elements (C3D4) were employed for the residual femur and the distal epiphysis. The highly irregular anatomical geometry of these structures generated element quality issues when quadratic elements were used, and linear tetrahedral elements were therefore adopted to obtain a stable and computationally efficient mesh.

The mesh density was defined according to both the geometric complexity of each component and its relevance to the objectives of the study. Since stress evaluation within the prosthetic components was not a primary focus of the analysis and these parts exhibited relatively simple geometries, a larger element size of 3.5 mm was adopted for the prosthesis. In contrast, all remaining components of the assembly were meshed using element sizes equal to or smaller than 2 mm to achieve a more accurate representation of the stress distribution within the bone structures.

The growth plate required special consideration due to its very limited thickness. To accurately capture its geometry and ensure an adequate number of elements through its thickness, the mesh size was reduced to 1.2 mm. Despite the small dimensions of this anatomical structure, the geometry could still be successfully discretized using quadratic tetrahedral elements (C3D10), allowing a more accurate representation of the stress field in this region. The applied mesh is shown in Figure 3.18, below Table 4 reports the element type and the corresponding mesh size used for the residual femur, prosthesis, stem, distal epiphysis and growth plate.

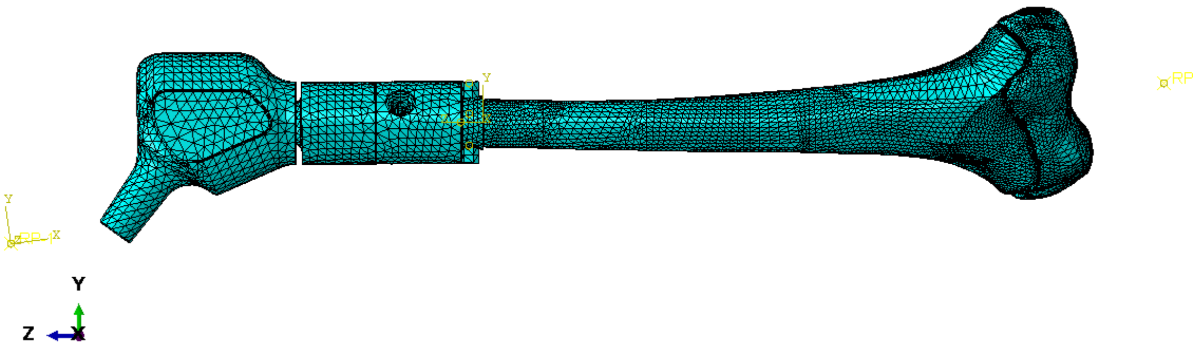

Figure 3.18: overall view of the meshed assembly.

Table 6 Summary of the finite element mesh characteristics adopted for each component of the reconstructed femur model.

Part	Type of elements	Size of elements [mm]
Resected femur	C3D4	2
Prosthesis	C3D10	3.5
Stem	C3D10	2

Growth Plate	C3D10	1.2
Distal Epiphysis	C3D4	2

3.3.7 Partition of the femur

To enable detailed and comparative analysis of von Mises stresses, the model was subdivided into five distinct anatomical regions, the same regions are identified in all the configurations. Proceeding from proximal to distal:

1. ROI 1: Interface stem-femur, it has a constant length of 20 mm.
2. ROI 2: Intermediate region of interest
3. ROI 3: Intermediate region of interest
4. ROI 4: stem tip region of interest, it has a constant length of 20 mm,10 mm before the stem end point and 10 mm after it;
5. ROI 5: defined as the distal diaphyseal region extending from the end of ROI 4 to the remaining distal portion of the femoral shaft.

Consequently, the longitudinal extension of ROI 5 varied depending on the investigated resection configuration. ROI 5 was mainly included to evaluate the distal propagation and redistribution of stresses along the residual femoral shaft. Since this region is located further from the primary bone–implant interaction zones, lower stress magnitudes were generally expected.

Creating ROI 2 and ROI 3 from the end point of ROI 1 to the starting point of ROI 4, divided by 2. In Figure 3.12 the partitioned femur can be observed.

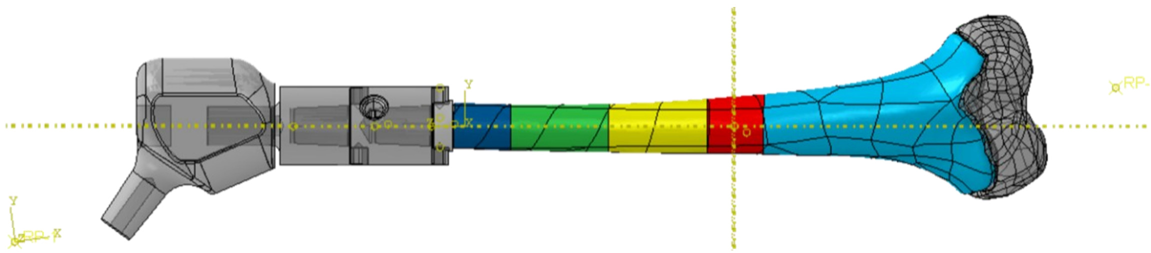

Figure 3.19: Partitions of the femur: ROI 1 is shown in blue, ROI 2 in green, ROI 3 in yellow, ROI 4 in red, ROI 5 in light blue.

4 Case study

This case study aims to investigate the biomechanical behavior of a proximal femoral reconstruction performed using the LINK Megasystem-C Tumor and Revision System following oncological proximal femoral resection. The primary objective of the study is to evaluate how stress distribution within the residual femoral bone changes as a function of different resection level and stem lengths.

The analysis focuses on five different levels of proximal femoral resection, representing progressive bone loss conditions commonly encountered in orthopedic oncology surgery. For each resection level, three different stem lengths were investigated to evaluate the influence of intramedullary fixation length on load transfer and structural stability of the implant-bone system.

To adapt the prosthesis to the different reconstruction configurations, the dimensions of two modular components were systematically modified:

- the stem segment;
- the upper cylindrical portion of the coupling component.

These components were progressively increased by 5 mm increments in each configuration, allowing maintenance of the overall prosthetic geometry and proper adaptation of the implant to the varying resection lengths.

The study was conducted through Abaqus CAE 2019, a Finite Element Analysis (FEA) software, under identical loading and boundary conditions (Section 3.3.4) for all models, ensuring direct comparison between configurations.

Furthermore, the residual femur and prosthetic assembly were divided into mechanically relevant regions to enable detailed local stress analysis (Section 3.3.7).

The comparative analysis allows investigation of how increasing resection length and varying stem dimensions influence stress redistribution within the remaining bone tissue. Attention is given to identifying potential stress concentration areas, stress shielding effects, and regions potentially susceptible to mechanical failure or aseptic loosening.

Through this systematic biomechanical evaluation, the study aims to provide useful insights into the optimization of prosthetic reconstruction strategies for proximal femoral replacement, supporting improved implant design and enhanced clinical outcomes in orthopedic oncological surgery.

4.1 Configuration 1

Configuration 1 represents the shortest prosthetic configuration among the investigated models, characterized by a neck segment of 45 mm and a resection length of approximately 215 mm, also the proximal cylindrical extension of the coupling component has been reduced to fit the new geometry of the neck segment. A cutting plane was created 10 mm along the positive direction of the global Z-axis, after which the neck segment was partitioned, and the generated cells were removed. The same procedure was applied to the coupling component. Figure 4.1 shows configuration 1 with the 100 mm stem inserted and all the dimensions values while Figure 4.2 (a) shows configuration 1 with the 130 mm stem inserted and Figure 4.2 (b) shows the configuration 1 with the 160 mm stem inserted.

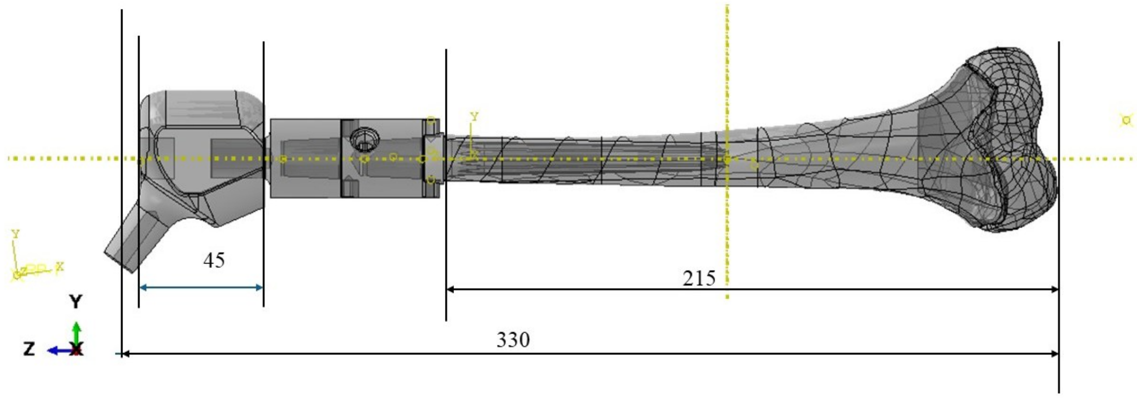

Figure 4.1: the dimensioned prosthetic assembly corresponding to Configuration 1 with 100 mm stem inserted.

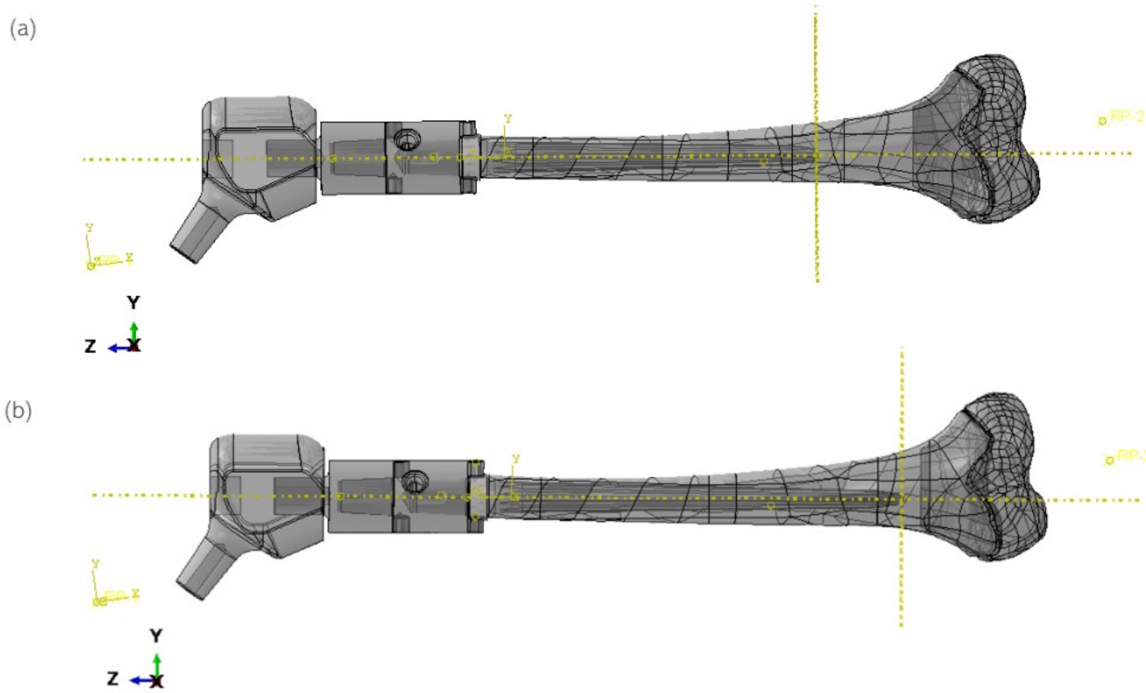

Figure 4.2 Configuration 1 with: a) 130 mm stem inserted; b) 160 mm stem inserted.

4.2 Configuration 2

For Configuration 2, the same procedure adopted for Configuration 1 was applied. However, in this case the cutting plane was positioned 5 mm along the positive direction of the global Z-axis resulting in a neck segment of 50 mm and a resection length of approximately 210 mm. After partitioning the component, the generated cell was removed, producing a 5 mm reduction in the length of the neck segment. The same modification was then applied to the second prosthetic component, resulting in the desired reconstruction length for Configuration 2.

Figure 4.3 shows configuration 2 with the 100 mm stem inserted and all the dimensions values while Figure 4.4-a shows configuration 1 with the 130 mm stem inserted and Figure 4.4-b shows the configuration 1 with the 160 mm stem inserted.

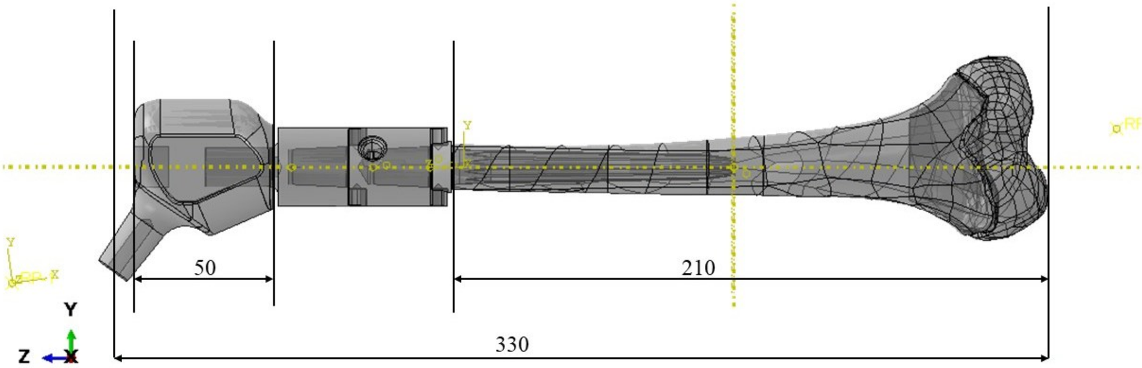

Figure 4.3: the dimensioned assembly corresponding to Configuration 2 with 100 mm stem inserted.

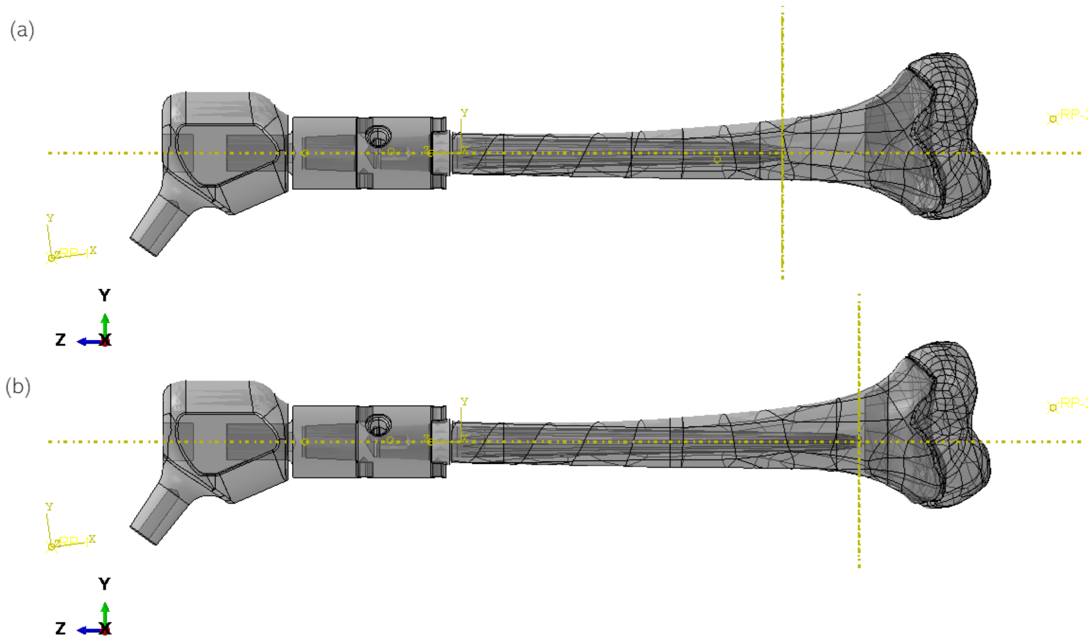

Figure 4.4: Configuration 2 with: a) 130 mm stem inserted; b) 160 mm stem inserted.

4.3 Configuration 3

Configuration 3 corresponds to the reference reconstruction scenario provided by LINK. In this configuration, no geometric modifications were applied to the prosthetic components, and the original CAD geometries supplied by the manufacturer were maintained. Consequently, the neck segment and the coupling component retained their initial dimensions and served as the baseline configuration for subsequent comparisons. The configuration is characterized by a neck segment of 55 mm and a resection length of approximately 205 mm.

Figure 4.5 shows configuration 3 with the 100 mm stem inserted and all the dimensions values while Figure 4.6-a shows configuration 3 with the 130 mm stem inserted and Figure 4.6-b shows the configuration 3 with the 160 mm stem inserted.

As it's possible to see from the picture here the stem tip reaches the trabecular bone.

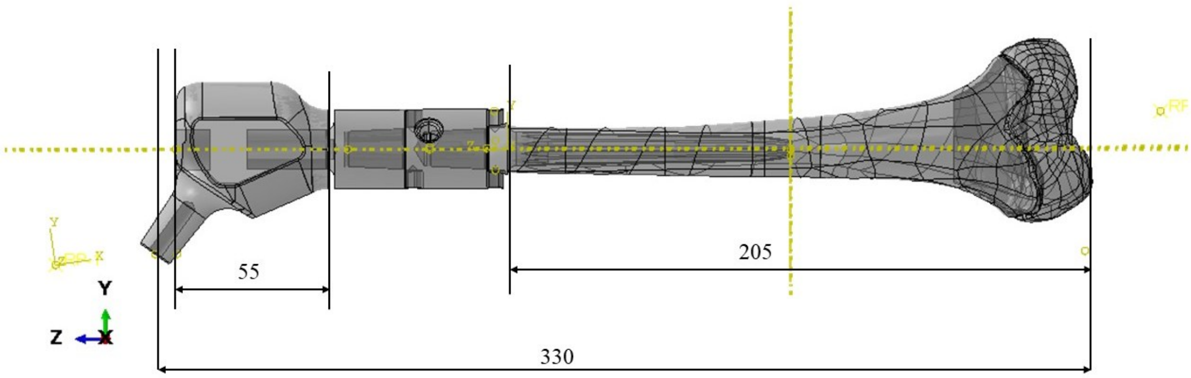

Figure 4.5: the dimensioned assembly corresponding to Configuration 3 with 100 mm stem inserted.

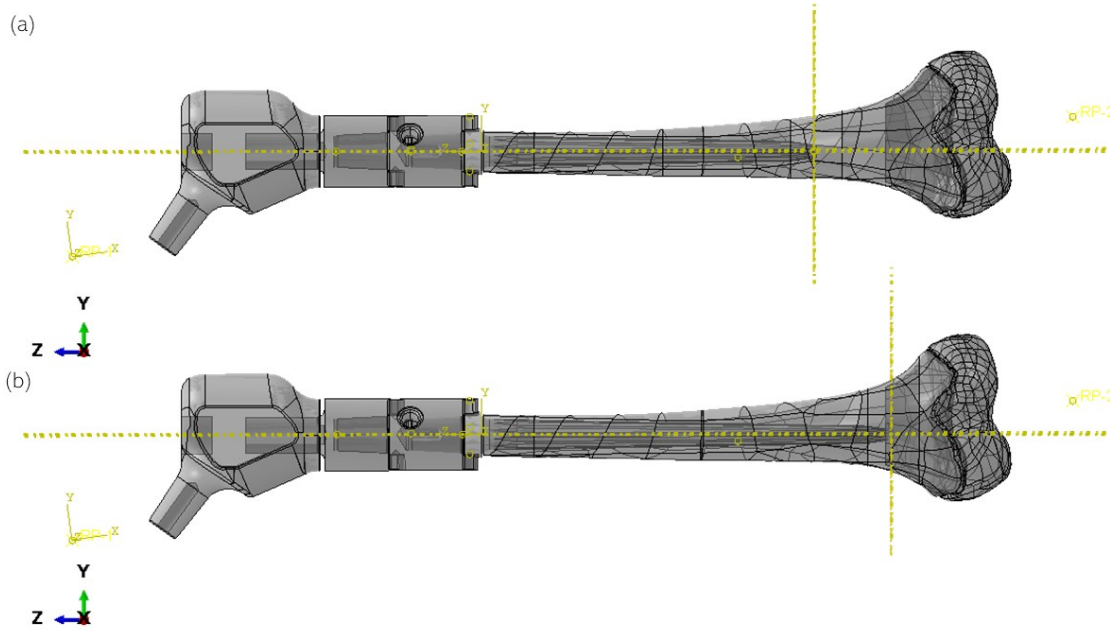

Figure 4.6: Configuration 3 with: a) 130 mm stem inserted; b) 160 mm stem inserted.

4.4 Configuration 4

For Configuration 4, the overall reconstruction length was increased by modifying both the neck segment and the coupling component. Specifically, a 5 mm extrusion was applied to the distal surface of the neck segment along the negative direction of the global Z-axis reaching a length of 60 mm.

In addition, a 5 mm extrusion was applied to the proximal cylindrical portion of the coupling component along the positive direction of the global Z-axis. The resected femur for this configuration is 200 mm. These modifications resulted in an increase in the overall prosthetic length while preserving the original geometry of the remaining prosthetic components.

Figure 4.7 shows configuration 4 with the 100 mm stem inserted and all the dimensions values while Figure 4.8-a shows configuration 4 with the 130 mm stem inserted.

Figure 4.8-b shows configuration 4 with the 160 mm stem inserted and also in this configuration placing the longest stem, the tip reaches the trabecular bone.

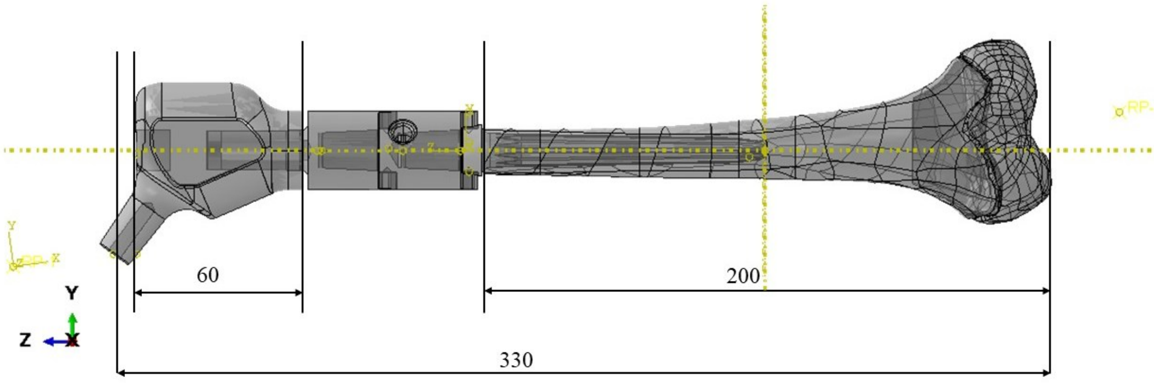

Figure 4.7: the dimensioned assembly corresponding to Configuration 4 with 100 mm stem inserted.

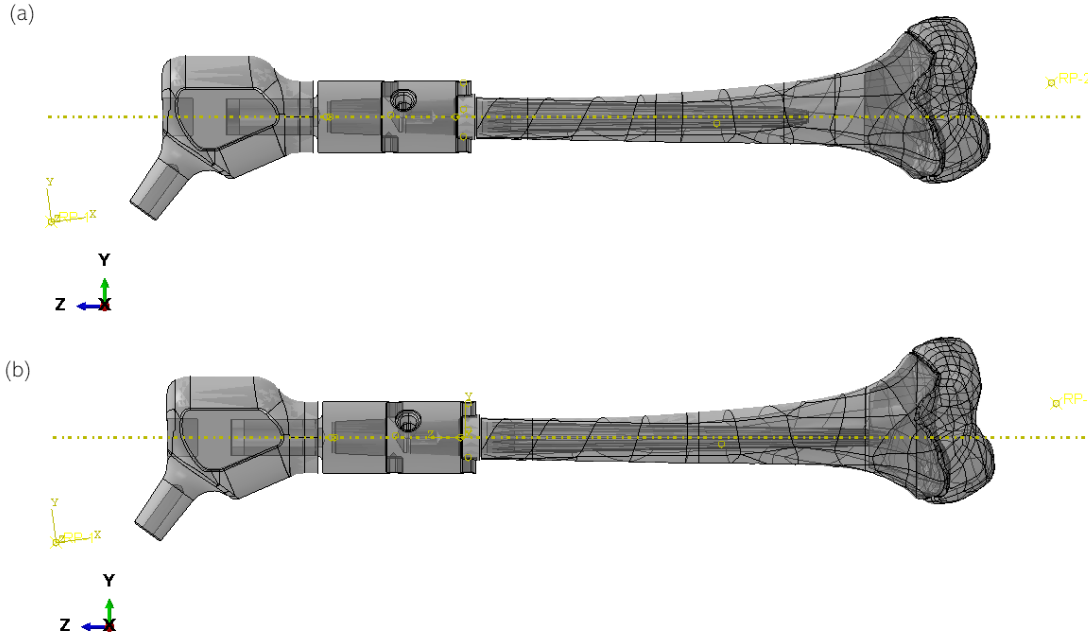

Figure 4.8: Configuration 4 with: a) 130 mm stem inserted; b) 160 mm stem inserted.

4.5 Configuration 5

For Configuration 5, the same procedure adopted for Configuration 4 was applied. However, the extrusion distance was increased from 5 mm to 10 mm.

Specifically, a 10 mm extrusion was performed on the neck segment in the negative direction of the global Z-axis, while a corresponding 10 mm extrusion was applied to the coupling component in the positive direction of the global Z-axis. This resulted in the longest prosthetic reconstruction investigated in the present study with a neck segment of 65 mm and a resected femur of 195 mm.

Figure 4.9 shows configuration 5 with the 100 mm stem inserted and all the dimensions values while Figure 4.10-a shows configuration 5 with the 130 mm stem inserted and Figure 4.10-b shows the configuration 5 with the 160 mm stem inserted, it reaches the trabecular bone as well as configuration 3 and 4.

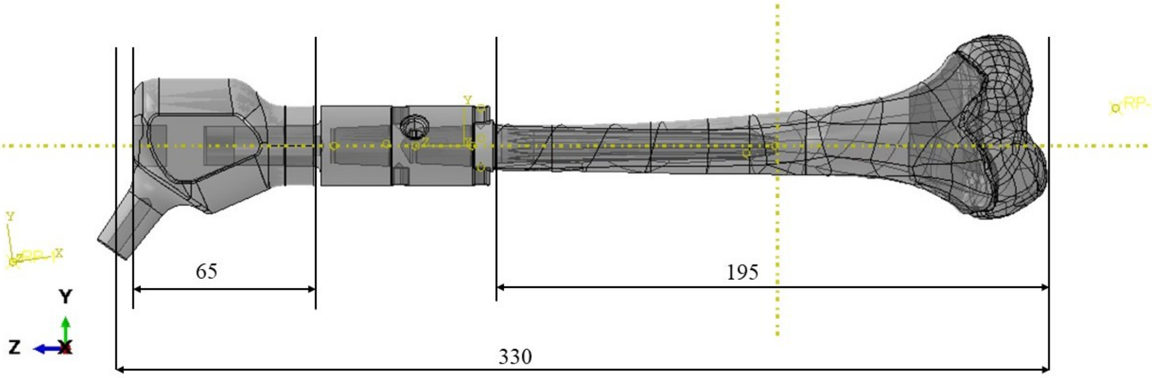

Figure 4.9: the dimensioned assembly corresponding to Configuration 5 with 100 mm stem inserted.

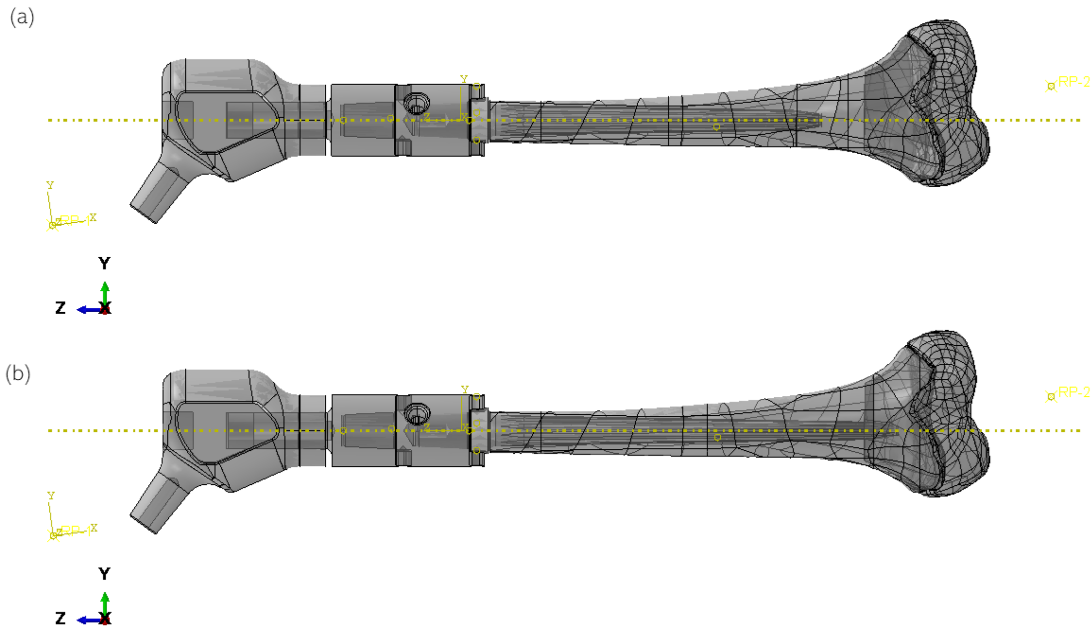

Figure 4.10: Configuration 5 with: a) 130 mm stem inserted; b) 160 mm stem inserted.

5 Results and discussion

The finite element analysis results are presented through a comprehensive evaluation of Von Mises stress, compressive stress, and shear stress distributions within the residual femur for the five investigated resection levels and three stem length configurations.

Attention is given to the analysis of Von Mises stress, which was used to assess the mechanical response of the reconstructed femur under physiological loading conditions representative of static standing with bilateral support. To enable comparison among the different reconstruction configurations, the stress distribution was evaluated both qualitatively and quantitatively within the five predefined regions of interest (ROIs).

Von Mises stress is a scalar quantity derived from the stress tensor and is widely used in biomechanical analyses to evaluate the response of biological tissues and engineering structures under complex loading conditions [37].

A comparative assessment was performed to investigate the biomechanical influence of resection level and stem length on the reconstructed femur. The results are presented according to the different reconstruction configurations and anatomical regions of interest, allowing a detailed evaluation of local mechanical variations throughout the femur.

5.1 Qualitative Evaluation of Von Mises Stress Distribution

The qualitative evaluation of Von Mises stress distribution is first presented in order to provide an overview of the stress transfer mechanisms within the reconstructed femur for the investigated configurations. The contour maps allow visualization of stress concentration regions, load transfer pathways and areas potentially affected by stress shielding phenomena.

The qualitative analysis also provides an initial comparison among the investigated configurations before proceeding with the quantitative evaluation of stress values in the selected anatomical regions of interest.

Figures from 5.1 to 5.5 present the Von Mises stress distribution for the five investigated resection levels combined with the three prosthetic stem length configurations (100 mm, 130 mm and 160 mm).

For each configuration, stress distributions are reported on both the transverse (XY) and longitudinal (ZY) planes to provide a comprehensive representation of the mechanical behavior of the residual femur.

For the longitudinal views, an X-plane cut was applied to all models using the same cut position (X=-0.47).

This sectional view was introduced to visualize the internal stress distribution within the femur and to facilitate the assessment of stress transfer mechanisms, particularly in the region surrounding the distal end of the prosthetic stem.

Maintaining the same cut location for all configurations ensured a consistent qualitative comparison between the different stem lengths and resection levels.

Maximum stress values for each configuration are reported in black within the corresponding contour maps.

The stress distributions are represented through a color map ranging from dark blue, corresponding to low stress values, to red, indicating regions of maximum stress concentration. Regions displayed in grey correspond to stress values exceeding 5 MPa.

This upper visualization limit was intentionally selected to maintain a consistent and readable representation of the stress patterns across all investigated configurations, allowing easier qualitative comparison between different stem lengths and resection levels.

Overall, all investigated configurations exhibited similar global stress patterns, suggesting coherent and mechanically consistent load transfer within the reconstructed femur. This similarity in stress distribution also supports the reliability of the numerical model, since comparable mechanical behavior was observed despite variations in resection level and stem length.

In all configurations, most of the residual femur remained subjected to stress values below 5 MPa, while only localized regions exhibited higher stress peaks.

Figure 5.1 presents the Von Mises stress distributions obtained for Configuration 1 with stem lengths of 100 mm, 130 mm, and 160 mm. For all stem lengths, the highest stress concentrations are located either at the proximal bone–implant interface or around the distal stem tip, confirming that these regions play a major role in load transfer between the prosthesis and the residual femur, in accordance with the literature [37].

A qualitative difference can be observed in the location of the maximum stress. For the 100 mm stem, the most critical region is located around the distal stem tip. In contrast, for the 130 mm and 160 mm stems, the highest stress concentration is observed at the proximal bone–implant interface. Furthermore, the stress field surrounding the stem tip appears more diffuse for the shorter stems, whereas the longest stem exhibits a more localized stress concentration around the distal end of the implant.

The stress distributions obtained for Configuration 2 show a pattern like the one observed in Configuration 1, and it can be observed in Figure 5.2Figure 5.3.

Stress concentrations are mainly located at the proximal interface and near the distal end of the stem, while the central portion of the femur shows relatively low stress levels.

As in Configuration 1, the 100 mm stem exhibits the highest stress concentration around the stem tip, whereas for the 130 mm and 160 mm stems the most stressed region is located at the proximal bone–implant interface. The longest stem again produces a more localized stress field around the distal end of the implant.

Figure 5.3 illustrates the stress distributions obtained for Configuration 3. The overall stress pattern remains comparable to that observed in the previous configurations, with elevated stresses at the proximal interface and around the stem tip.

Unlike the other configurations, Configuration 3 exhibits a different behavior regarding the location of the maximum stress. The highest stress concentration is located at the proximal interface for the 100 mm and 160 mm stems, whereas the 130 mm stem exhibits its maximum stress around the distal stem tip. This configuration therefore represents an exception to the trend observed in the remaining cases.

In addition, due to the increased resection length, the distal end of the longer stems approaches a region characterized by trabecular bone, which may contribute to the differences observed in the stress contours around the stem tip.

Figure 5.4 shows the stress maps corresponding to Configuration 4 exhibit the same general distribution pattern observed previously. The highest stresses are concentrated at the proximal bone–implant interface and around the stem tip, while the central diaphyseal region remains characterized by relatively low stress levels.

The 100 mm stem shows its maximum stress concentration at the distal stem tip, whereas for the 130 mm and 160 mm stems the maximum stress is located at the proximal interface. Moreover, the stress field surrounding the stem tip becomes progressively more localized as stem length increases.

Lastly, Figure 5.5 presents the Von Mises stress distributions obtained for Configuration 5. Despite the larger resection length, the overall stress pattern remains consistent with the previous configurations.

The 100 mm stem exhibits the highest stress concentration around the distal stem tip, while the 130 mm and 160 mm stems show their maximum stress at the proximal bone–implant interface. Like Configuration 4, the distal end of the longest stem lies within a region containing a greater amount of trabecular bone, which may influence the observed stress distribution.

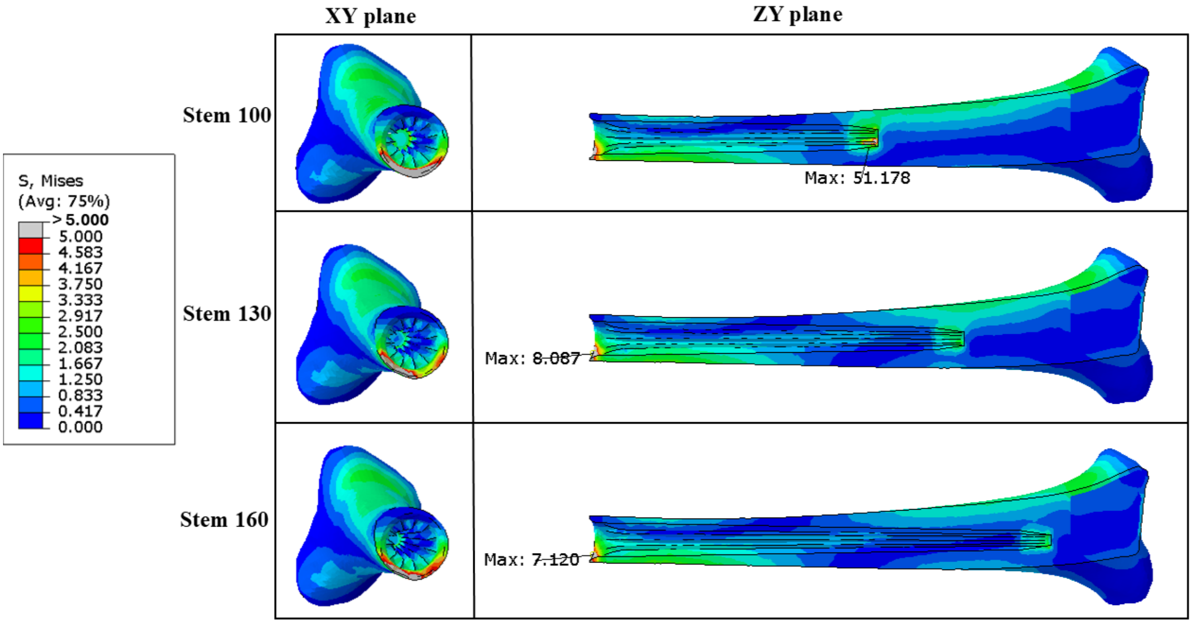

Figure 5.1: Von Mises stress distribution for the first configuration combined with the three prosthetic stem lengths (100 mm, 130 mm and 160 mm).

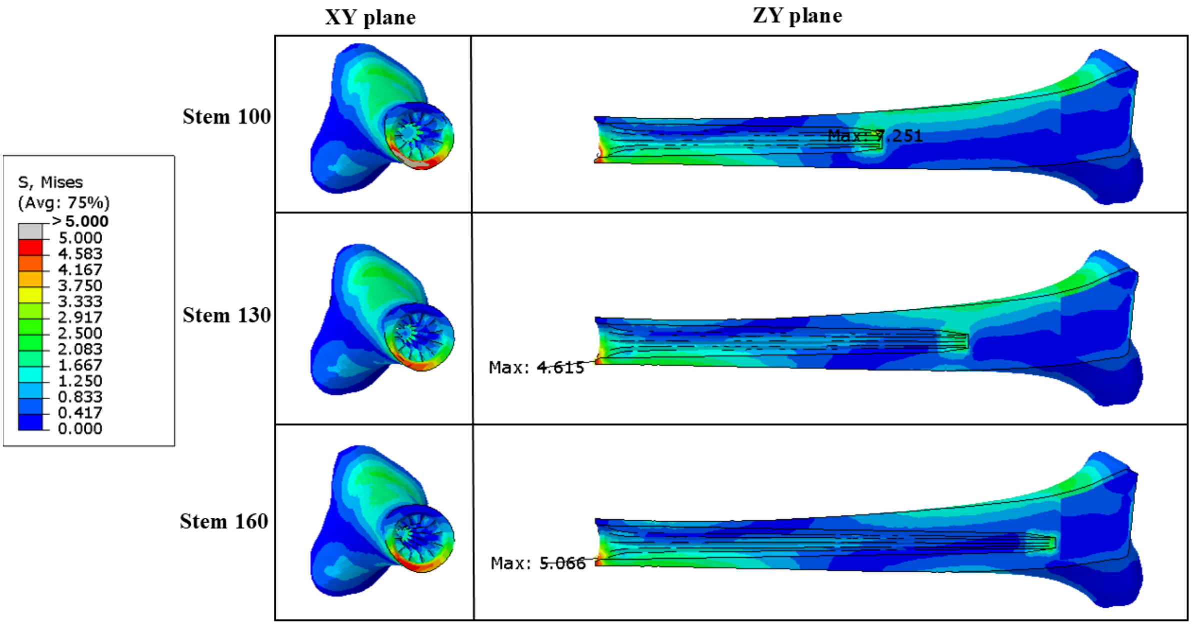

Figure 5.2: Von Mises stress distribution for the second configuration combined with the three prosthetic stem lengths (100 mm, 130 mm and 160 mm).

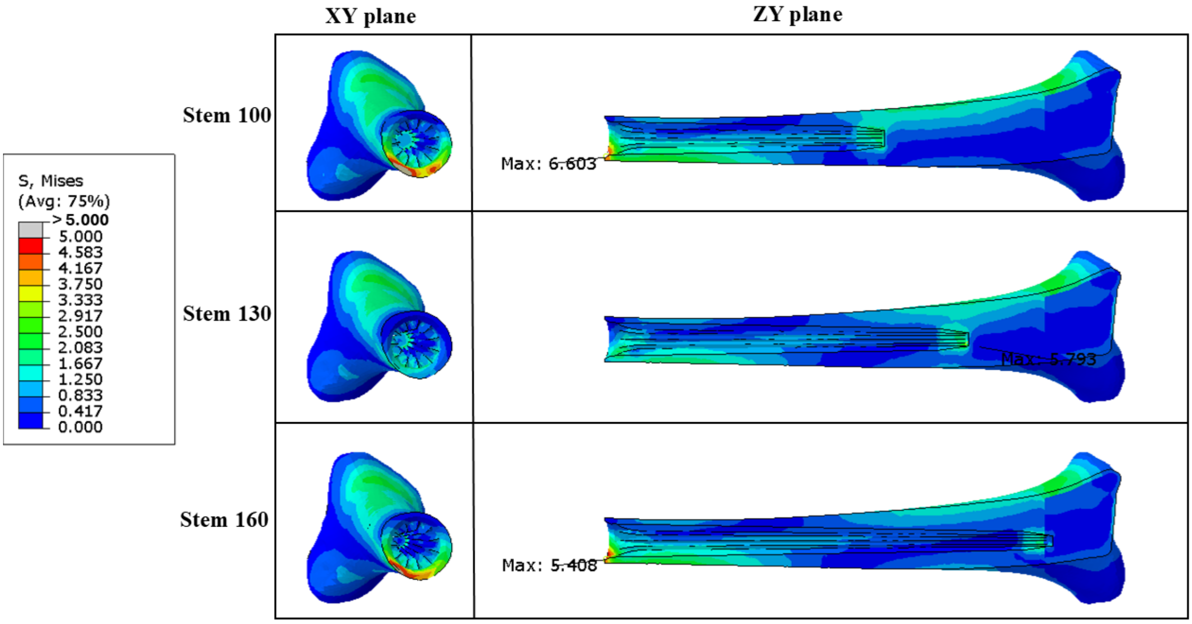

Figure 5.3: Von Mises stress distribution for the third configuration combined with the three prosthetic stem lengths (100 mm, 130 mm and 160 mm).

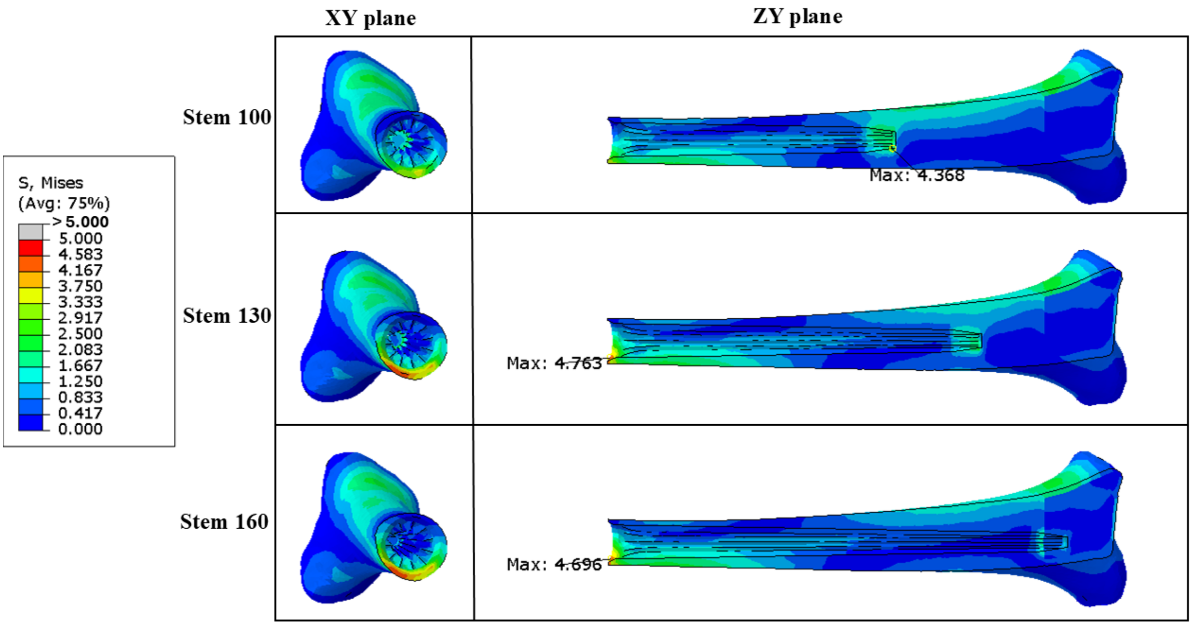

Figure 5.4: Von Mises stress distribution for the fourth configuration combined with the three prosthetic stem lengths (100 mm, 130 mm and 160 mm).

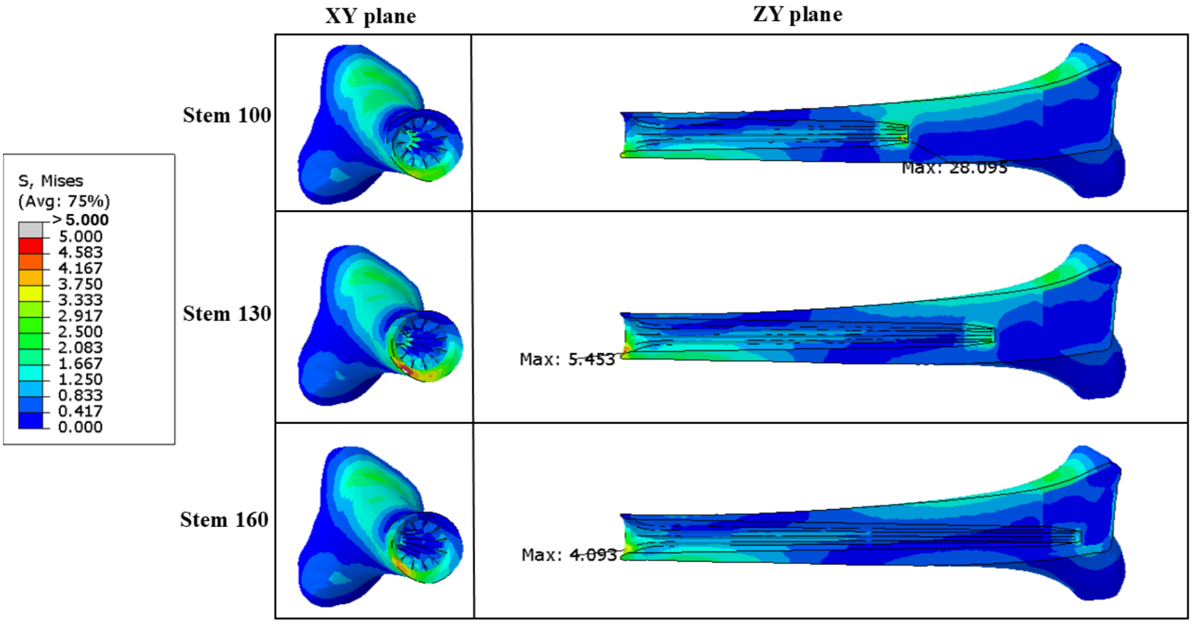

Figure 5.5: Von Mises stress distribution for the fifth configuration combined with the three prosthetic stem lengths (100 mm, 130 mm and 160 mm).

Overall, the qualitative analysis demonstrates that all configurations exhibit a similar stress distribution pattern, with stress concentrations occurring mainly at the bone–implant interface and near the stem tip. Increasing stem length generally reduces the maximum Von Mises stress, while increasing resection length leads to a progressive decrease in stress levels throughout the residual femur.

Moreover, the qualitative analysis suggests that the position of the stem tip relative to the cortical and trabecular regions of the femur may influence the shape and extent of the stress field surrounding the distal end of the implant.

5.2 Quantitative Evaluation of Von Mises Stress Distribution

The von Mises stress values presented in the analysis were calculated by extracting stress data from Abaqus output files for each anatomical part of the femur across all prosthetic configurations. The extracted values were processed in Excel, where the average stress for each femoral part was computed.

Due to the presence of multiple investigated variables, specific parameters were fixed during the analysis to enable clearer comparison among the different configurations.

Some graphs were generated by maintaining a constant stem length or resection configuration while evaluating the influence of the remaining variables.

Figures 5.6, 5.7 and 5.8 present the average Von Mises stress values for the investigated stem lengths and resection configurations across the five anatomical regions of interest.

Overall, Von Mises stress appears to be influenced by both stem length and extent of resection. A progressive reduction in stress magnitude can generally be observed moving from Configuration 1 to Configuration 5 for all investigated stem lengths. This behavior suggests that increasing resection extent progressively modifies the physiological load transfer within the reconstructed femur.

Despite the variations in stress magnitude, the general stress distribution pattern remained relatively consistent across all investigated configurations.

In particular, ROI 1 and ROI 4 consistently exhibited the highest Von Mises stress values for all stem lengths and resection configurations. This behavior is biomechanically consistent with the mechanical role of these regions within the reconstructed femur.

ROI 1 corresponds to the proximal region directly interacting with the prosthetic reconstruction and therefore represents one of the primary load transfer areas between the implant and the residual femur. The elevated stress values observed in this region suggest that a significant portion of the mechanical load is transferred proximally through the bone–implant interface.

A second stress peak was frequently observed in ROI 4, particularly for the shorter stem configurations. Since this region approximately corresponds to the distal stem tip area, the increase in stress may be associated with localized load transfer concentrations occurring near the end of the prosthetic stem.

The identification of elevated stress values around the stem tip is consistent with previous finite element investigations.

El-Zayat et al. reported that both short and long stem reconstructions generated stress peaks in the region surrounding the stem tip, identifying this area as one of the most mechanically loaded regions of the reconstructed bone. Although their study was performed on an adult tibial reconstruction and therefore differs substantially from the present pediatric proximal femoral model, both investigations highlight the important role of the stem tip in load transfer between the implant and the host bone [40].

The authors suggested that the stem tip plays a critical role in load transfer and may represent a potential site of mechanical complications, including stem-end pain and cortical overload [40].

For the 160 mm stem configuration, stress values appeared more uniformly distributed along the investigated anatomical regions, while localized stress peaks became less pronounced compared to the shorter stem configurations.

The progressive reduction of proximal stress observed for the longer stem configurations may indicate conditions associated with proximal stress shielding, which may indicate a tendency toward proximal stress shielding, as the surrounding bone appears to participate less in the overall load transfer mechanism.

Similar observations were reported by Innocenti et al., who investigated the influence of stem length using finite element analysis [37].

The authors observed that increasing stem length altered load transfer mechanisms within the reconstructed bone and could promote stress shielding phenomena.

However, unlike their findings, the present study did not show an increase in stress concentration around the stem tip with increasing stem length. On the contrary, stress levels in this region generally decreased as stem length increased.

Nevertheless, the reduction of stress observed within the residual femur for longer stem configurations is consistent with the observations of Innocenti et al. and may indicate a tendency toward stress shielding.

Although the long-term effects of stress shielding were not investigated in the present work, these findings suggest that stem length may play an important role in balancing implant stability and preservation of physiological bone loading.

Similar considerations were proposed by Campanacci et al. in a clinical study on pediatric proximal femoral reconstruction using allograft–prosthesis composites.

The authors chose short-stem fixation constructs in skeletally immature patients to preserve bone stock and avoid the use of long intramedullary stems, which were considered more likely to induce stress shielding and reduce physiological loading of the residual bone.

Although no finite element analysis was performed in their study, the present results support the concept that stem length can substantially influence load transfer within the reconstructed pediatric femur and should therefore be carefully considered during surgical planning [22].

For what regard the influence of resection length, only a limited number of studies have been reported in literature, particularly in the pediatric field.

Streitbürger et al. reported higher rates of aseptic stem loosening in reconstructions characterized by limited residual bone available for implant fixation. The authors suggested that the reduced amount of supporting bone and the consequent alterations in load transfer may compromise the long-term mechanical stability of the reconstruction. Although implant loosening was not investigated in the present study, the observed modifications in Von Mises stress distribution associated with increasing resection length support the hypothesis that preservation of adequate residual bone stock is essential to ensure a more physiological load transfer between the implant and the host bone. These findings may help explain the increased risk of mechanical complications reported in cases with extensive bone resections [28].

For completeness, an alternative representation of the same results is provided in Figure 8.1 of the Appendix, where the average von Mises stress values are plotted as a function of stem length for each Region of Interest (ROI 1–ROI 5).

In contrast to the figures presented in this chapter, each graph in the Appendix corresponds to a fixed ROI rather than to a fixed stem length.

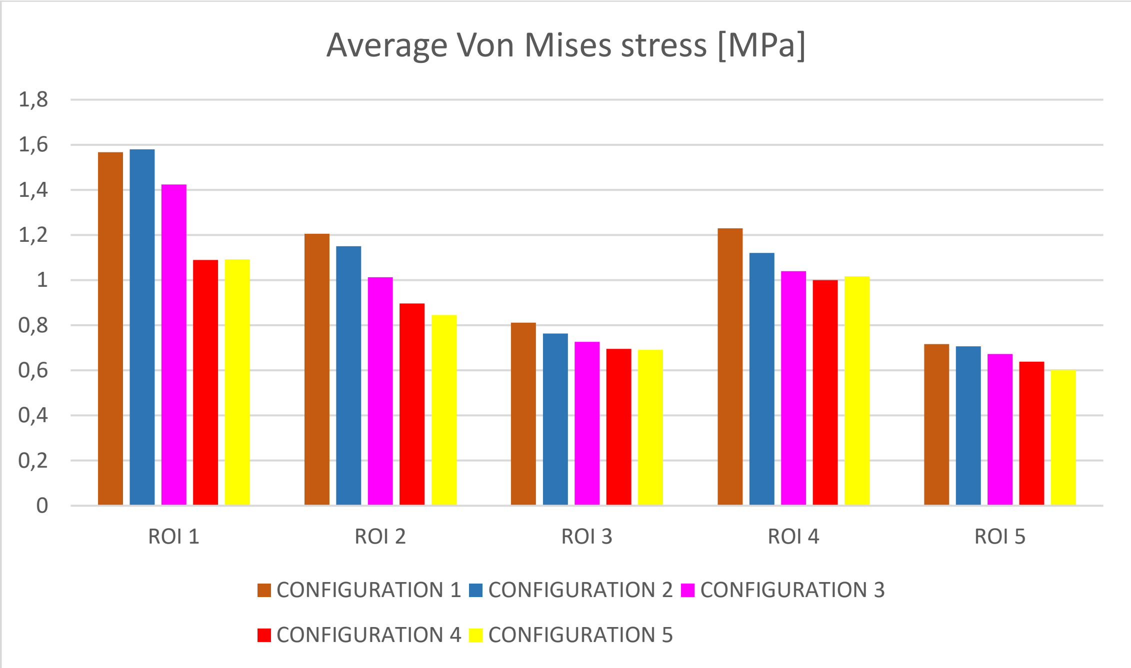

Figure 5.6: Average von mises equivalent stress for the five investigated resection configurations in each region of interest for the 100 mm stem configuration.

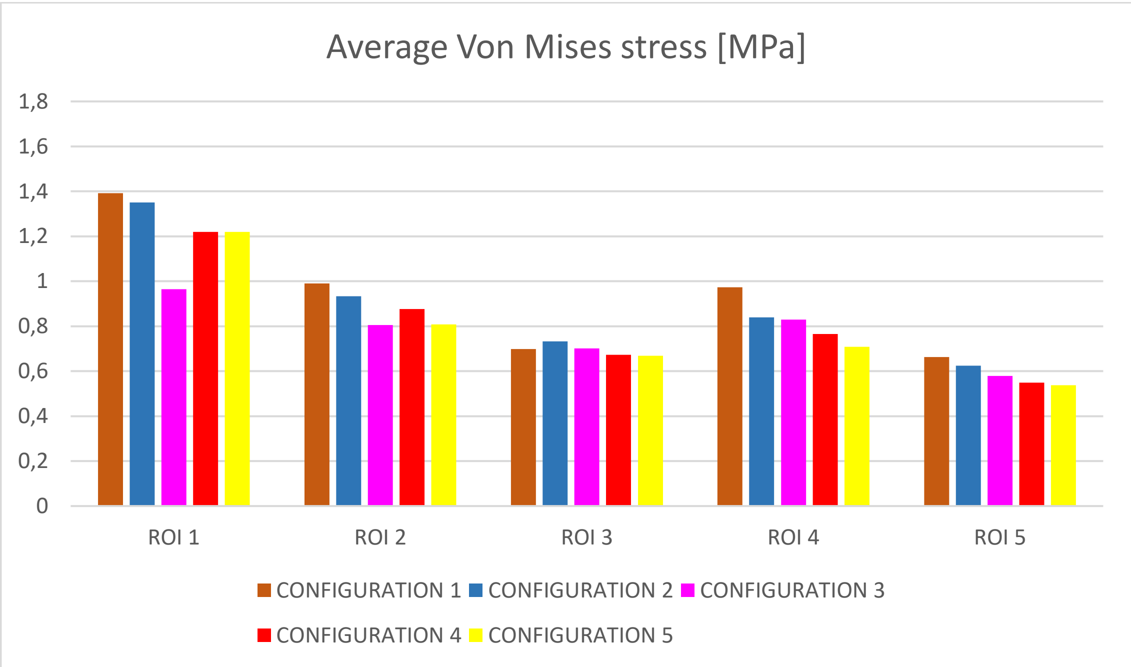

Figure 5.7: Average von mises equivalent stress for the five investigated resection configurations in each region of interest for the 130 mm stem configuration.

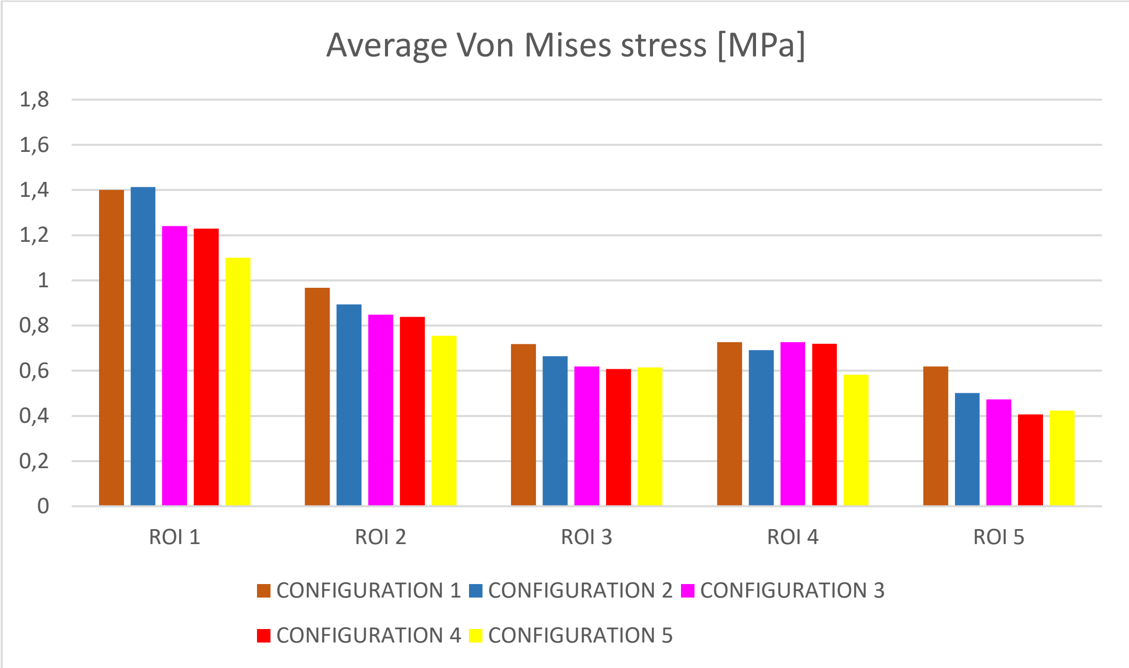

Figure 5.8: Average von mises equivalent stress for the five investigated resection configurations in each region of interest for the 160 mm stem configuration.

5.3 Compressive Stress Analysis

The compressive stress values presented in the analysis were calculated by extracting the S33 stress component from Abaqus output files for each anatomical region of the femur across all prosthetic configurations.

The extracted values were subsequently processed in Excel. Since the objective of the analysis was to evaluate compressive loading within the resected femur, only negative S33 values were considered during post-processing. Positive values, corresponding to tensile stresses, were excluded from the averaging procedure to isolate the compressive stress contribution along the anatomical axis of the femur.

Figures 5.9 present the average compressive stress values for the investigated stem lengths and resection configurations across the five anatomical regions of interest.

Compressive stress appears to be sensitive to variations in resection configuration. A progressive reduction in compressive stress magnitude can generally be observed moving from Configuration 1 to Configuration 5 for all investigated stem lengths. This behavior suggests that increasing resection extent progressively modifies the axial load transfer within the reconstructed femur.

Among the investigated anatomical regions, ROI 1 and ROI 2 consistently exhibited the highest compressive stress values, indicating that these regions sustain the largest portion of axial loading transferred through the prosthetic reconstruction.

For the 100 mm and 130 mm stem configurations, shown in Figures 5.9 and 5.10 respectively, after the progressive decrease in compressive stress from ROI 1 to ROI 3, a secondary peak can be observed in ROI 4, generating a distal stress peak. This behavior suggests a localized concentration of axial load transfer near the stem tip region.

Conversely, for the 160 mm stem configuration, shown in Figure 5.11, the distal peak becomes less evident and compressive stress progressively decreases across all investigated regions. This behavior indicates a more distributed transfer of compressive loads along the residual femur.

Despite these variations, the overall stress distribution pattern remained relatively consistent across all investigated stem lengths.

For completeness, Figure 8.2 in the Appendix reports the compressive stress values as a function of stem length, with a separate graph provided for each Region of Interest (ROI 1–ROI 5), thus offering a complementary representation to the plots presented in this section.

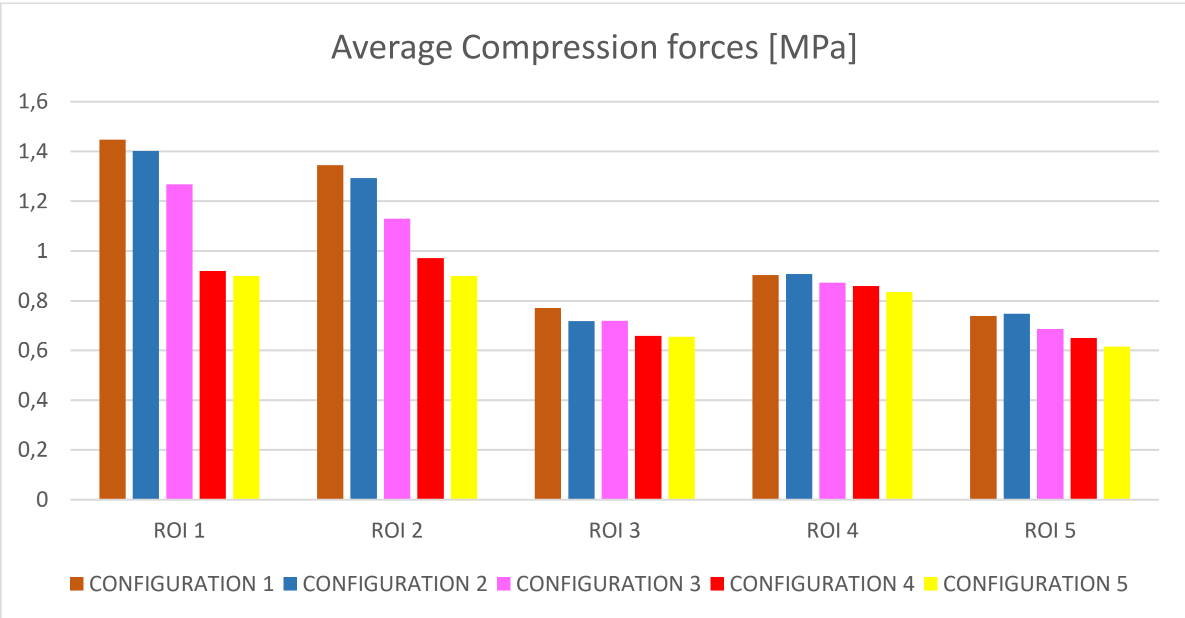

Figure 5.9: Average compression stress values for the five investigated resection configurations in each region of interest for the 100 mm stem configuration.

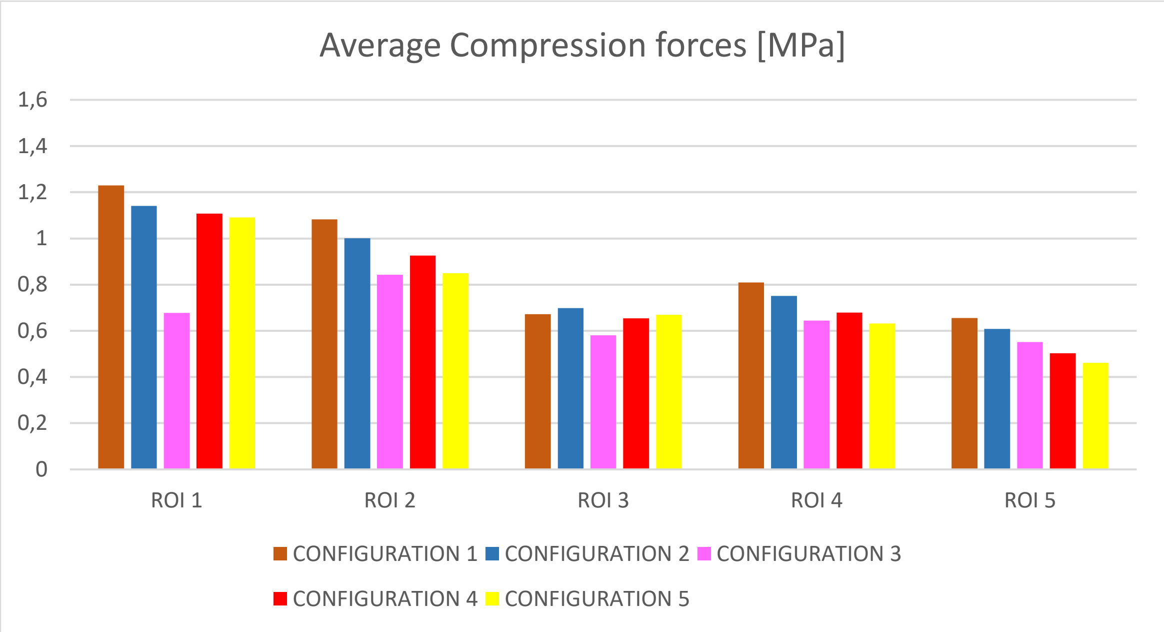

Figure 5.10: Average compression stress values for the five investigated resection configurations in each region of interest for the 130 mm stem configuration.

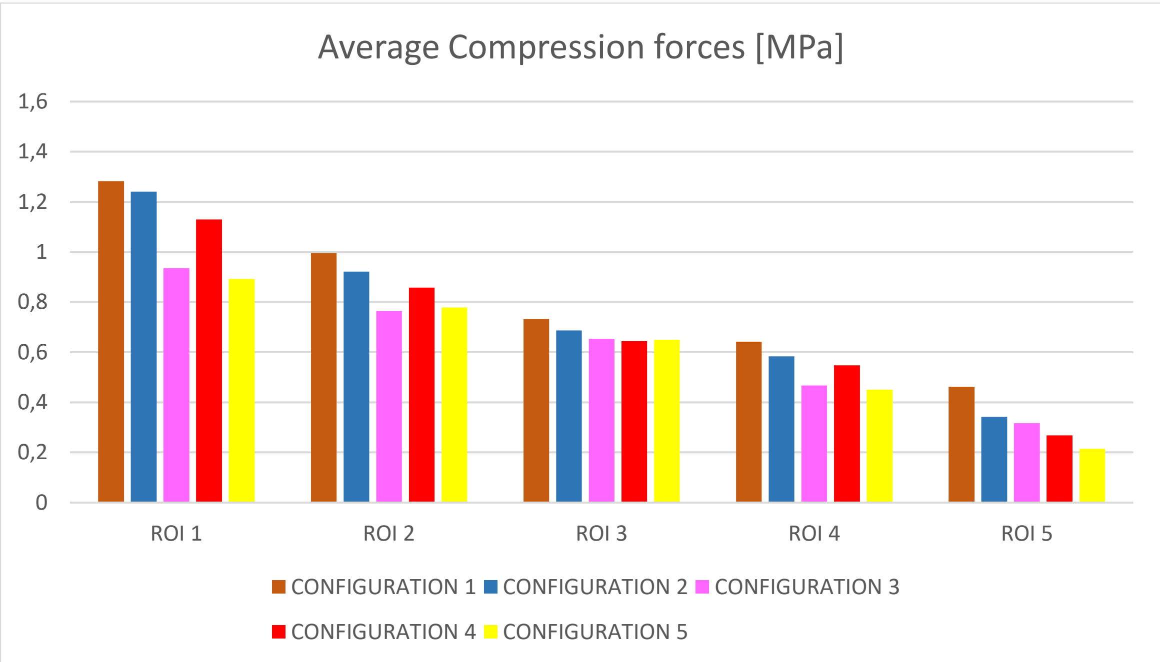

Figure 5.11: Average compression stress values for the five investigated resection configurations in each region of interest for the 160 mm stem configuration.

5.4 Shear Stress Analysis

The shear stress values presented in the analysis were calculated by extracting the S12 stress component from Abaqus output files for the same anatomical region of the femur across all prosthetic configurations. The S12 component was defined in the anatomical reference system. The extracted values were subsequently processed in Excel, where all values were converted to positive magnitudes and averaged for each region of interest.

Shear stress analysis is particularly important given that bone tissue exhibits significantly lower resistance to shear, and torsional forces compared to normal stresses. Elevated shear stress values can lead to the formation of microfractures, making this parameter critical for assessing implant safety and long-term stability.

Figure 5.12, 5.13, 5.14 present the shear stress distribution obtained for the three investigated stem lengths (100 mm, 130 mm and 160 mm) across the five resection configurations.

Although the overall magnitude of shear stress slightly decreases with increasing stem length, the general stress distribution pattern remains consistent across all investigated configurations.

For each stem length, a first stress peak is observed in ROI 1, followed by a pronounced decrease in ROI 2, a slight increase in ROI 3, and a second peak in ROI 4. In ROI 5, shear stress values remain higher than those measured in ROI 2 and ROI 3, suggesting persistence of stress transfer toward the distal portion of the reconstructed femur.

For the 100 mm stem (Figure 5.12), the most critical region is ROI 4, where Configuration 1 reaches the highest shear stress value observed in the study, of 0.183 MPa, indicating relatively limited tangential loading within the investigated regions.

The remaining configurations show comparable stress levels, particularly in ROI 2, ROI 3 and ROI 5.

For the 130 mm stem (Figure 5.13), the stress peak in ROI 4 remains evident, although its magnitude becomes comparable to that observed in ROI 1.

Configuration 1 continues to exhibit the highest shear stress values among the resection levels investigated.

For the 160 mm stem (Figure 5.14), ROI 1 and ROI 4 remain the most stressed regions. However, a noticeable increase in shear stress can be observed in ROI 5 compared with the 100 mm and 130 mm stem configurations.

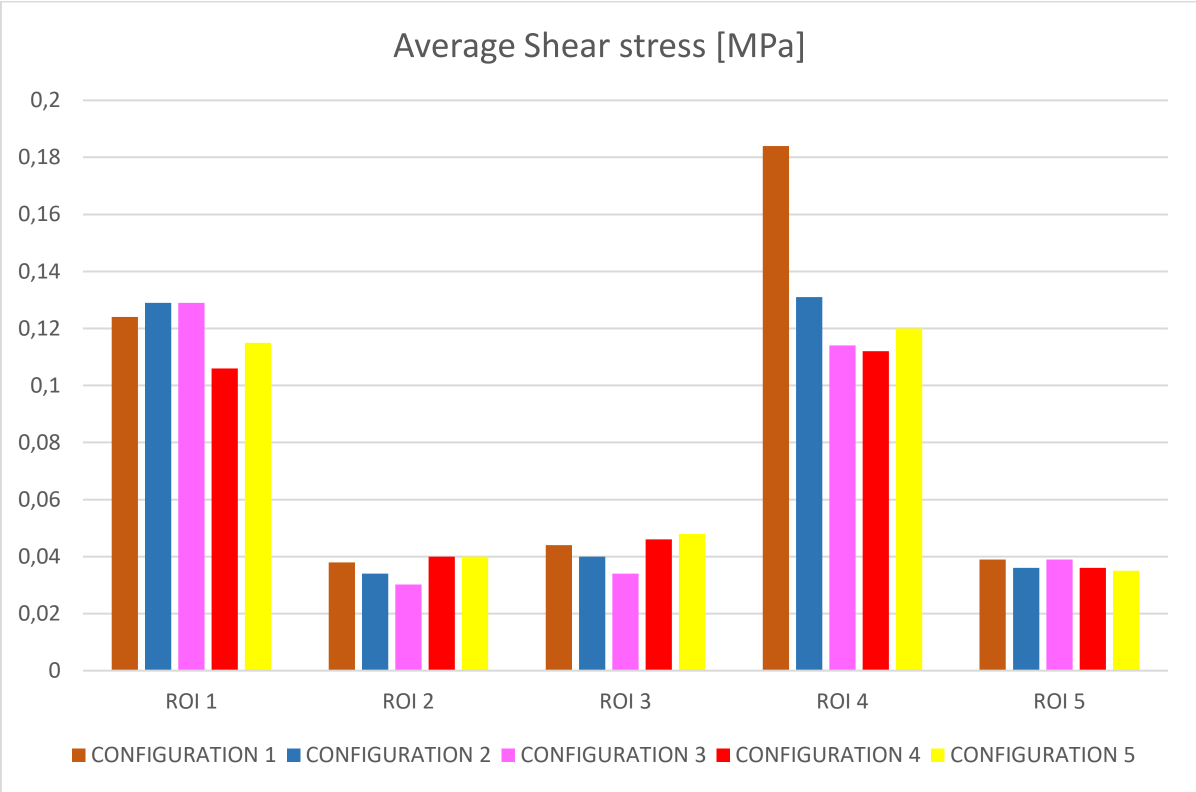

Figure 5.12 Average shear stress values for the five investigated resection configurations in each region of interest for the 100 mm stem configuration.

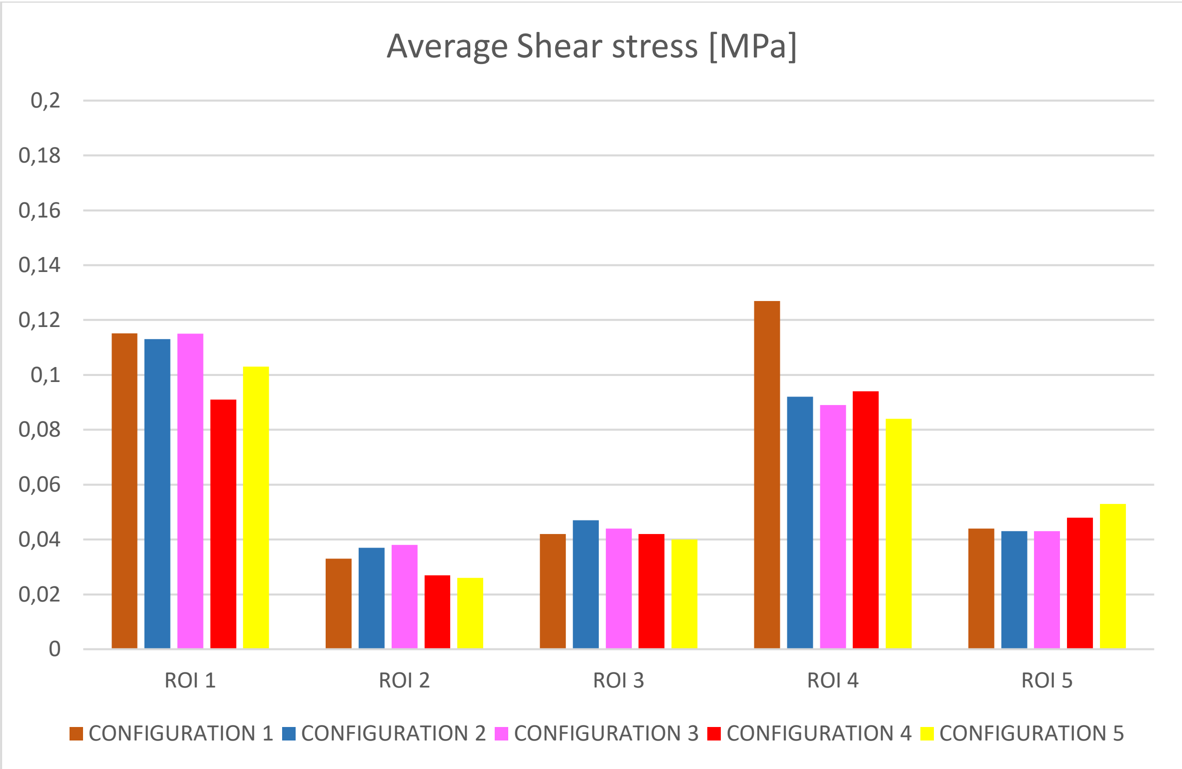

Figure 5.13: Average shear stress values for the five investigated resection configurations in each region of interest for the 130 mm stem configuration.

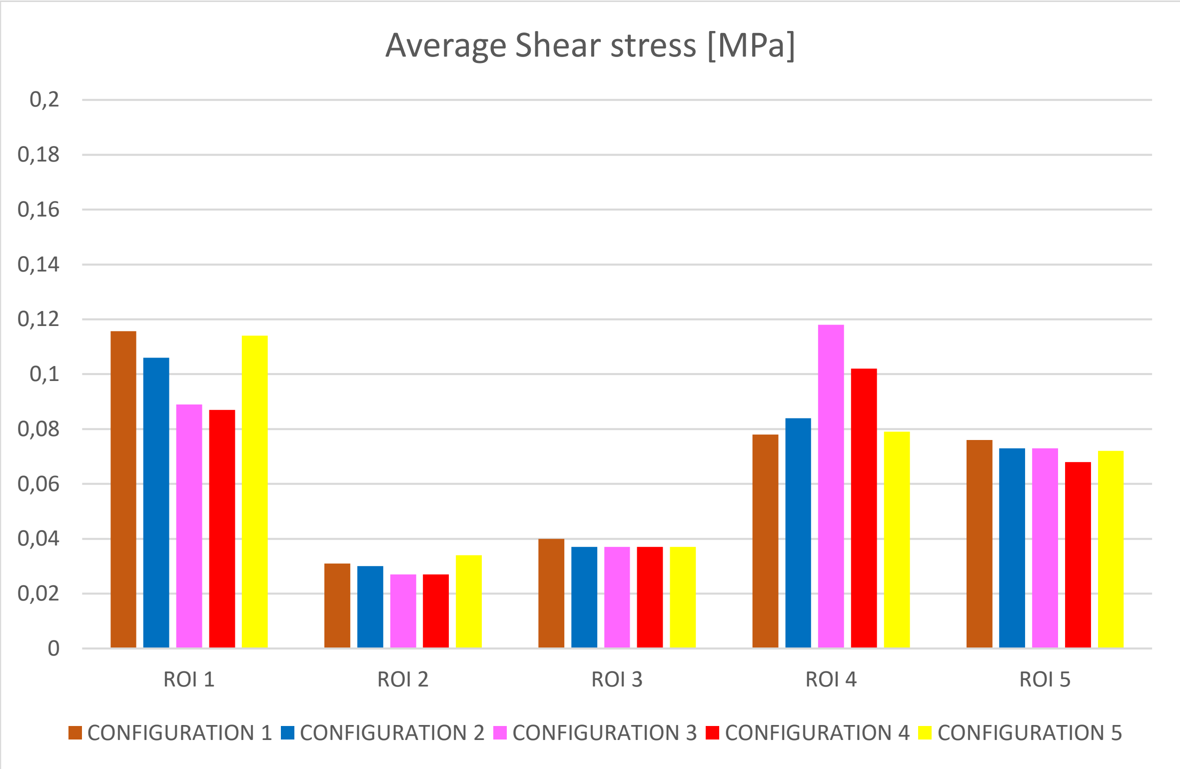

Figure 5.14: Average shear stress values for the five investigated resection configurations in each region of interest for the 160 mm stem configuration.

Shear stress appears to be more sensitive to stem length than to prosthesis configuration. The influence of stem length is region-dependent, with the most evident effects observed in ROI 4 and ROI 5.

Figure 8.3 in the Appendix presents the shear stress values as a function of stem length for all five investigated Regions of Interest (ROI 1–ROI 5) and the five resection configurations. Among these regions, ROI 4 and ROI 5 show the most pronounced dependence on stem length.

In ROI 4, the shear stress generally decreases as stem length increases, whereas in ROI 5 the opposite trend is observed, with progressively higher shear stress values for longer stems.

A comparable trend toward distal load transfer with increasing stem length has been reported by Arno et al. [38], who observed a reduction of proximal strain and an increase of distal strain in femoral reconstructions with longer stems.

The obtained shear stress values remain remarkably low across all configurations and anatomical regions. Literature indicates that acceptable shear stress levels for bone tissue should remain below 51.6 MPa [39] to prevent mechanical failure.

The present analysis yields values that are orders of magnitude lower than this threshold, indicating that all investigated configurations maintain shear stresses within safe biomechanical limits.

This finding suggests that from a shear stress perspective, all configurations provide adequate mechanical safety margins, with the primary differentiating factors being the optimization of normal stress distribution and compression force patterns as previously discussed.

5.5 Limitation

There were several limitations to this study. First, the FEM was developed from a single patient-specific geometry, and therefore the results may not be representative of the entire pediatric population.

Furthermore, cortical, cancellous bones and growth plate were modeled as homogeneous and isotropic materials, consequently, variations in bone properties within the femur were not taken into account and may have influenced the predicted stress distribution.

In addition, the simulations were performed under a simplified static loading condition represented by an axial force of 250 N.

Daily activities such as walking, running, or stair climbing generate more complex loading patterns that were not included in the present analysis. Muscle forces and ligament contributions were also neglected, which may affect the actual stress distribution within the reconstructed femur.

Another limitation is that ideal contact conditions between the implant and the surrounding bone were assumed, whereas clinical situations may involve variations in fixation quality and implant positioning.

A further aspect that should be considered is the limited availability of biomechanical studies focusing on pediatric proximal femoral reconstructions.

Compared to adult orthopedics, the development of patient-specific finite element models in pediatric patients is particularly challenging due to the complex anatomy of the immature skeleton, the continuous growth-related changes in bone morphology, and the limited availability of subject-specific imaging and mechanical property data.

Consequently, direct comparisons with previous studies remain difficult. Nevertheless, these challenges further emphasize the importance of patient-specific investigations such as the present study, which contribute to improving the understanding of load transfer mechanisms and implant behavior in pediatric oncological reconstructions.

Despite these limitations, the developed model provides useful biomechanical insights into the influence of resection level and stem length on stress distribution within the pediatric femur with a modular megaprosthesis inserted.

6 Conclusions

This thesis has focused on investigating the biomechanical behavior of different designs of a megaprosthesis used for the proximal femoral replacement in a pediatric patient affected by bone tumor.

In details, the goal was to check how and if parameters such as stem length and resection level influence the stress within the femur.

The finite element analysis was conducted using a 3D model reconstructed from computed tomography images of a fourteen-year-old patient, including cortical bone, trabecular bone, and the distal growth plate, thus capturing the complex anatomical and material heterogeneity of the pediatric femur. The prosthetic implant was virtually inserted after simulating 5 different proximal bone resections, and an axial load of 250 N was applied along the mechanical axis to mimic physiological conditions during static standing.

Three different stem lengths were then analyzed (100 mm, 130 mm and 160 mm) to evaluate their influence on implant stability and stress distribution.

Throughout the modelling process, several challenges were encountered, including the lack of pediatric-specific mechanical property data and threshold values for bone failure necessitated careful interpretation of stress levels relative to available adult data.

The use of finite element analysis in orthopedic oncology provides valuable insights into the mechanical behavior of reconstructed anatomical structures.

In particular, patient-specific modelling offers important advantages by allowing the evaluation of different surgical and prosthetic configurations based on the individual anatomy of the patient.

This approach may support pre-operative planning and contribute to the optimization of reconstruction strategies aimed at preserving physiological load transfer and implant stability.

The results of this study indicate that both the resection level and the stem length influence the average Von Mises stress and compression forces, while shear stress appears to be more sensitive to stem length than to resection level.

The numerical results showed that increasing the resection length generally led to a reduction in Von Mises stress and compressive stress within the residual femur. Although the overall stress distribution pattern remained consistent across all investigated configurations, larger resections progressively modified the load transfer mechanism by reducing the amount of residual bone available to participate in load sharing.

Stem length was also found to play a significant role in determining the mechanical response of the reconstruction.

Longer stems produced a more uniform stress distribution and reduced stress concentrations, particularly in the region corresponding to the stem tip.

However, the reduction of stress observed in the residual bone may also indicate a tendency toward stress shielding, suggesting that excessively long stems could decrease the physiological mechanical stimulation of the surrounding bone.

Overall, the results suggest that both preservation of residual bone stock and careful selection of stem length are essential for achieving a balance between implant stability and physiological load transfer in pediatric proximal femoral reconstructions.

Future studies could involve several fields, for example they could incorporate more realistic physiological loading scenarios, including gait, stair climbing, and other daily activities, to better reproduce the mechanical environment experienced by the femur.

Furthermore, the present work was based on a single patient-specific model. Future investigations should involve a larger number of pediatric patients to evaluate the inter-subject variability and improve the generalizability of the results.

The inclusion of different ages, anatomical geometries, and tumor locations could provide a more comprehensive understanding of the biomechanical behavior of pediatric oncological reconstructions.

Although the acquisition of patient-specific data in pediatric orthopedic oncology is particularly challenging due to the rarity of these conditions and the limited availability of medical images, larger patient cohorts would substantially strengthen the clinical relevance of future studies.

Another important aspect concerns the material assumptions adopted in the model. Future studies could incorporate heterogeneous and anisotropic material properties derived from medical imaging data, as well as bone remodeling algorithms capable of predicting long-term adaptation of the residual femur following implantation.

An additional direction for future research would be the investigation of different fixation strategies. The present study focused exclusively on cementless reconstruction; however, cemented stems are still widely used in orthopedic oncology. A comparative finite element analysis between cemented and cementless stems could provide valuable insights into differences in stress distribution, load transfer mechanisms, and implant stability.

Understanding how these factors influence the mechanical response of the reconstructed femur may contribute to the optimization of patient-specific surgical planning and prosthetic design in pediatric orthopedic oncology.

By addressing these aspects, future research could further improve the understanding of the biomechanical behavior of pediatric proximal femoral reconstructions and contribute to the optimization of implant design and surgical strategies.

Ultimately, this work highlights the potential of patient-specific finite element modelling as a valuable tool for supporting surgical decision-making and improving the biomechanical understanding of complex reconstructions in pediatric orthopedic oncology.

7 References

[1] Chang A, Breeland G, Black AC, Hubbard JB. Anatomy, Bony Pelvis and Lower Limb: Femur. 2023 Nov 17. In: StatPearls [Internet]. Treasure Island (FL): StatPearls Publishing; 2026 Jan–. PMID: 30422577.

[2] OpenStax. (2026). *Anatomy and Physiology 2e* (2nd ed.). Rice University. https://openstax.org/details/books/anatomy-and-physiology-2e

[3] Zaghloul, A. (2018). Hip Joint: Embryology, Anatomy and Biomechanics. *Biomedical Journal of Scientific & Technical Research*, *12*(3). https://doi.org/10.26717/bjstr.2018.12.002267

[4] Stewart, T. D., & Hall, R. M. (2006). (iv) Basic biomechanics of human joints: Hips, knees and the spine. *Current Orthopaedics*, *20*(1), 23–31. https://doi.org/10.1016/j.cuor.2005.12.004

[5] Nguyen, J. C., & Caine, D. (2024). The Immature Pediatric Appendicular Skeleton. In *Seminars in Musculoskeletal Radiology* (Vol. 28, Issue 4, pp. 361–374). Thieme Medical Publishers, Inc. https://doi.org/10.1055/s-0044-1786151

[6] Zimmermann, E. A., Riedel, C., Schmidt, F. N., Stockhausen, K. E., Chushkin, Y., Schaible, E., Gludovatz, B., Vettorazzi, E., Zontone, F., Püschel, K., Amling, M., Ritchie, R. O., & Busse, B. (2019). Mechanical Competence and Bone Quality Develop During Skeletal Growth. *Journal of Bone and Mineral Research*, *34*(8), 1461–1472. https://doi.org/10.1002/jbmr.3730

[7] Tiffany, A. S., & Harley, B. A. C. (2022). Growing Pains: The Need for Engineered Platforms to Study Growth Plate Biology. In *Advanced Healthcare Materials* (Vol. 11, Issue 19). John Wiley and Sons Inc. https://doi.org/10.1002/adhm.202200471

[8] The Royal Children's Hospital Melbourne. Available from: Fracture Education : Anatomic differences: child vs. adult

[9] Öhman, C., Baleani, M., Pani, C., Taddei, F., Alberghini, M., Viceconti, M., & Manfrini, M. (2011). Compressive behaviour of child and adult cortical bone. *Bone*, *49*(4), 769–776. https://doi.org/10.1016/j.bone.2011.06.035

[10] TL, S., LP, M., Holm S, S., & C, W. (2017). Using a Finite Element Pediatric Hip Model in Clinical Evaluation - A Feasibility Study. Journal of Bioengineering & Biomedical Science, 07(05). https://doi.org/10.4172/2155-9538.1000241

[11] Incze-Bartha, Z., Incze-Bartha, S., Simon Szabó, Z., Feier, A. M., Vunvulea, V., Nechifor-Boilă, I. A., Pastorello, Y., Szasz, D., & Dénes, L. (2023). Finite Element Analysis of Normal and Dysplastic Hip Joints in Children. Journal of Personalized Medicine, 13(11). https://doi.org/10.3390/jpm13111593

[12] Petrescu, D. I., Yustein, J. T., & Dasgupta, A. (2024). Preclinical models for the study of pediatric solid tumors: focus on bone sarcomas. In *Frontiers in Oncology* (Vol. 14). Frontiers Media SA. https://doi.org/10.3389/fonc.2024.1388484

[13] Ryan, R. E. (2003). Living with juvenile diabetes: A practical guide for parents and caregivers. *Journal of Pediatric Nursing*, *18*(2), 139. https://doi.org/10.1053/jpdn.2003.18

[14] Nie, Z., & Peng, H. (2018). Osteosarcoma in patients below 25 years of age: An observational study of incidence, metastasis, treatment and outcomes. *Oncology Letters*, *16*(5), 6502–6514. https://doi.org/10.3892/ol.2018.9453

[15] Brisse, H., Ollivier, L., Edeline, V., Pacquement, H., Michon, J., Glorion, C., & Neuenschwander, S. (2004). Imaging of malignant tumours of the long bones in children: Monitoring response to neoadjuvant chemotherapy and preoperative assessment. In *Pediatric Radiology* (Vol. 34, Issue 8, pp. 595–605). Springer Verlag. https://doi.org/10.1007/s00247-004-1192-x

[16] van der Woude, H.-J., Bloem, J. L., Hogendoorn, P. C. W., van der Woude, H.-J., Bloem, J. L., & Hogendoorn, P. C. W. (1998). Preoperative evaluation and monitoring chemotherapy in patients with high-grade osteogenic and Ewings sarcoma: review of current imaging modalities. In *Skeletal Radiol* (Vol. 27). International Skeletal Society.

[17] Ilyas, I., Pant, R., Kurar, A., Moreau, P. G., & Younge, D. A. (2002). Modular megaprosthesis for proximal femoral tumors. *International Orthopaedics*, *26*(3), 170–173. https://doi.org/10.1007/s00264-002-0335-7

[18] Yadav, P., Shefelbine, S. J., & Gutierrez-Farewik, E. M. (2016). Effect of growth plate geometry and growth direction on prediction of proximal femoral morphology. *Journal of Biomechanics*, *49*(9), 1613–1619. https://doi.org/10.1016/j.jbiomech.2016.03.039

[19] Guder, W. K., Engel, N. M., Streitbürger, A., Polan, C., Dudda, M., Podleska, L. E., Nottrott, M., & Hardes, J. (2024). Incidence and management of secondary deformities after megaendoprosthetic proximal femur replacement in skeletally immature bone sarcoma patients. *Archives of Orthopaedic and Trauma Surgery*, *144*(6), 2501–2510. https://doi.org/10.1007/s00402-024-05334-1;

[20] Salvini, M., Malerba, G., Meschini, C., el Motassime, A., Venturini, E., Campanacci, D. A., Muratori, F., Checcucci, S., Scanferla, R., Vitiello, R., & Maccauro, G. (2025). Proximal femur replacement in oncologic lesion: hemiarthroplasty vs total hip arthroplasty—a multicentric retrospective study. *Journal of Orthopaedic Surgery and Research*, *20*(1). https://doi.org/10.1186/s13018-025-05910-0;

[21] Zoccali, C., Careri, S., Attala, D., Florio, M., Milano, G. M., & Giordano, M. (2021). A new proximal femur reconstruction technique after bone tumor resection in a very small patient: An exemplificative case. Children, 8(6). https://doi.org/10.3390/children8060442

[22] Campanacci, D. A., Scanferla, R., Muratori, F., Scolari, F., Scoccianti, G., Tamburini, A., & Beltrami, G. (2024). Allograft-prosthesis composite after proximal femur bone tumor resection in pediatric age: Is it effective in preserving bone stock? *Journal of Children's Orthopaedics*, *18*(5), 531–539. https://doi.org/10.1177/18632521241269338;

[23] Mavrogenis, A. F., & Papagelopoulos, P. J. (2012). Expandable prostheses for the leg in children. In *Orthopedics* (Vol. 35, Issue 3, pp. 173–175). https://doi.org/10.3928/01477447-20120222-03

[24] Neel, M. D., Letson, G. D., & Moffitt, H. L. (n.d.). Modular Endoprostheses for Children With Malignant Bone Tumors From the Interdisciplinary Oncology Program at the. In *Cancer Control* (Vol. 8, Issue 4).

[25] implantcast GmbH. (2017). *MUTARS® Xpand: Non-invasive Growing Prosthesis*. Buxtehude, Germany: implantcast GmbH. Available at: www.implantcast.de

[26] Brzeszczyński, F. F., Karpiński, M., Brzeszczyński, M. A., Bończak, O., & Hamilton, D. F. (2025). Rehabilitation Protocols and Functional Outcomes in Oncological Patients Treated with Modular Megaprosthesis: A Systematic Review. In *Cancers* (Vol. 17, Issue 18). Multidisciplinary Digital Publishing Institute (MDPI). https://doi.org/10.3390/cancers17182951

[27] Waldemar Link GmbH & Co. KG. (2020). *MEGASYSTEM-C Tumor and Revision System: Surgical Technique*. Hamburg, Germany: Waldemar Link GmbH & Co. KG. Available at: https://www.link-ortho.com

[28] Streitbürger, A., Hardes, J., Nottrott, M., & Guder, W. K. (2022). Reconstruction survival of segmental megaendoprostheses: a retrospective analysis of 28 patients treated for intercalary bone defects after musculoskeletal tumor resections. *Archives of Orthopaedic and Trauma Surgery*, *142*(1), 41–56. https://doi.org/10.1007/s00402-020-03583-4

[29] Floerkemeier, T., Gronewold, J., Berner, S., Olender, G., Hurschler, C., Windhagen, H., & von Lewinski, G. (2013). The influence of resection height on proximal femoral strain patterns after Metha short stem hip arthroplasty: an experimental study on composite femora. *International Orthopaedics*, *37*(3), 369–377. https://doi.org/10.1007/s00264-012-1725-0

[30] Fraterrigo, G., Schileo, E., Simpson, D., Stevenson, J., Kendrick, B., & Taddei, F. (2023). Does a novel bridging collar in endoprosthetic replacement optimise the mechanical environment for osseointegration? A finite element study. *Frontiers in Bioengineering and Biotechnology*, *11*. https://doi.org/10.3389/fbioe.2023.1120430

[31] Bahamonde, L., & Zecchetto, P. (2023). Resection and reconstruction of the proximal femur with revision stems: a cost-effective alternative. *Annals of Joint*, *8*. https://doi.org/10.21037/aoj-20-104;

[32] Li, J., Xiong, L., Lei, C., Wu, X., & Mao, X. (2023). Is it reasonable to shorten the length of cemented stems? A finite element analysis and biomechanical experiment. *Frontiers in Bioengineering and Biotechnology*, *11*. https://doi.org/10.3389/fbioe.2023.1289985;

[33] Hou, Z. W., Zheng, K., & Yu, X. C. (2025). Biomechanical comparison of a novel triangular fixation stem and a conventional fixation stem in a model of a prosthesis for ultrashort residual proximal femur reconstruction: a finite element analysis study. *BMC Musculoskeletal Disorders*, *26*(1). https://doi.org/10.1186/s12891-025-08805-7

[34] Cook-Et-Al-Concepts-and-Applications-of-Finite-Element-Analysis-4ed. (n.d.).

[35] Taylor, M., & Prendergast, P. J. (2015). Four decades of finite element analysis of orthopaedic devices: Where are we now and what are the opportunities? *Journal of Biomechanics*, *48*(5), 767–778. https://doi.org/10.1016/j.jbiomech.2014.12.019

[36] Kluess, D., Wieding, J., Souffrant, R., Mittelmeier, W., & Bader, R. (n.d.). *Finite Element Analysis in Orthopaedic Biomechanics 151 x Finite Element Analysis in Orthopaedic Biomechanics*. Retrieved www.intechopen.com

[37] Innocenti, B. (2025). Cemented fixation improves bone stress and stability in distal femoral replacement. *Knee Surgery, Sports Traumatology, Arthroscopy*. https://doi.org/10.1002/ksa.70143

[38] Arno, S., Fetto, J., Nguyen, N. Q., Kinariwala, N., Takemoto, R., Oh, C., & Walker, P. S. (2012). Evaluation of femoral strains with cementless proximal-fill femoral implants

of varied stem length. *Clinical Biomechanics*, *27*(7), 680–685. https://doi.org/10.1016/j.clinbiomech.2012.03.006

[39] Turner, C. H., Wang, T., & Burr, D. B. (2001). Shear strength and fatigue properties of human cortical bone determined from pure shear tests. *Calcified Tissue International*, *69*(6), 373–378. https://doi.org/10.1007/s00223-001-1006-1

[40] El-Zayat, B. F., Heyse, T. J., Fanciullacci, N., Labey, L., Fuchs-Winkelmann, S., & Innocenti, B. (2016). Fixation techniques and stem dimensions in hinged total knee arthroplasty: a finite element study. *Archives of Orthopaedic and Trauma Surgery*, *136*(12), 1741–1752. https://doi.org/10.1007/s00402-016-2571-0

8 Appendix

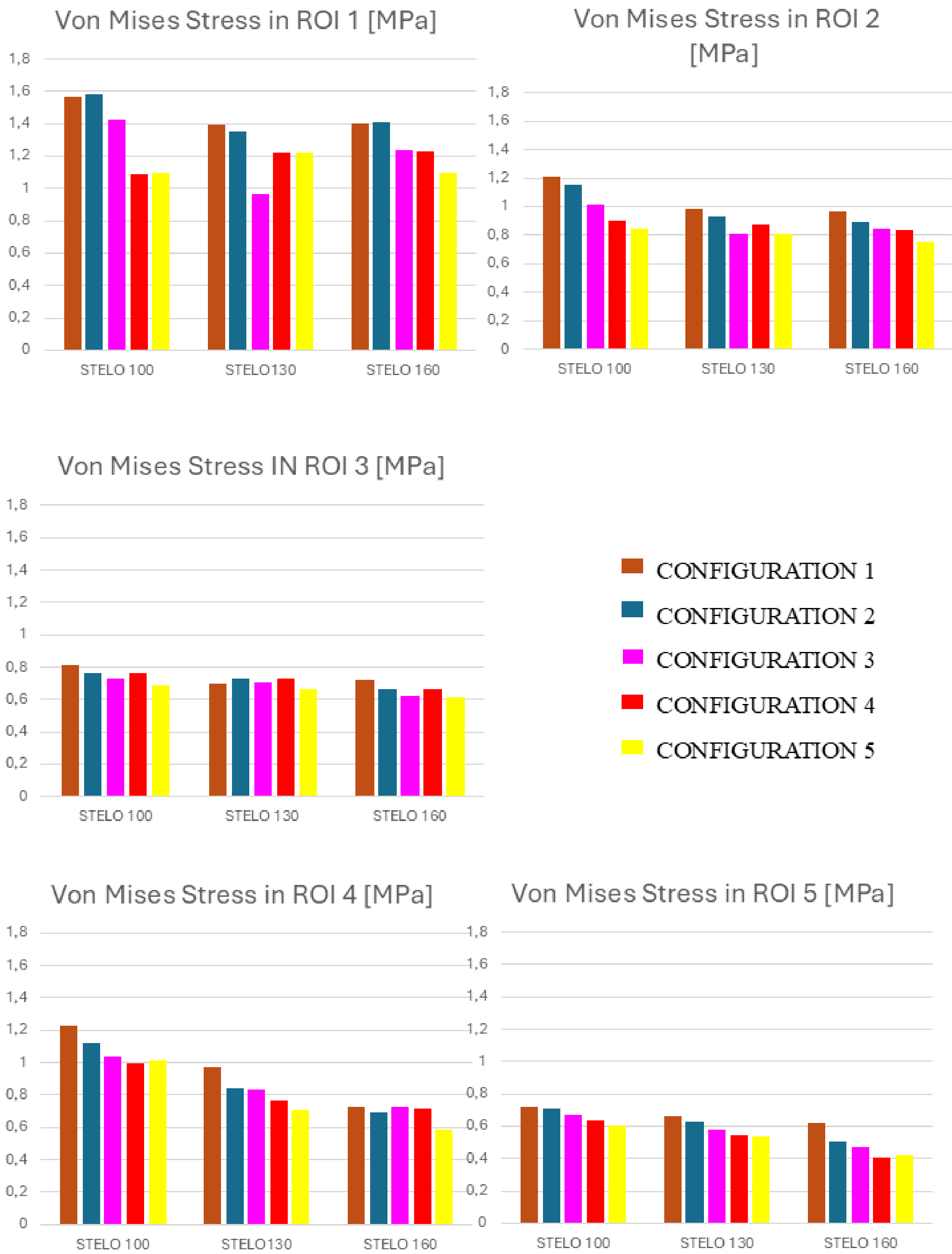

Figure 8.1: Average Von Mises stress in the five Regions of Interest (ROI 1–ROI 5). Each graph represents a different ROI and compares the five implant configurations for stem lengths of 100, 130, and 160 mm.

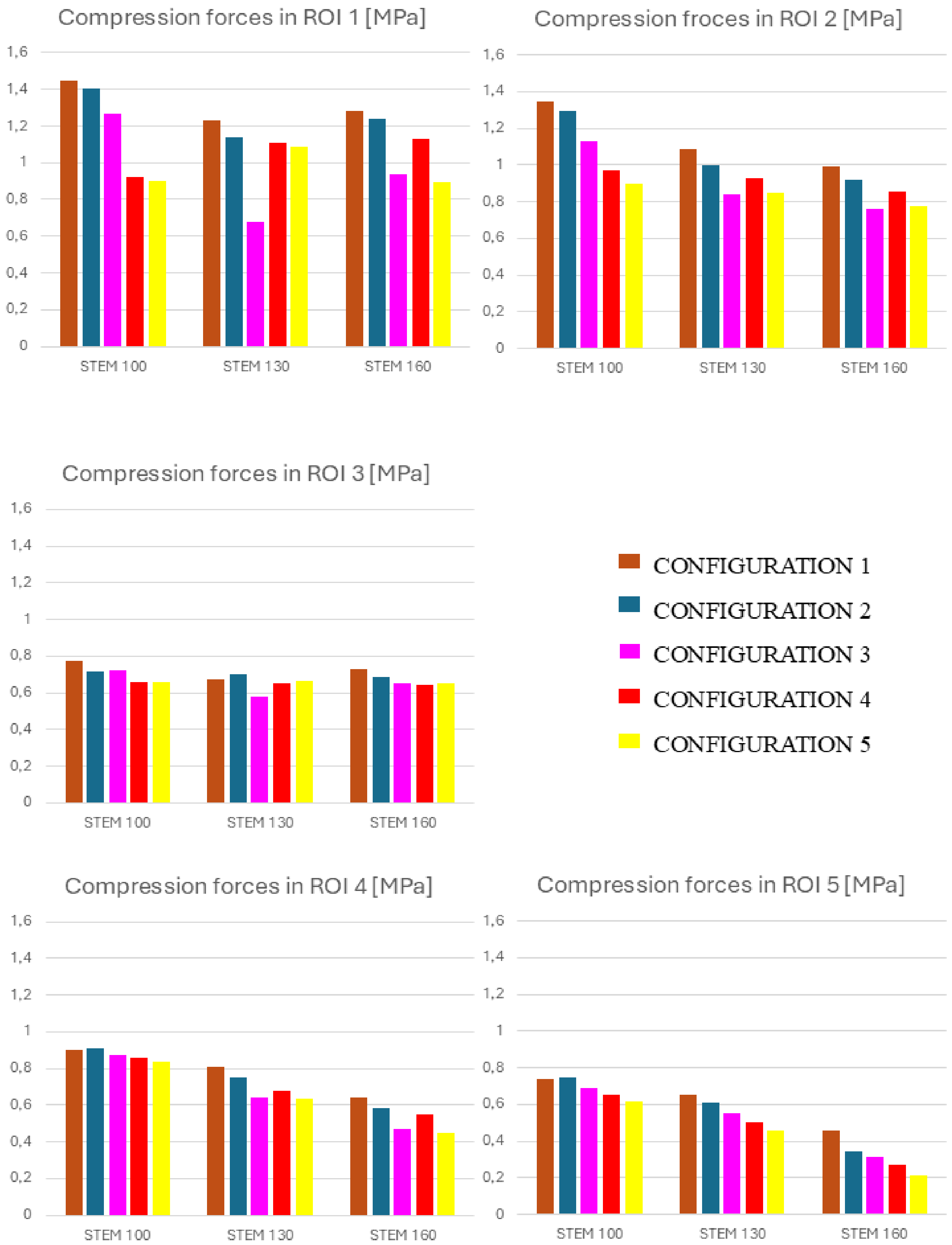

Figure 8.2: Compression forces in the five Regions of Interest (ROI 1–ROI 5). Each graph represents a different ROI and compares the five implant configurations for stem lengths of 100, 130, and 160 mm.

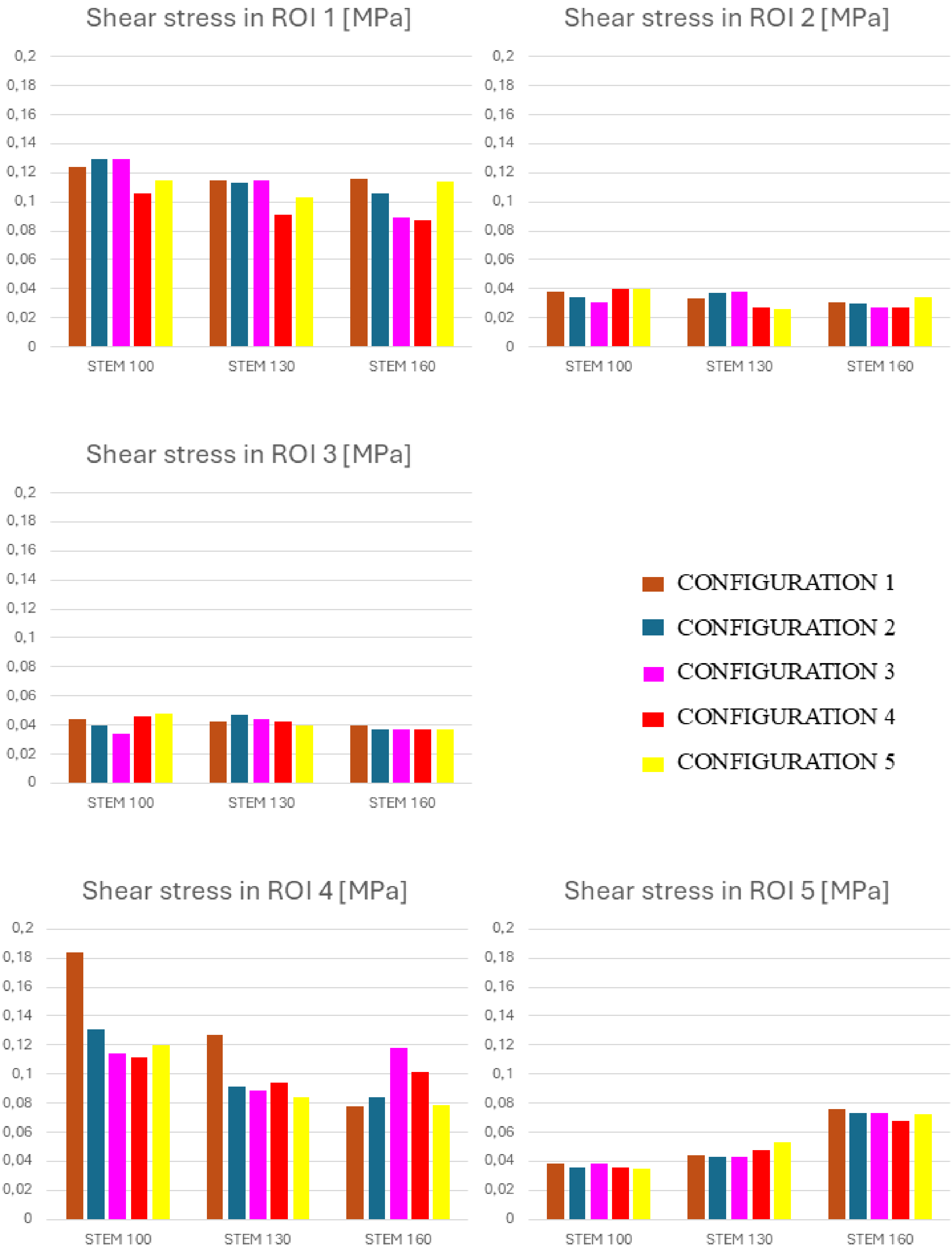

Figure 8.3: Shear stress in the five Regions of Interest (ROI 1–ROI 5). Each graph represents a different ROI and compares the five implant configurations for stem lengths of 100, 130, and 160 mm.